

An-Najah National University

Faculty of Graduate Studies

Recycling of Waste CdS Film Solar Cells by Different Depositions

By

Majd Ibrahim Rashid Sbeah

Supervisor

Prof. Hikmat Hilal

Co-Supervisor

Dr. Ahed Zyoud

This Thesis Is Submitted in Partial Fulfillment of the Requirements for The Degree of Master of Chemistry, Faculty of Graduate Studies, An-Najah National University, Nablus, Palestine.

2020

Recycling of Waste CdS Film Solar Cells by Different Depositions

By


Majd Ibrahim Rashid Sbeah

This Thesis was defended successfully on 24/12/2020, and approved by:

Defense Committee Members

- Prof. Hikmat S. Hilal / Supervisor**
- Dr. Ahed Zyoud / Co. Supervisor**
- Dr. Muayad Abusaa / External Examiner**
- Dr. Maen Ishtaiwi / Internal Examiner**

Signature



.....

.....

.....

.....

III

Dedication

I dedicate my dissertation to my great loving parents Mr. Ibrahim Sbeah and Mrs. Sawsan Sbeah, with my special feeling of gratitude to them, whose words of encouragement and motivation for tenacity ring in my ears.

To my lovely and supportive sister, Reem. To my brothers Ahmad and Abdalrahman, and all my family who supported me throughout my study.

To people who paved my way of science and knowledge, all my distinguished teachers.

Also, I dedicate this dissertation to my friends who supported me and shared with me the most beautiful moments.

To all chemical researchers in Palestine and the world.

Majd Ibrahim Sbeah

Acknowledgments

First and foremost, I acknowledge my thanks to Allah, the Ever-Thankful; the Ever-Magnificent, for His blesses and helps. I am really sure that this work would never have succeeded and become truth, without His guidance.

I would like to take this opportunity to say deep thanks to all my supervisors; Professor Hikmat S. Hilal, and Dr. Ahed Zyoud for their help, guidance, and encouragement and their moral support throughout research work and writing up.

Thanks for the technical help from the Chemistry Department Laboratory staff at An-Najah N. University, especially Mr. Nafith Dwekat.

Last and not least, I would like to express my profound and deepest gratitude to my great parents, lovely sister, and brothers, for their encouragement and support, along this work.

I hope that this modest work will obtain the degree of the anticipated expectations.

Majd Ibrahim Sbeah

الإقرار

أنا الموقعة ادناه مقدمة الرسالة التي تحمل عنوان

Recycling of Waste CdS Film Solar Cells by Different Depositions

أقر بأن ما اشتملت عليه هذه الرسالة إنما هو نتاج جهدي الخاص، باستثناء ما تمت الإشارة إليه حيثما ورد، وان هذه الرسالة ككل من أو جزء منها لم يقدم من قبل لنيل أية درجة أو بحث علمي أو بحثي لدى أية مؤسسة تعليمية أو بحثية أخرى

Declaration

The work provided in this thesis, unless otherwise referenced, is the researcher's own work, and has not been submitted elsewhere for any other degree or qualification.

Student's name:

اسم الطالبة: مجد إبراهيم راشد صبيح

Signature:



التوقيع:

Date:

التاريخ: 24/12/2020

List of Contents

No.	Contents	Page
	Dedication	III
	Acknowledgements	IV
	Declaration	V
	List of Contents	VI
	List of Tables	X
	List of Figures	XII
	List of Abbreviations	XVI
	Abstract	XVII
	Chapter 1: Introduction	1
1.1	Solar Energy	2
1.2	Semiconductors (SCs)	3
1.2.1	General properties of semiconductors	4
1.2.2	Classification of semiconductors (SCs)	5
1.2.2.1	Intrinsic SCs	5
1.2.2.2	Extrinsic SCs	6
1.2.2.2.1	<i>P</i> -type	7
1.2.2.2.2	<i>N</i> -type	8
1.2.3	Fermi Level (E_F)	9
1.2.4	Popular semiconductors in solar cells	10
1.3	Active technologies for solar energy conversion	11
1.3.1	Photovoltaic Devices (PV)	11
1.3.2	Photo-Electrochemical Cells (PECs)	12
1.3.2.1	Dark current in <i>N</i> -type PEC technique	17
1.3.2.2	Photo current in <i>N</i> -type PEC technique	17
1.4	Thin film technology	18

VII

1.5	Cadmium Sulfide (CdS)	19
1.6	CdS thin film deposition techniques	20
1.6.1	Electrochemical Deposition technique (ECD)	21
1.6.2	Chemical Bath Deposition technique (CBD)	23
1.7	Annealing of CdS semiconductors	25
1.8	Recycling of solar cells (polycrystalline CdS film electrodes)	25
1.9	Objectives	26
1.10	Hypothesis	27
1.11	Novelty of this work	28
	Chapter 2: Experimental Part	30
2.1	Materials	31
2.1.1	Chemicals and Solvents	31
2.1.2	Substrate cleaning	31
2.2	Preparation of CdS films	32
2.2.1	Chemical Bath Deposition (CBD)	32
2.2.2	Electrochemical Deposition (ECD)	33
2.2.3	Combined ECD/CBD	35
2.3	Modification of CdS thin films	36
2.3.1	Annealing process	36
2.3.2	Cooling rate control	37
2.3.2.1	Fast Cooling (Quenching)	37
2.3.2.2	Slow Cooling	38
2.4	Coating with Multi-wall Carbon Nanotube	38
2.5	Recycling of CdS films by recovering the Cd ²⁺ ions	39
2.6	CdS film prepared from recovered Cd ²⁺ ions	40
2.7	Film characterization	41

VIII

2.7.1	Electronic absorption spectra	41
2.7.2	Scanning Electron Microscopy (SEM)	41
2.7.3	X-ray Diffraction (XRD)	41
2.8	PEC experiment	42
2.9	Effect of Redox Couple	43
2.10	Current density vs potential plots	44
2.11	Electrode stability testing	44
	Chapter 3: Results and Discussions	46
3.1	General Remarks	47
3.2	Part 1: Fresh CdS thin film electrodes	48
3.2.1	Electronic absorption spectra	48
3.2.1.1	Effect of deposition time on CBD-CdS thin film spectra	48
3.2.1.2	Effect of deposition cycle on CBD-CdS thin film spectra	51
3.2.1.3	Effect of deposition on ECD/CBD-CdS thin film spectra	53
3.2.1.4	Effect of CdS film preparation method on spectra	55
3.2.1.5	Effect of annealing and cooling rate on CdS thin film electrodes prepared by fourth cycle of deposition by CBD (fresh electrodes)	57
3.2.2	XRD patterns	60
3.2.2.1	CBD-CdS thin film electrodes at fourth cycle of deposition	62
3.2.2.2	Effect of annealing and cooling rate on CdS thin film electrodes	64
3.2.3	SEM micrographs	64
3.2.3.1	SEM images for CBD-CdS thin film electrodes at the fourth cycle of deposition	66

3.2.3.2	Effect of annealing and cooling rate on CdS thin film electrodes	68
3.2.4	PEC studies on fresh CdS thin film electrodes	68
3.2.4.1	Effect of deposition time	70
3.2.4.2	Effect of cycle of deposition	72
3.2.4.3	Effect of different annealing temperature	73
3.2.4.4	Effect of annealing (at 125 °C)	75
3.2.4.5	Effect of deposition method	76
3.3	Effect of Redox Couple on PEC	78
3.4	Part 2: Coated CdS thin film electrodes by multi-wall carbon nano tube (MWCNT)	78
3.4.1	Electronic absorption spectra	80
3.4.2	XRD patterns for coated CdS thin films electrodes	81
3.4.3	SEM micrographs	83
3.4.4	PEC studies for coated and fresh CdS thin film electrodes	85
3.5	Part 3: Recycled CdS thin film electrodes	85
3.5.1	Electronic absorption spectra	85
3.5.2	PEC studies for recycled and fresh CdS thin film electrodes	88
3.6	Stability of the CdS thin film electrodes	90
	Chapter 4: Conclusions	92
	Suggestions for Further Works	93
	References	94
	الملخص	ب

List of Tables

No.	Table	Page
Table (1.1)	Common semiconductor materials used in solar cells	11
Table (1.2)	Different techniques for deposition of CdS	21
Table (2.1)	The parts of the ECD device technique	34
Table (3.1)	Effect of deposition time on energy band gap value for CBD-CdS thin film electrodes	51
Table (3.2)	Effect of the cycle of deposition on energy band gap value for CBD-CdS thin film electrodes	53
Table (3.3)	Effect of deposition time on energy band gap value for ECD/CBD-CdS thin film electrodes	55
Table (3.4)	Effect of the time deposition on energy band gap value for CBD & combined CdS thin film electrodes	56
Table (3.5)	Effect of annealing and cooling rate on energy band gap value for CBD-CdS thin film electrodes	60
Table (3.6)	Crystallite size values from XRD results for CBD-CdS film	61
Table (3.7)	Crystallite size values from XRD results for annealed and fast cooled the CBD-CdS film	63
Table (3.8)	EDX atomic analysis for fourth deposition cycle of CBD-CdS	65
Table (3.9)	EDX atomic analysis for annealed CBD-CdS at 125 °C with fast cooling rate	67
Table (3.10)	Effect of deposition time on PEC characteristics of fresh CBD-CdS thin film electrodes	69
Table (3.11)	Effect of deposition cycle on PEC characteristics of fresh CBD-CdS thin film electrodes	71
Table (3.12)	Effect of different annealing temperature and cooling rate on PEC characteristics of fresh CBD-CdS thin film electrodes	73
Table (3.13)	Effect of annealing and non-annealing on PEC characteristics of fresh CBD-CdS thin film electrodes	74
Table (3.14)	Comparison the PEC characteristics of CdS thin film electrodes prepared by different techniques	76
Table (3.15)	Effect of redox couple on PEC characteristics of fresh CBD-CdS thin film electrodes	77
Table (3.16)	Effect of coated with (MWCNT) on energy band gap value of CBD thin film electrodes, by electronic absorption spectra	80
Table (3.17)	XRD results for coated CBD-CdS thin film	81
Table (3.18)	EDX atomic analysis for coated CBD-CdS	82
Table (3.19)	Comparison the PEC characteristics of coated and fresh CdS thin films electrodes prepared by fourth deposition	84

Table (3.20)	Effect of annealing and cooling rate on energy band gap values of CBD-CdS thin film electrodes (fresh and recycled)	87
Table (3.21)	Effect of annealing and cooling rate on PEC characteristics of fresh and recycled CBD-CdS thin film electrodes	89

List of Figures

No.	Figure	Page
Fig. (1.1)	Energy diagrams of band gap for the three types of materials.	4
Fig. (1.2)	Schematic of thermally excited electron in intrinsic semiconductor.	6
Fig. (1.3)	Portion of the periodic table around (Ga) and (As) (groups III and V). Elements from groups II - VI, can act as dopants.	6
Fig. (1.4)	Classes of extrinsic semiconductors.	7
Fig. (1.5)	Doped semiconductor showing energy levels of (a) <i>n</i> -type doping (b) <i>p</i> -type doping.	9
Fig. (1.6)	Fermi level in intrinsic SC.	10
Fig. (1.7)	Fermi level diagram, a) <i>n</i> -type SC and b) <i>p</i> - type SC.	10
Fig. (1.8)	Energy level diagram for a <i>p-n</i> junction, showing band bending and creation of an electron-hole pair upon absorption of a photon.	12
Fig. (1.9)	The energy schemes for: a) <i>n</i> -type and b) <i>p</i> -type semiconductors in electrolyte solution.	13
Fig. (1.10)	Energy level diagram for a) <i>n</i> - type, and b) <i>p</i> -type SC before and after equilibrium with an electrolyte which is containing redox couple.	14
Fig. (1.11)	Photo voltage formation under illumination. E = electron potential; EC = lower conduction band edge; EV = upper valence band edge; E_F = Fermi level; $E_{Red/Ox}$ = standard redox potentials.	15
Fig. (1.12)	Regenerative cell energy level diagram at a) equilibrium, and b) during illumination	16
Fig. (1.13)	Dark current for <i>n</i> -type SC.	17
Fig. (1.14)	Photo-current generation for <i>n</i> -type SC.	18
Fig. (1.15)	Dark and Photo currents Voltammograms for <i>n</i> -type SC.	18
Fig. (1.16)	The crystal structure of CdS (a) cubic zinc-blend (b) hexagonal (wurtzite)	20
Fig. (2.1)	Experimental setup for solution growth of CdS film through the CBD technique.	32
Fig. (2.1)	Experimental arrangement for CdS film growth.	34
Fig. (2.3)	A schematic showing CdS, ITO/Plastic substrate prepared by combined ECD/CBD technique.	35
Fig. (2.4)	Experimental arrangement for CdS film growth through the ECD/CBD technique.	36
Fig. (2.5)	The annealing system with Pyrex cylinder.	37

XIII

Fig. (2.6)	Photo of fast cooling process for Pyrex cylinder.	38
Fig. (2.7)	Coating process of CdS film with MWCNT.	39
Fig. (2.8)	a) Photo of the immerse process of pre-used CdS films and excess powder in HCl acid b) Photo of remain solution after removing the $H_2S_{(g)}$	40
Fig. (2.9)	Two-electrode photo-electrochemical cell (PEC).	42
Fig. (2.10)	Solar radiation and Halogen spot lamp spectrum.	43
Fig. (3.1)	Electronic absorption spectra measured for prepared CBD-CdS thin films, deposited at different times a) 30 min, b) 60 min, c) 90 min, d) 120 min e) 150 min and f) 180 min (all one cycle)	49
Fig. (3.2)	Tauc Plot from UV-Vis analysis of fresh prepared CBD-CdS thin films, deposited at different times a) 30 min, b) 60 min, c) 90 min, d) 120 min e) 150 min and f) 180 min	50
Fig. (3.3)	Electronic absorption spectra measured for prepared CBD-CdS thin films, deposited in different cycles a) first b) second c) third d) fourth e) fifth and f) sixth cycle.	52
Fig. (3.4)	Tauc Plot of fresh prepared CBD-CdS thin films, deposited in different cycles a) first b) second c) third d) fourth e) fifth and f) sixth cycle.	52
Fig. (3.5)	Electronic absorption spectra for the ECD/CBD of CdS thin films, deposited in different times a) 30 min, b) 60 min, c) 90 min, d) 120 min, e) 150 min and f) 180 min.	54
Fig. (3.6)	Tauc Plot of ECD/CBD-CdS thin films, deposited in different times a) 30 min, b) 60 min, c) 90 min, d) 120 min, e) 150 min and f) 180 min (all one cycle deposition)	54
Fig. (3.7)	Electronic absorption spectra for the CBD & EC/CBD of CdS thin films, deposited at 120 min a) 120 min for CBD and b) 120 min for ECD/CBD (one cycle)	56
Fig. (3.8)	Electronic absorption spectra for annealed CBD-CdS thin films, at different temperature a) after annealing at 100 °C and slowly cooled b) after annealing at 100 °C and quickly cooled c) after annealing at 125 °C and slowly cooled d) after annealing at 125 °C and quickly cooled e) after annealing at 150 °C and slowly cooled f after annealing at 150 °C and quickly cooled	57
Fig. (3.9)	Electronic absorption spectra for a) annealed CBD-	58

	CdS thin film after annealing at 125 °C and slowly cooled, b) after annealing at 125 °C and quickly cooled and c) non-annealed CBD- CdS thin film	
Fig. (3.10)	Tauc Plots from UV-Vis analysis for a) annealed CBD- CdS thin film after annealing at 125 °C and slowly cooled, b) after annealing at 125 °C and quickly cooled and c) non-annealed CBD- CdS thin film	59
Fig. (3.11)	XRD patterns for CBD-CdS at fourth cycle of deposition	61
Fig. (3.12)	XRD patterns for annealing film at 125 °C a) after cooling slowly, b)after cooling quickly	62
Fig. (3.13)	XRD patterns for fast cooling film at 125 °C	63
Fig. (3.14)	SEM surface for CBD-CdS thin film at fourth cycle of deposition	64
Fig. (3.15)	EDX patterns for CBD-CdS thin film at fourth cycle of deposition	65
Fig. (3.16)	SEM surface for CBD-CdS thin film after annealing at 125 °C with fast cooling	66
Fig. (3.17)	EDX patterns for CBD-CdS thin film after annealing at 125 °C with fast cooling	67
Fig. (3.18)	Photo J-V plots for CBD- CdS/ITO/Plastic thin film fresh electrodes, deposited in different times a)30 min, b) 60 min, c) 90 min, d) 120 min, e) 150 min and f) 180 min (all one cycle)	69
Fig. (3.19)	Photo J-V plots for CBD-CdS thin film non-annealed fresh electrodes, effect of deposition cycles a) first, b) second, c) third, d) fourth, e) fifth and f) sixth cycle	71
Fig. (3.20)	Photo J-V plots for CBD-CdS annealed thin film at different temperature a) after annealing at 100 °C and slowly cooled b) after annealing at 100 °C and quickly cooled c) after annealing at 125 °C and slowly cooled d) after annealing at 125 °C and quickly cooled e) after annealing at 150 °C and slowly cooled f after annealing at 150 °C and quickly cooled	72
Fig. (3.21)	Photo J-V plots for a) non-annealed CBD-CdS thin film b) annealed CBD- CdS thin film after annealing at 125 °C and slowly cooled and c) after annealing at 125 °C and quickly cooled	74
Fig. (3.22)	Photo J-V plots for a) ECD/CBD and b) CBD- CdS thin films which deposited for 120 min at first cycle of deposition	75
Fig. (3.23)	Photo J-V plots for fresh CdS thin film, with effect	77

	of redox couple a) Iron and b) poly sulfide redox couples	
Fig. (3.24)	Electronic absorption spectra for a) coated and b) fresh CBD-CdS thin films, deposited in the fourth cycle (120 min)	79
Fig. (3.25)	Tauc Plot from UV-Vis analysis for a) coated and b) fresh CBD-CdS thin films, deposited in the fourth cycle (120 min)	79
Fig. (3.26)	XRD patterns measured for coated CdS thin film	80
Fig. (3.27)	SEM surface for coated CdS thin film	82
Fig. (3.28)	EDX patterns for coated CdS thin film	83
Fig. (3.29)	Photo J-V plots for a) coated CBD-CdS b) fresh CBD-CdS thin films and c) back side of coating electron, which deposited in fourth cycle	84
Fig. (3.30)	Electronic absorption spectra for a) non- annealed fresh electrodes, b) after annealing at 125 °C and quickly cooled fresh, c) after annealing at 125 °C and slowly cooled fresh, d) non-annealed recycled, e) after annealing at 125 °C and slowly cooled recycled, f) after annealing at 125 °C and quickly cooled recycled	86
Fig. (3.31)	Tauc Plot from UV-Vis analysis for a) non- annealed fresh electrodes, b) after annealing at 125 °C and quickly cooled fresh, c) after annealing at 125 °C and slowly cooled fresh, d) non-annealed recycled, e) after annealing at 125 °C and slowly cooled recycled, f) after annealing at 125 °C and quickly cooled recycled	87
Fig. (3.32)	Photo J-V plots for a) non- annealed recycled, b) non-annealed fresh c) after annealing at 125 °C and slowly cooled fresh, d) after annealing at 125 °C and quickly cooled fresh, e) after annealing at 125 °C and slowly cooled recycled, f) after annealing at 125 °C and quickly cooled recycled	88
Fig. (3.33)	Short circuit current density vs. time measured for a) non-annealed fresh, b) non- annealed recycled c) after annealing at 125 °C and quickly cooled recycled, d) after annealing at 125 °C and quickly cooled fresh	91

List of Abbreviations

Symbol	Abbreviations
E_g	Energy band gap
CB	Conduction Band
VB	Valence Band
eV	Electron-Volt
SCs	Semiconductors
PEC	Photo-electrochemical cell
PV	Photovoltaic
E_F	Fermi energy-level
E_C	Conduction band energy
E_V	Valence band energy
E_{Redox}	Redox energy level
SCL	Space Charge Layer
Red	Reductant
Ox	Oxidant
ECD	Electrochemical Deposition
CBD	Chemical Bath Deposition
ECD/CBD	Combined between Electrochemical Deposition and Chemical Bath Deposition
FTO	Fluorine doped Tin Oxide
ITO	Indium doped Tin Oxide
DC	Direct Current
V_{oc}	Open circuit-potential
J_{sc}	Short circuit current density
J-V	Current density potential
η	Conversion Efficiency
FF	Fill Factor
XRD	X-ray Diffraction
SEM	Scanning electron microscope
EDX	Energy-dispersive X-ray spectroscopy

XVII
Recycling of Waste CdS Film Solar Cells by Different Depositions
By
Majd Ibrahim Rashid Sbeah
Supervisor
Prof. Hikmat Hilal
Co-Supervisor
Dr. Ahed Zyoud

Abstract

Nano-sized CdS films were deposited onto ITO/Plastic substrates for the first time by different techniques, namely: electrochemical (ECD), chemical bath (CBD) and electrochemical followed by chemical bath (ECD/CBD) deposition techniques. Scanning electron microscopy (SEM), X-Ray diffraction (XRD), and electronic absorption spectra confirmed the presence of CdS in the films. Photo-electrochemical (PEC) characteristics of different films, such as photo (J-V) plots, conversion efficiency and stability, were all investigated. Method of deposition and treatment affected the CdS film characteristics.

PEC characteristics of different films showed different behaviors. ECD films gave a CdS film that was too thin to be characterized. ECD/CBD films showed lower light-to-electricity conversion efficiency than CBD films. Moreover, the CBD films, which were prepared through the fourth cycle of deposition showed higher values of conversion efficiency and stability than other counterparts. This shows how advantageous the new described films are. Coating the CBD-CdS film with multi-wall carbon nanotube (MWCNT) did not improve its PEC characteristics.

XVIII

The effect of redox couple on the photo J - V plots was measured for fresh CBD- CdS thin film electrodes. The most efficient redox couple was the Poly-Sulfide system, which showed higher efficiency than the iron redox couple. Therefore, the Poly-Sulfide redox couple was used throughout this work.

Due to the hazardous nature of Cd ions, and their negative impact on the environment, this work described how the waste CdS films can be recycled into useful films. Again ITO/Plastic substrates were used for recycling the CdS films using CBD.

The effect of annealing (125 °C), and cooling rate (slow & fast), on fresh CdS film characteristics, such as electronic absorption spectra was studied. Different film PEC characteristics, such as photo (J - V) plots, open-circuit voltage (V_{oc}), short photo-current density (J_{sc}), efficiency and stability, were also studied. Films treated by annealing & fast cooling showed higher conversion efficiency and stability than non-annealed ones. The recycled CdS film showed lower PEC efficiency when annealed 125 °C under N_2 , despite the cooling rate.

Chapter One

Introduction

Chapter one

Introduction

1.1 Solar Energy

Recently, the world is gradually attempting to phase out and replace the use of non-renewable energy sources with renewable energy sources, as renewable energy sources are characterized by being clean, economical, inexpensive, and available at all times.

Renewable energy is very important to help us to develop energy independence and stability. Because of the abundance of solar energy and its excess distribution in nature compared to any other type of renewable energy, it can be considered very necessary.

Solar energy and its technologies are directly related to the sun's endless power and use that energy to produce heat, light, and electricity for household uses and industries.

While fossil fuels play a major role in environmental pollution and increasing global warming, ozone depletion, climate change, and the effects of acid rain; solar energy lowers these environmental problems and reduces toxic emissions to the atmosphere [1, 2].

Sunlight gives plenty of energy. The amount of solar radiation that falls from the sun to the earth is greater total amount of needed energy. Therefore, sunlight reaches the Earth is sufficient to cover all energy

consumption. Moreover, the sun doesn't harm the environment. Solar radiation is mainly visible and near-infrared at the surface of the earth, with a small proportion (~5 percent) in the near-ultraviolet region [3-8].

One of the most important uses of solar energy is electricity generation, especially in remote areas where it is too expensive to extend the electricity. Solar energy benefits can thus be summarized as:

- 1) It is the cleanest energy source with no cost.
- 2) It is an infinite natural energy source.
- 3) It needs cheap distribution networks.

Solar light can be converted to electricity by two methods: photovoltaic (PV) solar cells or photo-electrochemical (PEC) solar cells. These two methods use the sun without creating by-products or hazards of emissions [9-13]. In both methods semiconductor electrodes are needed.

1.2 Semiconductors (SCs)

Materials are classified into three groups: conductors, semiconductors and insulators. The difference in energy between the valence band and the conduction band, which is called an energy gap or band gap (E_g), depends on these properties of solid materials. The three types of materials have different values of E_g : a conductor, where interference between the valence and conduction bands occurs at the E_g is equal to zero, insulator that has E_g above ~4, and semiconductors with E_g between two previous values, Figure (1.1) [14-17].

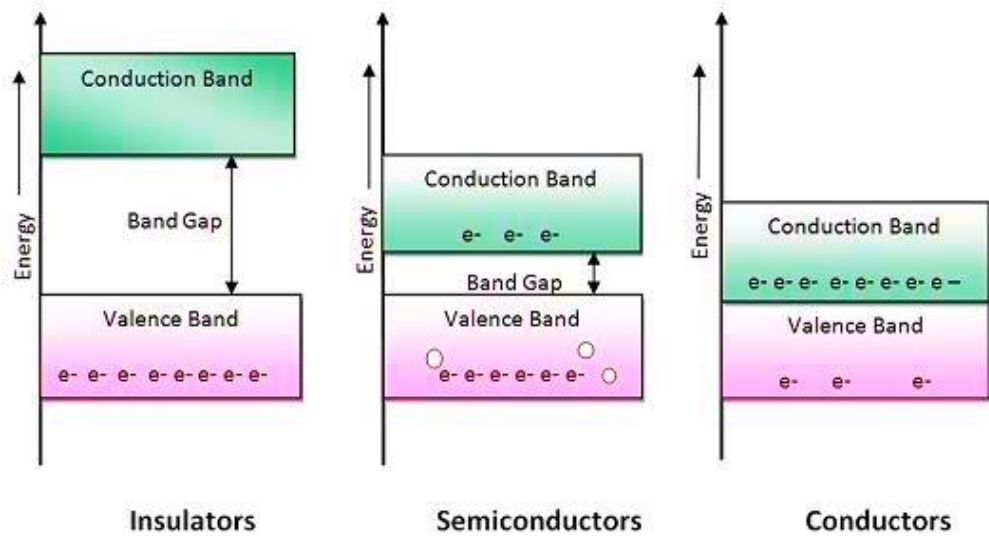


Figure (1.1): Energy diagrams of band gap for the three types of materials[13].

A semiconductor is a material that has an ability to conduct electrical current in between conductors (as copper (Cu), silver (Ag), gold (Au), and aluminum (Al)) and insulators (as rubber, plastics, glass)[15]. Semiconductors are used in many modern devices such as computers, radio, telephone, and recently in solar cells.

Now, large expectations are set in photovoltaic technology to become a major energy supplying technology before 2030 [17-20].

1.2.1 General properties of semiconductors.

Semiconductors are known as materials with conductivity varying from insulators to conductors. The main property can be considered as its band gap energy, where this band gap usually ranges from 1 to 4 eV. In various types, semiconductors are found: pure elements, compounds, and alloys.

The most popular elemental semiconductors are considered to be silicon and germanium, with InSb, InAs, GaP, GaSb, CdS, GaAs, SiC, ... Compound semiconductors, etc., are an example. The structure of the semiconductor is a crystalline structure and called the diamond lattice.

In semiconductors, current is based on either flow of electrons "negatively charged" or flow of holes "positively charged" in the material, but actually in both cases only the electrons move when excited. The electron passes from the valence band to the conduction band to form an "electron-hole pair" and leaves a hole behind in the valence band [21-24].

1.2.2 Classification of semiconductors (SCs).

Semiconductors are mainly classified into two categories: intrinsic and extrinsic.

1.2.2.1 Intrinsic SCs

It is a chemically pure semiconductor, also called an undoped semiconductor, and has a weak conductivity. In this SC, the number of electrons and holes are equals, so it can be formed in pairs at room temperature, Figure (1.2).

The holes in the valence band are created by few electrons which have been thermally excited to the conduction band; hence, these intrinsic semiconductors have limited conductivity only [24, 25].

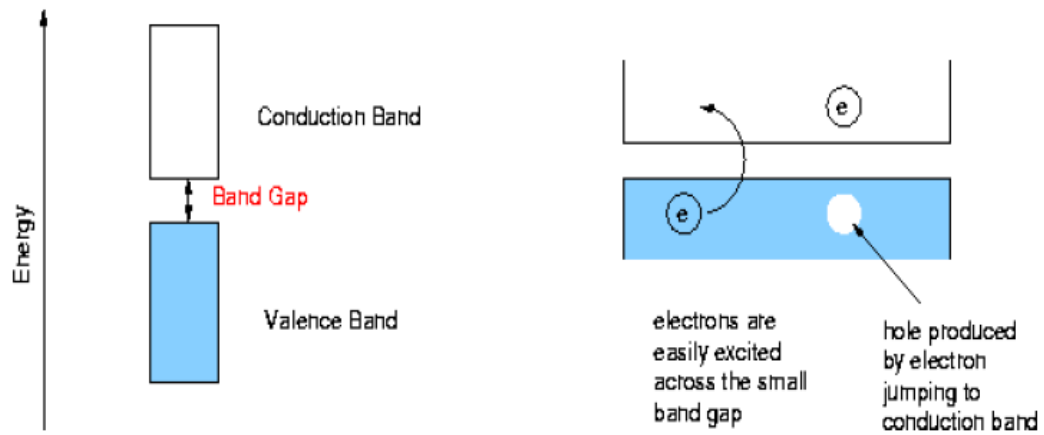


Figure (1.2): schematic of thermally excited electron in intrinsic semiconductor[13].

1.2.2.2 Extrinsic SCs

It is an improved intrinsic semiconductor with a small number of impurities (dopant atoms) Figure (1.3)), which is added by a special process known as doping, to improves the conductivity of the electrical properties of the semiconductor [23, 24].

	13 IIIA 3A	14 IVA 4A	15 VA 5A	16 VIA 6A
	5 B Boron 10.811	6 C Carbon 12.011	7 N Nitrogen 14.0074	8 O Oxygen 15.9994
12 IIB 2B	13 Al Aluminum 26.981539	14 Si Silicon 28.0855	15 P Phosphorus 30.973762	16 S Sulfur 32.065
30 Zn Zinc 65.38	31 Ga Gallium 69.723	32 Ge Germanium 72.64	33 As Arsenic 74.92159	34 Se Selenium 78.96
48 Cd Cadmium 112.411	49 In Indium 114.818	50 Sn Tin 118.71	51 Sb Antimony 121.760	52 Te Tellurium 127.6
80 Hg Mercury 200.59	81 Tl Thallium 204.3833	82 Pb Lead 207.2	83 Bi Bismuth 208.98037	84 Po Polonium [209,9824]

Figure (1.3): Portion of the periodic table around (Ga) and (As) (groups III and V).

Elements from groups II - VI, can act as dopants [22].

The impurities which are added include "extra" electrons or "missing" electrons so that the extrinsic semiconductors can be classified into two types, Figure (1.4):

- 1) *N*-type Semiconductors.
- 2) *P*-type Semiconductors.

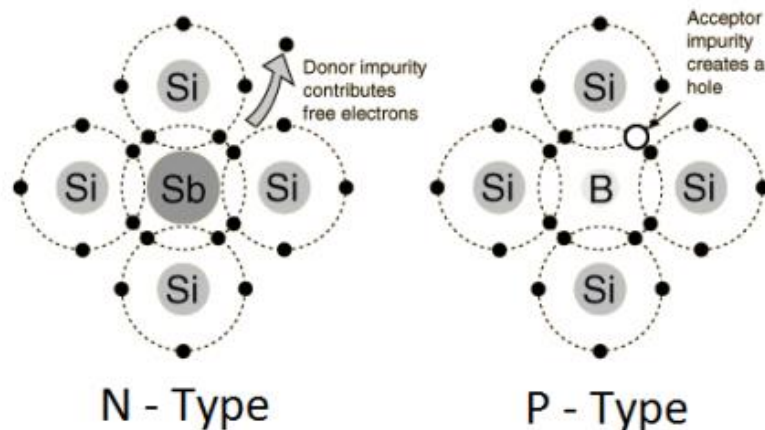


Figure (1.4): classes of extrinsic semiconductors [26].

1.2.2.2.1 *P*- type

This type includes atoms with a hole in their valence shell. For silicon, these dopant atoms act as acceptors. In this type, the more abundant charge carrier is the hole, and the less abundant charge carrier is the electron. This is due to the electrons that jump to the valence shell of the acceptor atoms in the valence band.

Aluminum (Al), gallium (Ga) and Indium (In) are examples of the atoms which can act as *p*- type SC. [22-28].

1.2.2.2.2 *N- type*

In a special atom, only one of the electrons will jump to the conduction band from the valence shell band. These atoms are known as dopant atoms "impurities", and it acts as donor atoms since they have to give an extra electron to the conduction band, because the energy level of this atom is closer to the conduction band (CB) than valence band (VB), thus cause increasing the conductivity of SC.

Antimony (Sb), arsenic (As) and phosphorus (P) are examples of these atoms. When an SC is doped with this dopant it is called *n*-type material.

In contrast, when the dopant energy level lies closer to the valence band (VB), and the atoms are acceptor as in the P-type case, the electrons are transmitted from the valence band to the electron acceptor atom, and leaving an excess positive charge "holes"[22-28]. Figure (1.5) energy levels for both types of semiconductor [29].

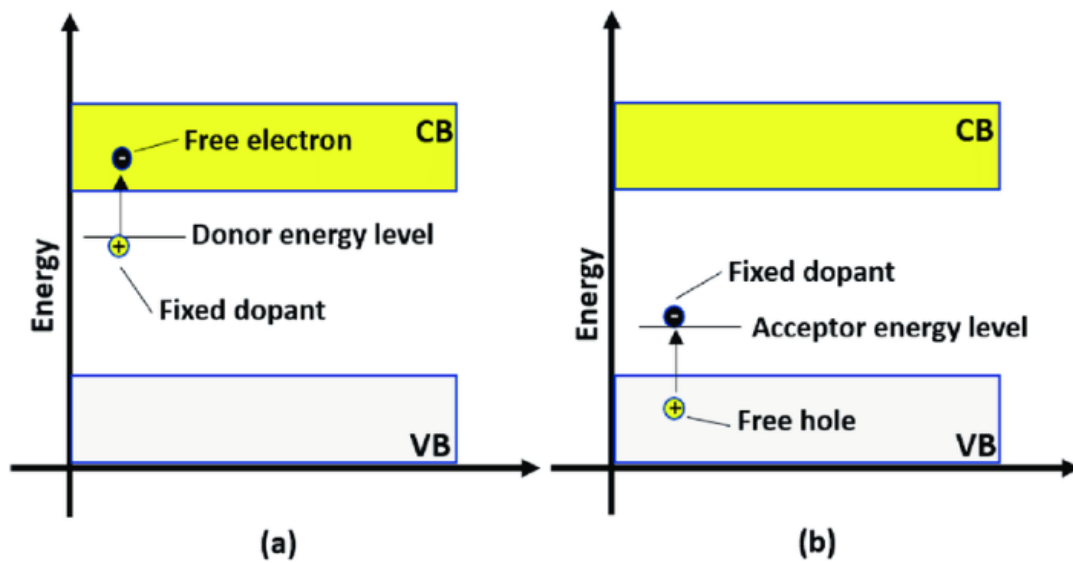


Figure (1.5): Doped semiconductor showing energy levels of (a) *n*-type doping (b) *p*-type doping [29]

1.2.3 Fermi level (E_F)

It is a concept that defines the maximum amount of occupied energy contained at absolute zero temperature (0 kelvins or -273oC) in the material. It is an important parameter for semiconductor electrochemistry since it plays an important role in explaining the action of doped semiconductors [30, 31].

Depending on the kind of SC, the Fermi level has a different location in an SC material. The Fermi level lies roughly in the center of the forbidden energy gap for intrinsic SC, Figure (1.6). But for two extrinsic SC types, the Fermi level shifts upward toward the conduction band for *N*-type SC as shown in Figure (1.7 a), while it shifts downward toward the top of the valence band for *P*-type SC shown in Figure (1.7 b) [31, 32].

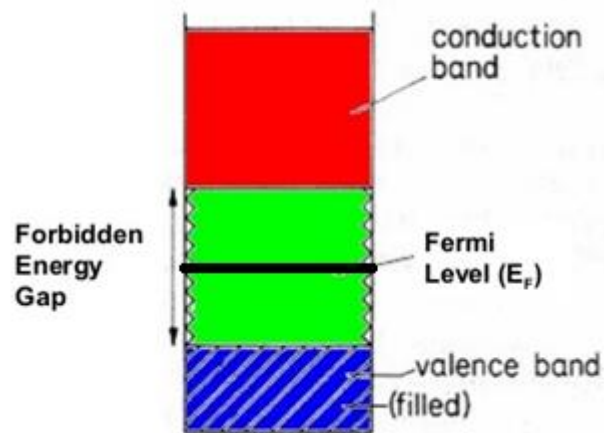


Figure (1.6): Fermi level in intrinsic SC [31].

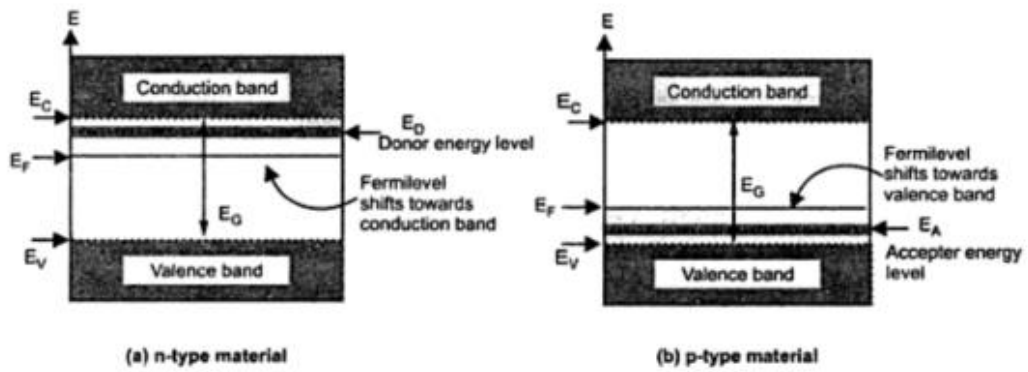


Figure (1.7): Fermi level diagram, a) *N*-type SC, *P*- type SC [32].

1.2.4 Popular semiconductors in solar cells

Solar cells technologies use many semiconductor materials. The most common ones are categorized in sets; Table (1.1) [10].

Table (1.1): Common semiconductor materials used in solar cells:

Class	Example
Elements	Si and Ge
II-VI compounds	CdS, CdTe and CdSe
III-V compounds	GaAs, InP and GaP
Oxides	TiO ₂ , WO ₃ and ZnO
Transition Metal Di- chalcogenides	MoSe ₂ and ZrS ₂
Ternary compounds	CuInS ₂ and CdIn ₂ Se ₄
Zinc phosphides	ZnP ₂

1.3 Active technologies for solar energy conversion.

Solar energy is converted into electricity through two main technologies, Photovoltaic Devices, and Photo-Electrochemical Cells. What distinguishes these two technics is that they use the sun without producing by-products or pollution risks.

1.3.1 Photovoltaic Devices (PV)

PV is important method for the future because it is a low cost, needs no fuel and produces electricity without emissions of greenhouse gases and renewable. On other hand, it has some drawback such as: it operates only in light and needs large areas to work.

It is based on the photovoltaic effect, which is the generation of potential difference, by using semiconductor materials in which a solid–solid junction (*p-n* junction) is used as the active layer [10, 33, 34].

PV cells consist of two or more thin layers of SC, on the first side it is a *p*-type but on the other side, it is *n*-type Figure (1.8).

When this SC absorbs photons, electrons and holes are separated in the electrode. Through the electrostatic force in this electrode, the electrons moving toward the n -type side, in contrast, the holes move toward the p -type side. Therefore, an electric current occurs as long as photons strike the SC cell [35].

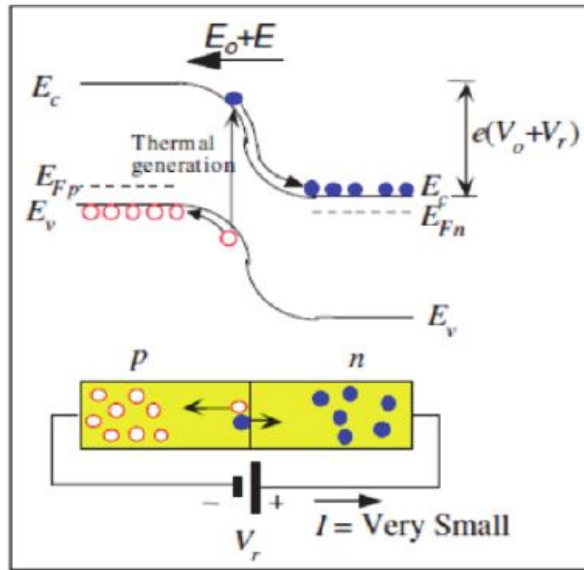


Figure (1.8): Energy level diagram for a p - n junction, showing band bending and creation of an electron-hole pair upon absorption of a photon [36]

1.3.2 Photo-Electrochemical Cells (PECs)

PECs are another technique that uses semiconductor material for converting solar energy into electricity. It is characterized by its high efficiency compared to the PV technique.

It is easy and more economic than PVs, because the electrolyte solution-based technique is low cost and provides large areas for reaction. PEC can also convert light to chemical energy and store it as well [37-40].

In this technique, the semiconductor-electrolyte junction is used instead of solid-state p - n junction in PVs, Figure (1.9)

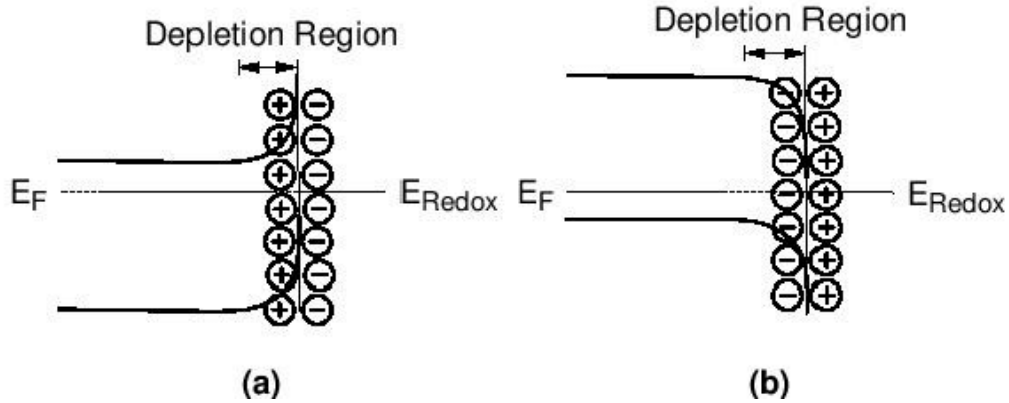


Figure (1.9): The energy schemes for: a) n -type and b) p -type semiconductors in electrolyte solution [38]

In PEC, the SC material that is used needs light at a wavelength that is equal or shorter than the threshold wavelength. Excitation of electrons from the upper valence band to the lowest conduction band is the result of this process, such that excess electrons occur in the conduction band and excess holes in the valence band [10, 38, 40].

As mentioned earlier, PEC cells depend on the formation of the SC-electrolyte junction. When the SC is immersed in an effective electrolyte solution, a depletion layer (the active layer) is formed as a result of the n -type (Figure 1.10 a) or p -type (Figure 1.11 b) SC electrolyte junction.

The Fermi level (E_F) is usually used in SC to determine the chemical potential of electrons. However, the chemical potential of electrons is determined for the electrolyte solution by the redox potential of redox pairs

already present in the electrolyte; these redox potentials are also determined by Fermi's electrolyte level, Figure (1.10)[41].

In *n*-type SC, when the SC material is immersed in an electrolyte solution and before the equilibrium state, the E_F is still above E_{redox} , Figure (1.10 a (1)). Therefore the electrons will flow toward the E_{redox} . After that, the electrons keep going until E_F be lowered and establish the equilibrium state, Figure (1.10 a (2)).

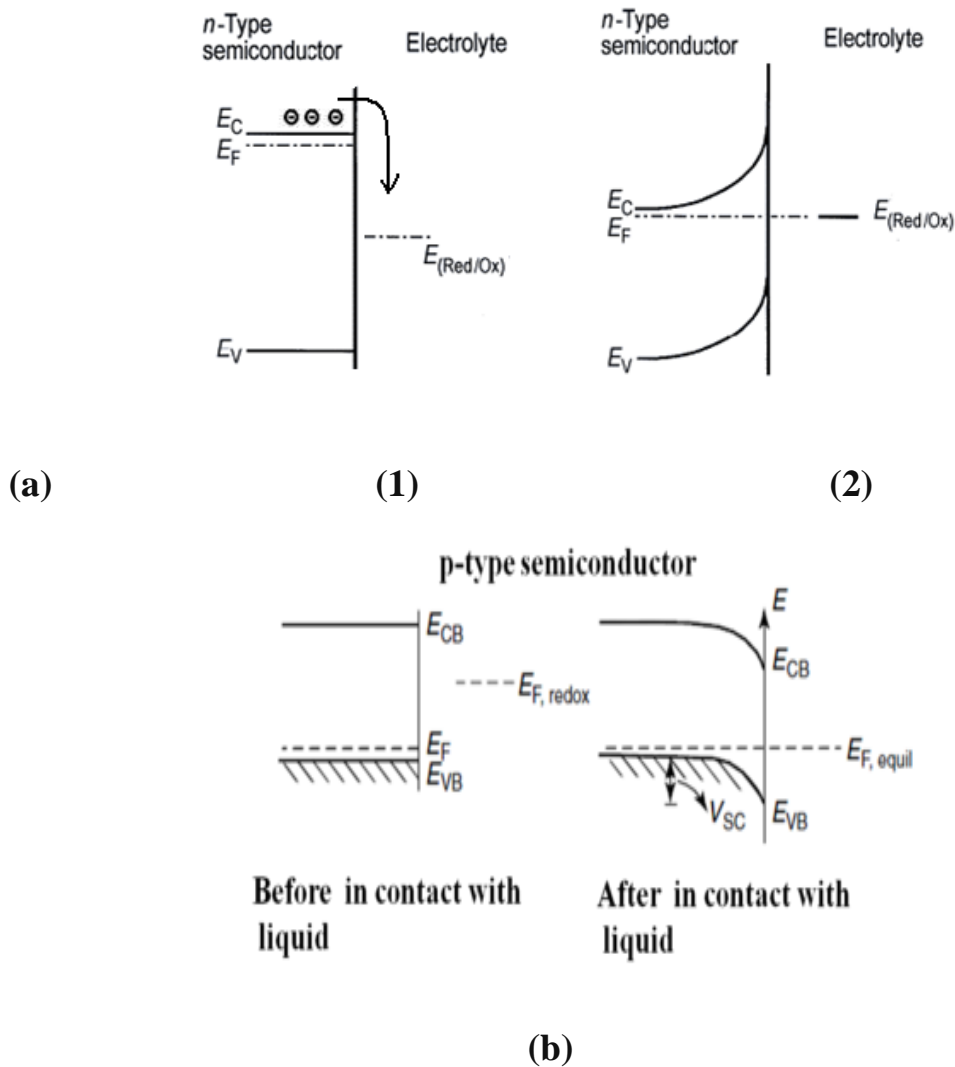


Figure (1.10): Energy level diagram for a) *n*- type, and b) *p*-type SC before and after equilibrium with an electrolyte, redox couple [41].

In the equilibrium state, the positive space charge layer (SCL) is formed in the SC, and an electric field in the depletion layer will result, because of the chemical reduction process of SC. As a result of this process, the edges of the two bands (Valence and Conduction) are bent, and the formation of a potential barrier and no more electrons move towards the electrolyte solution [42].

When the light of energy that exposed by SC is greater than the SC band gap, it will be absorbed within the electrode's SCL. The ($e^- - h^+$) pair will split apart. The holes (minority carriers) move toward the interface. In the contrast, the electrons (majority carriers) move toward the bulk of the n-type SC electrode, Figure (1.11) [43].

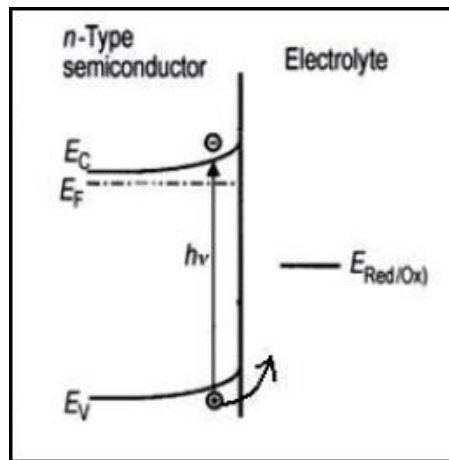


Figure (1.11): Photo voltage formation under illumination. E = electron potential; E_C = lower conduction band edge; E_V = upper valence band edge; E_F = Fermi level; $E_{Red/Ox}$ = standard redox potentials [44].

These types of PECs are regenerative cells, Figure (1.12).

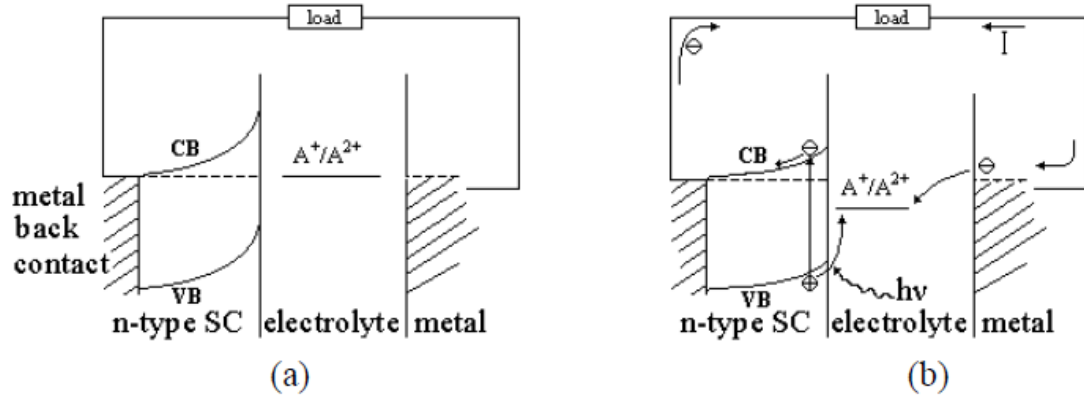
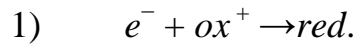
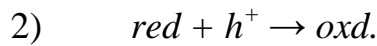


Figure (1.12): Regenerative cell energy level diagram at a) equilibrium, and b) during illumination [10].

At equilibrium state, the both E_F for SC and E_{Redox} potential of the electrolyte are at the same level. But during illumination, the E_F (for both SC and the counter electrode) is upward. As a result, the excited electron for metal moving toward the counter electrode through the external circuit and make a reduction of the redox couple:



To oxidize the reduced species of the same redox couple in the electrolyte solution, holes transfer from the valence band to the SC surface:



The photo-current generated in the external circuit is called short-circuit current (I_{SC}) and can be easily calculated by the value of this current [44].

1.3.2.1 Dark current in *N*-type PEC technique

Dark current occurs in the dark. It occurs by applying negative potential at the *n*-type section, and causes flat bands, Figure (1.13) [44, 45].

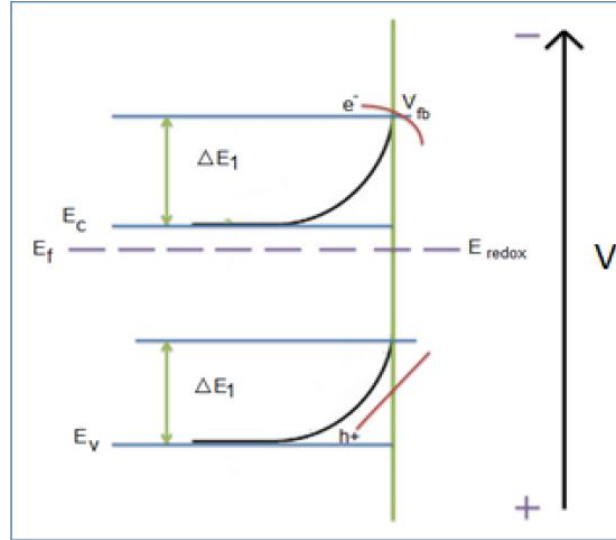


Figure (1.13): Dark current for *n*-type SC [44].

1.3.2.2 Photo current in *N*-type PEC technique

As a consequence of excited electrons and holes, photo current arises after light absorption, while the concentration of the majority carrier (electrons) changes relatively; the concentration of the minority carrier (holes) is enhanced greatly. When these minority carriers dominate the electrode response, the photo-effects are being greater.

This process occurs in the case of band bending only. The excited electrons move to the positive potential. Photocurrent occurs opposite to dark current, Figure (1.14) [44, 45].

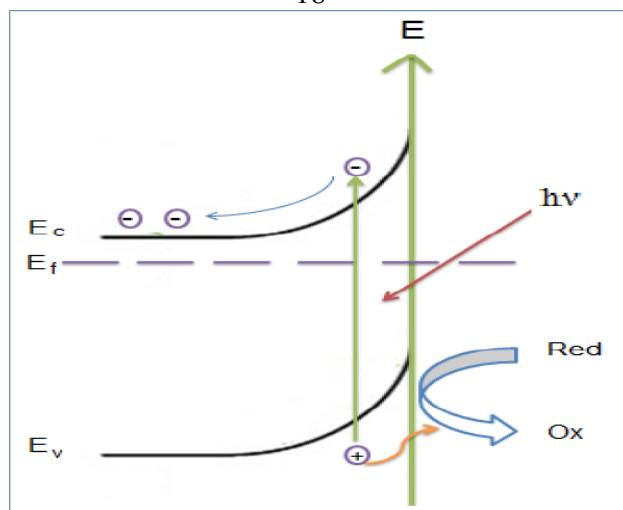


Figure (1.14): Photo-current generation for *n*-type SC [45].

Voltammograms for both currents (Dark and Photo) are shown in figure (1.15).

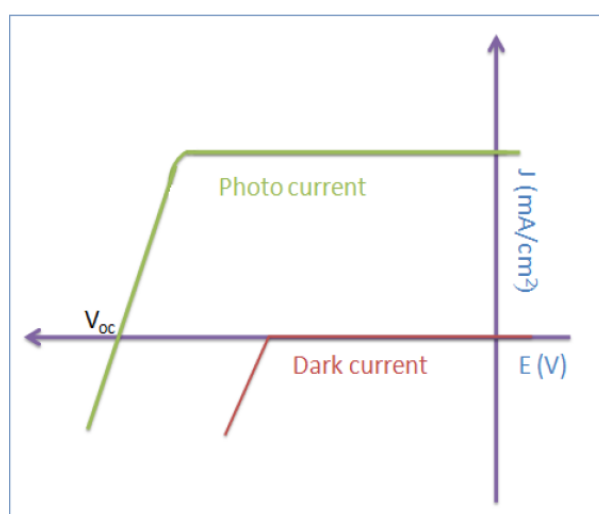


Figure (1.15): Dark and Photo currents voltammograms for *n*-type SC [45]

1.4 Thin film technology.

Thin film technology is a method of thin-film coating that is used for several applications to manufacturing ultra-thin, highly uniform, and

conformal material layers. This technology is widely use in an electronics, sensor industries, optics and solar cells.

These thin films of metal chalcogenides can be deposited onto glass, metal, plastics and other substrates through different techniques, by flash evaporation, vacuum evaporation, electro-deposition, and electroless chemical bath deposition (CBD).

The metal compound films that result from this are also used in photovoltaic cells. Most of the solar thin-film modules have slightly lower efficiencies for conversion but are cheaper to manufacture. Many semiconductors, such as CdS, CdSe, CdTe, CuSe, CuS, ZnS, ZnSe and others, have been used as thin-film electrodes in solar cells [46-49].

1.5 Cadmium Sulfide (CdS).

CdS is a semiconductor characterized by its suitable band gap (~ 2.42 - 3.12 eV). It has important optical properties, high absorption coefficients and it is easy to fabrication for numerous device applications.

The presence of sulfur in this semiconductor is very important, where this sulfur is deficient of the electrons, and possessing the sulfur vacancies with a high electron affinity. Therefore, the CdS will acquire the electrons easily which makes the material as n-type in nature [50, 51].

This CdS exists in two crystalline structures: hexagonal structure (wurtzite), Figure (1.16 a) and cubic structure (zinc blende), Figure (1.16 b).

In both these phases, it is possible to develop CdS films depending on the deposition conditions and techniques [52, 53].

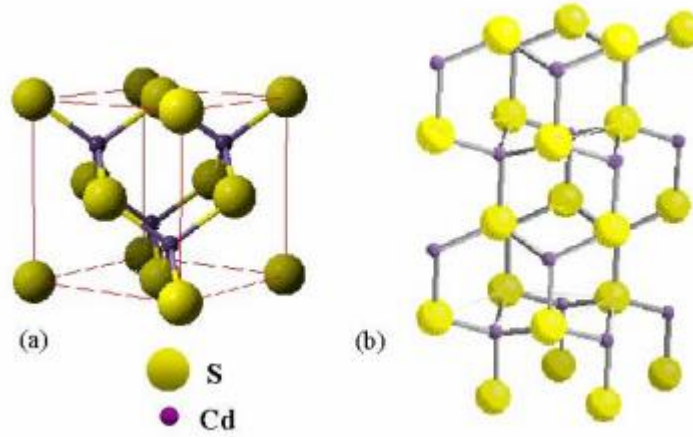


Figure (1.16): The crystal structure of CdS (a) cubic zinc-blend (b) hexagonal (wurtzite) [53].

1.6 CdS thin film deposition techniques.

Several deposition techniques can be used to deposit CdS films. Thin film properties depend on the method of deposition, the rate of deposition, the substrate temperature, and the background pressure. The deposition technique is determined by the application and the properties of the needed film. Different thin film deposition techniques are shown in Table (1.2) [53-55].

Table (1.2): Different techniques for deposition of CdS [53].

<i>CdS deposition techniques</i>
Vacuum evaporation (By resistive heating). Electron beam evaporation (EBE). Flash evaporation. Sputtering. RF sputtering. Chemical bath deposition. Spray pyrolysis. Electrolysis. Close space elimination. Close-spaced sublimation (CSS). Successive ionic layer adsorption & reaction (SILAR). Pulsed laser ablation. Molecular beam epitaxy (MBE). Metal organic chemical vapor deposition (MOCVD). Screen printing.

Chemical Bath Deposition (CBD) and Electro-Chemical Deposition (ECD) techniques are the most popular and cheapest methods for CdS thin film deposition [54].

1.6.1 Electrochemical Deposition technique (ECD)

ECD technique is simple and non-costly. It is one of the most important painting processes where particle size distribution is highly controllable. It is used to coat the film on the cathodic plate electrode by the action of an electric current inside an electrolytic cell.

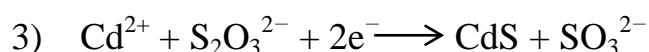
Advantages of ECD technique are [56, 57]:

- Smoothness and uniformity of surface.
- Environmental friendly (lower contamination).

- Good performance of protection against corrosion.
- Ease of utilization and control thickness of paint.
- Greater operating flexibility when compared with a non-electrophoretic coating, through controlling the concentration, pH, and temperature.
- Good contact with substrate.

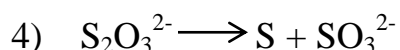
- Growth by ECD technique

Different research was made to describe the mechanism of formation of this CdS thin film from a solution which containing a sulfur atoms, through an ECD [58, 59]. The reaction mechanism of CdS formation is described as follows:

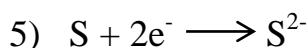


The electro-deposition of CdS layers occurs on the cathode at the proper cathodic applied voltage after the reaction of $\text{S}_2\text{O}_3^{2-}$ ions with Cd^{2+} ions, ECD is dependent on pH.

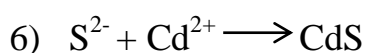
The source of sulfur ions is thiosulphate, this thiosulphate undergoes disproportion reaction, which depending on the pH values, as follows:



When the pH becomes lower, this causes decomposition of $S_2O_3^{2-}$ and forms colloidal sulfur. The sulfur will be reduced to sulfur ions by accepting two electrons as follows [59]:



Then the Cd^{2+} ions react with sulfur ions and precipitate as CdS on the cathodic plate as follows:



1.6.2 Chemical Bath Deposition technique (CBD)

CBD is a process to prepare various compound semiconductor thin films. It is simple, safe, and inexpensive. It is useful to prepare films at very low temperatures (near room), and reproducible large area thin films for solar applications.

To enhance efficiency, CBD can produce SC electrodes that can be deposited by other techniques, such as electrochemical. The deposition parameters, such as temperature, pH, concentrations of reactants (cadmium sulfate and thieourea), the concentration of complexing agents and composition control the stoichiometry and structure of the films [60-62].

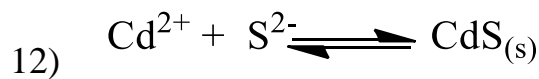
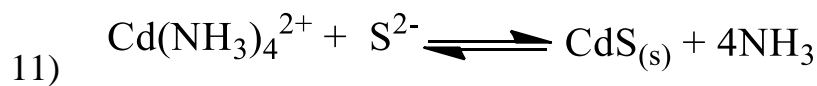
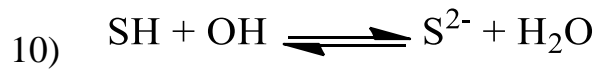
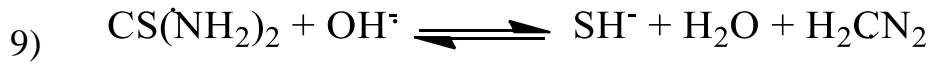
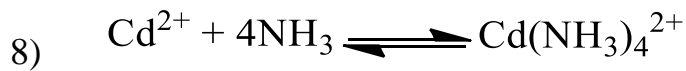
- CdS growth by CBD

Literature shows how the CBD-CdS process is based on control of precipitation of CdS. The CdS is deposited through two types of reactions,

homogeneous (which leads to CdS as colloids), and heterogeneous (where CdS is deposited on the surface of the substrate) [63, 64].

Controlling the concentration of free Cd^{2+} ions is the key parameter for CdS deposition and control of the precipitation process. The ammonia is a suitable compound for this purpose, where it is used as a complexing agent in the reaction to control the undesired homogeneous reaction [61].

Equations (7-12) identify the reaction mechanism of CdS formation: -



As a result, all the previous studies have shown that the resulting CdS thin films are conventionally deposited onto FTO/Glass through the two techniques ECD and CBD. In addition to this, modifications were proposed to enhance film efficiency and stability, depositing ITO/Plastic substrates is another research subject.

1.7 Annealing of CdS Semiconductor

The crystallization process of the semiconductor crystals and the crystal properties are controlled by the annealing of CdS semiconductor surfaces. Where the annealing process helps improves the SC crystals characteristics, such as its quality, homogeneity, and performance by increasing the efficiency of PEC cells.

The benefits of the annealing process are due to that the annealing will increase the grain size, which leads to reduce defects in semiconductor and lower surface roughness. Consequently, the minority carriers will diffuse increasingly to the electrolyte solution in PEC solar cell, and the device sheet resistance will decrease to obtain the space charge region in the active zone [65-69].

1.8 Recycling of solar cell (polycrystalline CdS film electrodes)

After the preparation of thin films of CdS, and using them in photovoltaic cells, it is necessary to clarify the negative environmental effects of cadmium ions. Cd ions are very dangerous and may cause cancer as they are slowly absorbed in the body.

When they are absorbed, they cause bone damage and possibly kidney and lung problems. Therefore it is very necessary to recycle CdS films [70].

In previous research, work was done to recycle cadmium, which was deposited on FTO/glass and prepared by CBD. For recycling of waste of CdS, different techniques were used for recovering residual Cd^{2+} ions.

An example of these techniques is ion exchange, coagulation, chemical precipitation, and others [71, 72]. Therefore, attention is made to recycling CdS films into new films.

In this work, we will prepare fresh CdS thin films, and produce CdS films from recycled in the recovery.

1.9 Objectives

This work aims primarily to prepare a new type of nano-sized CdS film onto Indium Tin Oxide (ITO)/Plastic substrate, this for PEC conversion of light-into-electricity. To achieve this goal, a new preparation technique is proposed here because we look for preparation for an efficient, non-costly and stable nano-film.

The new method involves using a new doping surface for deposition of CdS nanoparticles through the traditional deposition techniques.

The three preparation deposition techniques used are (CBD), (ECD), and the combined ECD/CBD.

The resulting films prepared by different methods will be compared in terms of PEC characteristics, including J-V plots, light-to-electricity conversion efficiency, electrode stability, SEM surface topography, XRD crystal structure, and others. In addition to that, the effect of the number of repetition of the Sedimentation process on the plastic sheet will also be studied. Moreover, recycling of CdS film electrodes into new ones is another objective here.

This is to purify contaminated waters from cadmium ions and to produce useful film materials. The technical objectives of this work are:

- 1) Recycling CdS thin films (used in solar cells).
- 2) Recovering residual Cd^{2+} and S^{2-} ions from waste CdS film electrodes.
- 3) The ITO/plastic substrates and sulfide ions will be recovered.
- 4) Preparing new recycled CdS film electrodes.
- 5) In PEC processes, the recycled CdS film electrodes can be assessed.
- 6) Enhancing the recycled electrode conversion efficiency will also be assessed.

1.10 Hypothesis

As stated previously, because of its sufficient band gap and high absorption coefficients, CdS is one of the significant SC materials used in photovoltaic and PEC solar cells. It is desirable to control the properties of this semiconductor. A major effort is also being made to enhance the PEC characteristics of the CdS film and the potential to recycle it.

The main assumptions of this work are:

1. ECD here gives good contact but thin films.
2. The CBD approach offers extremely thick layers sufficient for light-to-electricity conversion.

3. The EC/CBD technique is expected to give films that have good contact and suitable thickness.
4. The final CdS film, prepared by depositing onto ITO/Plastic is thus expected to give high conversion efficiency and stability.
5. Recycling will help purify water from cadmium ion, which is environmentally friendly.
6. Recycling will help utilize cadmium waste to produce film electrodes useful in electricity production from solar light. This shows economic and environmental value of the project.
7. Flexible property of the plastic film will help make easier and more popular, especially in homes, offices, and parks.

1.11 Novelty of this work

In this work, we suggest a new technique in this work to prepare CdS films. Different techniques, including ECD, CBD, and ECD / CBD techniques are used to prepare polycrystalline CdS thin films.

The films deposited onto ITO / Plastic, In order to obtain the best preparation technique by monitoring various parameters, such as short current density (J_{sc}), open circuit voltage (V_{oc}), efficiency and stability, then the prepared samples were compared with each other. This work includes innovative concepts for the recycling section as:

- Recycling of waste CdS films electrodes will be studied
- The recycled films will be deposited onto FTO/Glass and or ITO/plastic substrates for the first time.
- Recycling deposition will be achieved by ECD, CBD and combined ECD/CBD for the first time.
- Comparative study between recycled and fresh films will be made.

Chapter Two

Experimental Part

Chapter Two

Experimental Part

2.1 Materials

2.1.1 Chemicals and Solvents

Common chemicals such as: $\text{CdCl}_2 \cdot 2\text{H}_2\text{O}$, NH_3 , thieourea ($\text{CS}(\text{NH}_2)_2$), LiClO_4 , Na_2S , NaOH , and elemental sulfur, NH_4Cl , HCl , $\text{Na}_2\text{S}_2\text{O}_3$, Cadmium(II) Acetate Dihydrate ($\text{C}_4\text{H}_{12}\text{CdO}_6$) were purchased from Aldrich, Frutarom or Merck. Common solvents as acetone were purchased from Riedel-DeHaen in pure form. Indium Tin Oxide (ITO) coated PET (polyethylene terephthalate film) (ITO/Plastic) substrates with higher conductivity, were purchased from Sigma-Aldrich. The waste ITO/Plastic substrates were used for recycling.

2.1.2 Substrate cleaning

ITO/Plastic substrates were pre-cleaned before the CdS thin film deposition, in order to obtain uniformity and good adherence for the deposited CdS films in (ECD, CBD, and combined). The cleaning steps of substrates were washing with liquid soap (from Al-Rajeh Company), distilled water, acetone, washing again by using distilled water, and finally, the substrates were dried by leaving in the air to be ready for use.

2.2 Preparation of CdS films.

2.2.1 Chemical Bath Deposition (CBD)

CdS thin films were deposited on ITO/Plastic substrates for the first time using CBD technique. Figure (2.1) shows the experimental setup for preparation.

The chemical bath contained 2.5 ml of stirred deionized water, and the solution of CdCl_2 (2.50 ml, 0.358 M), NH_4Cl (10 ml, 0.60 M), and NH_3 (3 ml, 25% M Extra pure). The bath temperature was set at 75 - 80° C in a constant temperature water bath under constant stirring for 30 min.

Finally, the solution of thiourea (2.50 ml, 0.089 M) was added to the tube of the chemical bath as a source of sulfide ions. The total volume of the chemical bath mixture became 20.5 ml, and the final pH was ~10-10.5 as reported earlier [73].

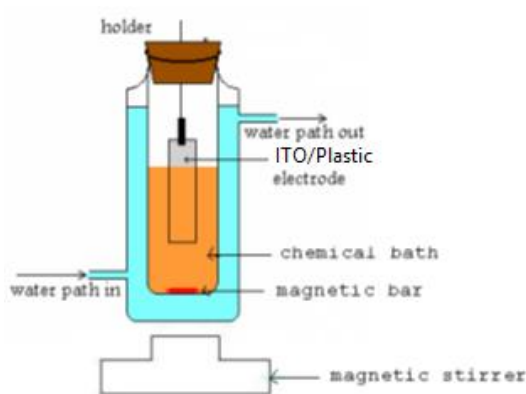


Figure (2.1): Experimental setup for solution growth of CdS film through the CBD technique

The pre-cleaned ITO/Plastic substrates, with dimensions (1x4) cm² were held by a substrate holder. The substrates were immersed in the tube solution partially, and the rubber seal was used in the system for firmly closed.

The minimum deposition time was 30 minutes. During the deposition, the solution color changed gradually, started from pale yellow to yellow and finally to bright orange. After the deposition, the resulted substrate was cleaned with distilled water and dried under atmospheric air.

2.2.2 Electrochemical Deposition (ECD)

For the first time, CdS films were deposited on pre-cleaned ITO / Plastic substrates using ECD. The experimental steps for CdS film preparation via the ECD are shown in figure (2.2).

A solution containing (10 ml of 0.598 M) Cadmium (II) Acetate Dihydrate ($C_4H_{12}CdO_6$), (10 ml of 0.148 M $Na_2S_2O_3$), a small quantity of $LiClO_4$ (approximately 0.741 g), 30 ml of distilled water, and HCl was used to control the value at pH for pH ~ 2.5 In a constant temperature water bath, the solution temperature was held at 90 °C and under constant stirring during deposition [58, 59].

Wires holders holding the platinum plate and the pre-cleaned substrate, with dimensions (1x4) cm² were used. Then the cleaned substrate and plate were partially immersed in the chemical solution. Metal clamps and wiring were isolated by Teflon sealing as in Figure (2.2).

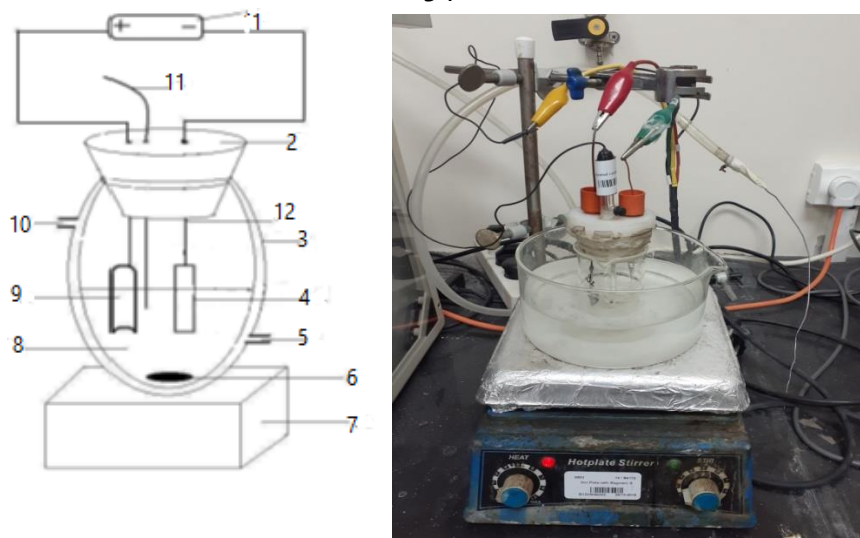


Figure (2.2): Experimental arrangement for CdS film growth

Table (2.1): The parts of the ECD device technique

Number	Name of part
1	Power Supply.
2	Rubber seal.
3	Beaker (60ml).
4	ITO/Plastic substrate.
5	Water input to keep the constant-temperature bath.
6	Magnetic stirrer.
7	Magnetic stirrer plate.
8	Solution containing (water, CdCl_2 , $\text{Na}_2\text{S}_2\text{O}_3$, LiClO_4 , NaOH and HCl).
9	Platinum electrode.
10	Water output to keep the constant -temperature bath.
11	Reference electrode.
12	Substrate holder.

The system was firmly closed. The deposition was carried out by adding a DC (direct current) stripping potential at the best negative potential (-0.9) V to the substrate. It was used in this work unless specified otherwise. Potential control was performed using a Potentiostat C.S model Electrochemical Workstation as described earlier [58].

The substrate was connected to the cathode (working electrode), and the platinum plate to the anode (counter electrode) of the power supply, with reference electrode (Saturated calomel electrode (SCE)).

The resulting substrate wasn't observable the CdS which means that the ECD may give very thin layer only.

2.2.3 Combined ECD/CBD

The CdS films deposited on ITO/Plastic substrates by using the ECD were cleaned with distilled water and then dried in the air atmosphere. After that, as previously stated, the CBD technique was applied over the ECD-CdS film. Figure (2.3) shows the resulting layers of CdS, where the two layers of non-homogeneous CdS films were thus prepared.

Finally, the coated CdS/ITO/Plastic substrates were washed with distilled water after deposition and dried with ambient air.

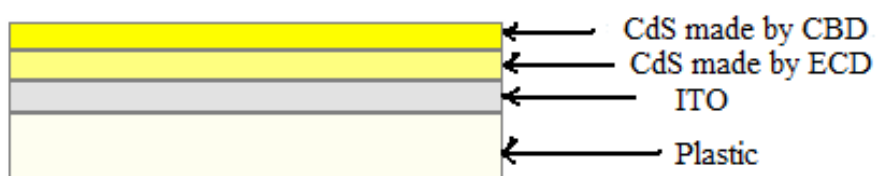


Figure (2.3): A schematic showing CdS, ITO/Plastic substrate prepared by combined EC/CBD

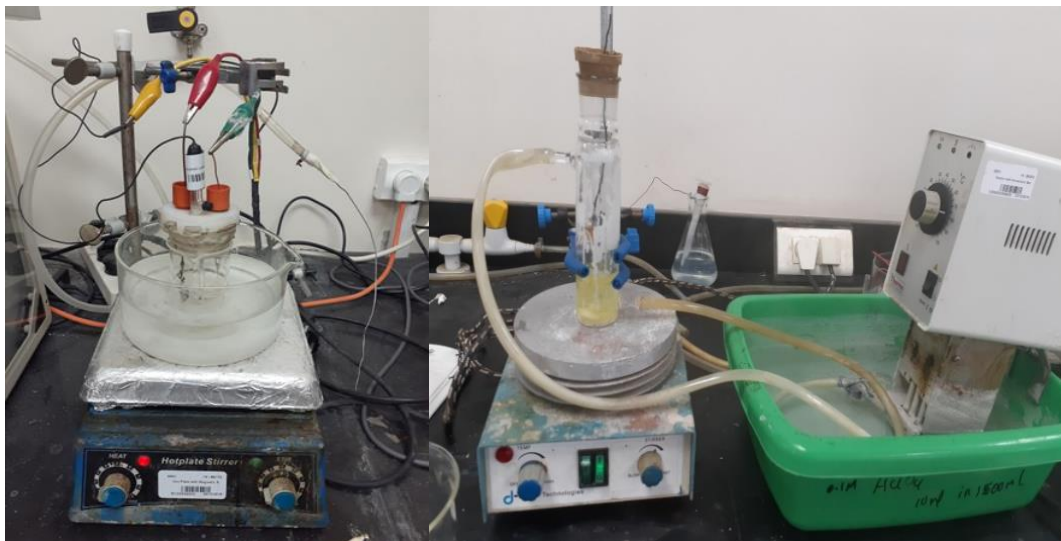


Figure (2.4): Experimental arrangement for CdS film growth through the EC/CBD technique

2.3 Modification of CdS thin films

Different methods were used to modify the prepared thin CdS films, such as annealing temperature, control of cooling rate, and multi-wall carbon nanotube coating of the prepared film (MWCNT).

2.3.1 Annealing Process

A thermostated horizontal tube furnace was used to perform film annealing (Lindberg Hevi-Duty Control Tube Furnace). In a 30 cm long Pyrex cylinder, which was then placed inside the tube furnace for the annealing process, the prepared CdS thin film substrate was inserted.

The temperature of the furnace was raised to the desired temperature (100 °C, 125 °C, 150 °C) under the N₂ atmosphere. Figure (2.5) shows a schematic for the tube furnace used. The annealing process

was continued for 15 minute at the desired temperature under N_2 atmosphere.

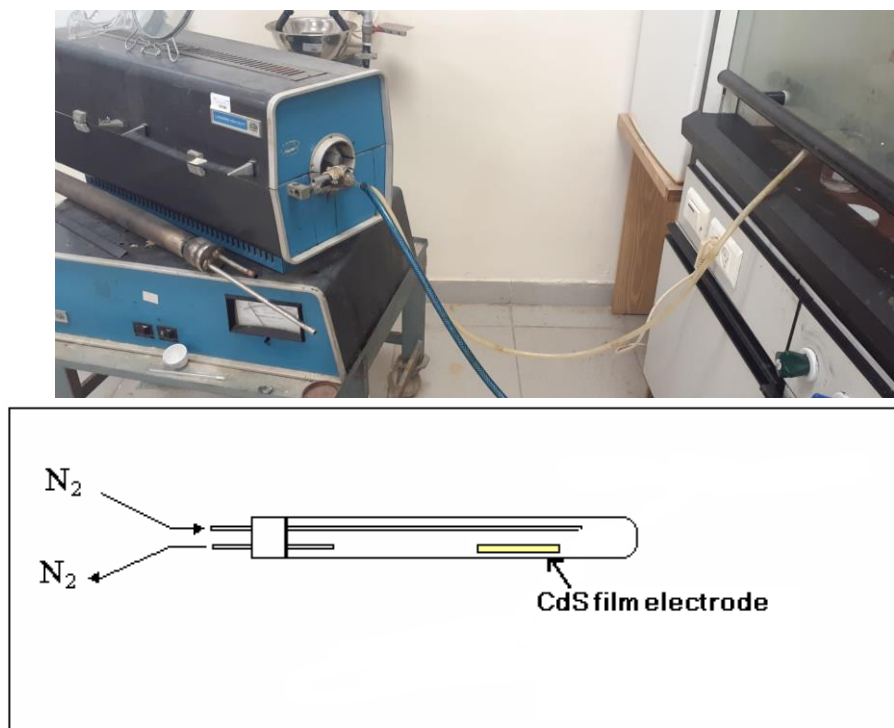


Figure (2.5): The annealing system with Pyrex cylinder

2.3.2 Cooling rate control process

2.3.2.1 Fast Cooling (Quenching)

The films annealed at 125°C for 15 min were cooled quickly. The furnace was shut down and the Pyrex cylinder was removed from the tube furnace (with the CdS thin film) and left to cool under N_2 atmosphere to room temperature for 5 minutes, as in Figure (2.6).



Figure (2.6): Photo of fast cooling process for Pyrex cylinder.

2.3.2.2 Slow Cooling

The film substrates heated at 125°C for 15 min, the furnace was shut down and left with the Pyrex cylinder inside to cool slowly to room temperature under the N_2 atmosphere. With an average cooling rate equal to $2.74^{\circ}\text{C} / \text{min}$, the time for the slow cooling process was around 2 hours or less.

2.4 Coating with Multi-Wall Carbon Nanotube.

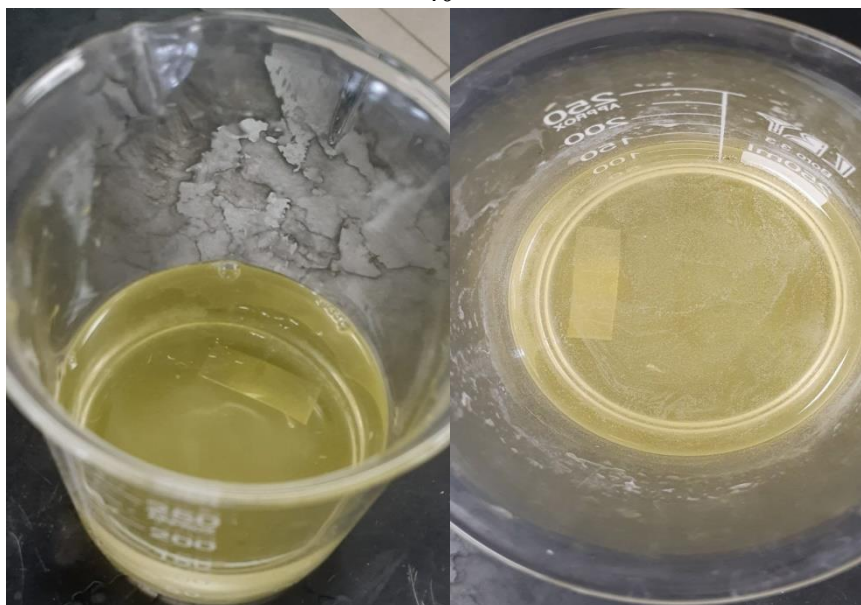
CdS thin films were coated by spraying the Multi-Wall Carbon Nanotube (CdS/MWCNT) through 2 seconds on the film surface. Within ethanol ($\text{C}_2\text{H}_5\text{OH}$), which was permitted to evaporate, the MWCNT was suspended and a thin layer of MWCNT matrices formed on the surface of the CdS thin film, Figure (2.7).



Figure (2.7): Coating process of CdS film with MWCNT

2.5 Recycling of CdS film by recovering the Cd^{2+} ions

After preparing CdS thin films by different technique, they were taken and immersed in 50 ml of 1 M HCl. This concentration of HCl was more suitable and used all the time. The pre-used CdS films and excess powder were immersed in HCl acid for 30 minute. The $\text{H}_2\text{S}_{(\text{g})}$ was transferred to the basic solution through a tube to form the Na_2S solution as shown in Figure (2.8):



a

b

Figure (2.8): a) Photo of the immerse process of pre-used CdS films and excess powder in HCl acid b) Photo of remain solution after removing the $\text{H}_2\text{S}_{(\text{g})}$

2.6 CdS film prepared from recovered Cd^{2+} ions

CBD was used to recycle films. The Cd^{2+} ions which were recovered from the earlier prepared films were used.

Atomic Absorption Spectroscopy (AAS) was subsequently used to determine the concentration of recovered Cd^{2+} ions from the thin films of CdS, which previously prepared [74, 75].

Finally, the solution of Cd^{2+} ions in HCl was transferred to the CBD, neutralized with 5-7 drops of concentrated NaOH basic solution to control the pH value of the solution at ~ 10 . The thiourea solution was added as the source of S^{2-} ions to deposit the CdS again on the cleaned ITO/Plastic.

2.7 Film characterization

2.7.1 Electronic absorption spectra

A Shimadzu UV-1601 spectrophotometer was used to measure the solid-state electronic absorption spectrum for different CdS thin films. ITO/Plastic substrate was used in absorbance measurements as baseline spectra. At 330-800 nm, the wavelength of the incident photons was varied.

2.7.2 Scanning Electron Microscopy (SEM)

The SEM was used to study the surface morphologies of CdS films prepared by different techniques. By means of field emission scanning electron microscopy (FESEM, JEOL JSM-6700F) with an energy dispersive X-ray spectrometer (EDS) instrument for measurement purposes, SEM measurements were kindly carried out on the Jeol-EO Scanning Electronic Microscope at UAE University, Al-Ain, and UAE.

2.7.3 X-ray Diffraction (XRD)

The X-ray diffraction technique was used to provide details on the crystallographic structure and chemical composition of CdS thin films prepared using different techniques.

In the laboratories of the United Arab Emirates University (UAEU), Al-Ain University, XRD measurements of this work were performed using an Analytical X'Pert PRO X-ray diffractometer (XRD), with CuK α ($\lambda =$

1.5418 Å) as the source. By comparing the measured diffraction patterns to JCPDS data-base cards, the XRD lines were established.

2.8 PEC experiment

The PEC cell involved two-electrodes; platinum counter electrode connected with and reference electrode, Figure (2.9). The prepared CdS thin film electrode was used as a working electrode into this PEC.

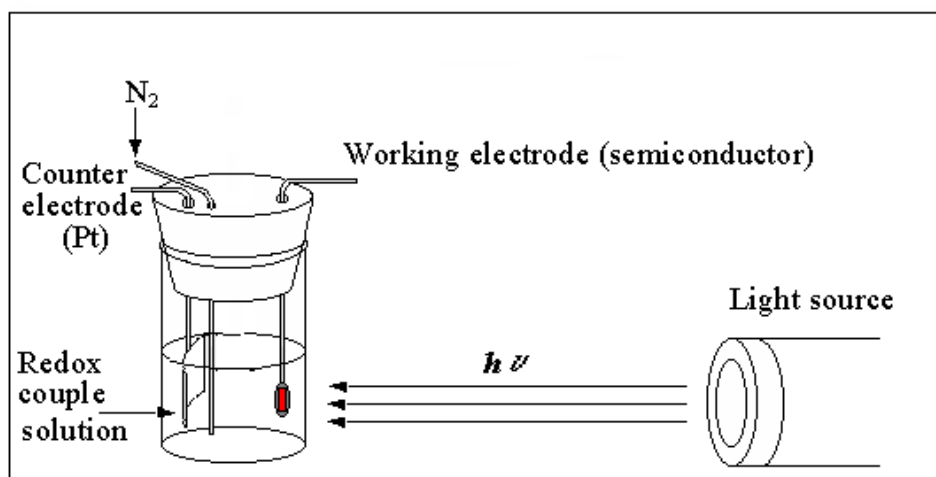


Figure (2.9): Two-electrode photo-electrochemical cell (PEC)

For preparation of the redox couple in this experiment, the Polysulfide $NaOH/S^{2-}/S_x^{2-}$ system was used with (0.1 M S, 0.1 M NaOH, 0.1M Na_2S). High purity N_2 gas (99.99999%) was bubbled through the solution for 5 minutes before each experiment, and to minimize air contamination, it was kept to flow above the solution during the experiment.

The solution was stirred at the beginning, and then stopped as the PEC experiment started, at temperature about 22-25 C° through work.

The 50 watt solar simulator halogen spot lamp was used as a source of light. The lamp was located at a given distance (57 cm) from the working electrode. As shown in figure (2.10), the halogen spot lamp spectrum was equivalent to the solar light spectrum. The LX-102 Light-meter measured the illumination intensity on the electrode and was ~ 59000 lux (equivalent to 0.0086 W.cm⁻²).

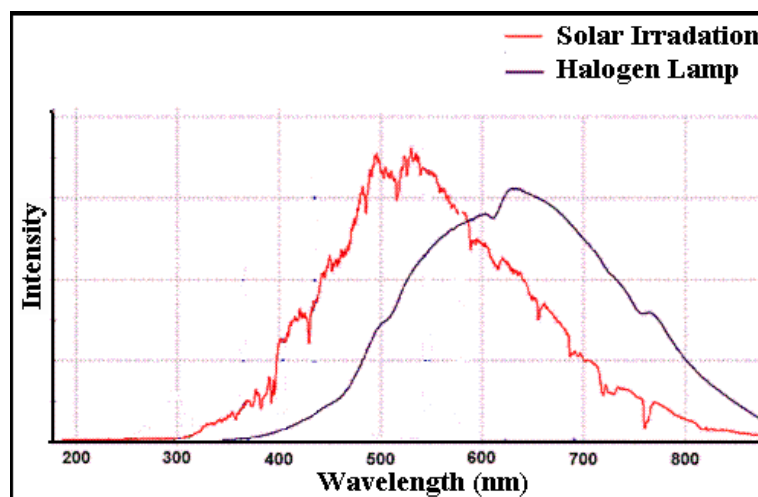


Figure (2.10): Solar radiation and Halogen spot lamp spectrum

2.9 Effect of Redox Couple

As mentioned earlier, where the Polysulfide NaOH/S⁻²/S_x²⁻ system was used as a redox couple in PEC which with (0.10 M NaOH, 0.10 M S, and 0.10 M Na₂S). Another redox couple with K₃Fe (CN)₆/K₄Fe (CN)₆/LiClO₄ solution was with (0.10 M K₃Fe (CN)₆, 0.10 M K₄Fe (CN)₆, and 0.10 M LiClO₄).

In this work, the Polysulfide $\text{NaOH/S}^{2-}/\text{S}_x^{2-}$ redox couple is more effective in measuring and finding the current than $\text{K}_3\text{Fe}(\text{CN}_6)/\text{K}_4\text{Fe}(\text{CN}_6)/\text{LiClO}_4$.

2.10 Current density vs potential plots

Current vs. voltage (J - V) plots were measured by using a computer-controlled CorrTest Electrochemical Workstation CS350 Potentiostat/Galvanostat. The measured electric current (I) was converted into current density (J), by dividing the measured electric current into the area of the illuminated electrode (A).

The photo-current experiments were carried out to measuring photo J - V characteristics by using the 50 Watt halogen spot lamp.

Experimental setup mentioned above (Figure 2.9) was used at room temperature under N_2 atmosphere, and the Polysulfide $\text{NaOH/S}^{2-}/\text{S}_x^{2-}$ system as a redox couple, unless otherwise stated. In order to obtain the best preparation technique, different types of films were compared with each other by monitoring different J_{sc} , V_{oc} , and conversion efficiency parameters from picture (J - V) plots.

2.11 Electrode stability testing

The electrode stability was tested under the same PEC conditions described above. At 0.00V potential (Calomel electrode), the illumination on the electrode was (0.0086 W.cm^{-2}). Short circuit current (I_{sc}) values were calculated vs. time at 7200 sec. The current density (J_{sc}) value was

determined by dividing the current (I_{sc}) value by the electrode region immersed in the solution of the redox pair. All measurements were made using Poly sulfide ($\text{NaOH}/\text{S}^{2-}/\text{Sx}^{2-}$ system Na_2S (0.1M), NaOH (0.1 M), S (0.1 M)) as a redox couple at room temperature, under the nitrogen atmosphere.

Chapter Three

Results and Discussions

Chapter Three

Results and Discussions

3.1 General Remarks

Thin films of CdS Nano-sized were deposited onto ITO/Plastic substrates by different techniques, namely: ECD, CBD and combined EC/CBD techniques. Moreover, different parameters were controlled to study the effects of annealing (at 125 °C under N₂ atmosphere), cooling rate (fast or slow cooling), deposition time and the deposition cycles (30 minutes each cycle) on film characteristics. Wide and suitable electrode was prepared under certain conditions; then it was divided and annealed at different temperatures.

We studied all film electrode PEC efficiencies and stabilities. Recycling for the CdS electrode was another purpose. For different films, the effects of deposition time, redox couple, the cycle of deposition, an annealing process, cooling rate, and coating with multiwall carbon nanotube coating were all studied. Characteristics as XRD, SEM, electronic absorption spectra, and PEC characteristics were all investigated for different prepared films.

3.2 Part 1:

Fresh CdS thin film electrodes

Different characteristics for prepared CdS thin-film electrodes, such as Electronic absorption, Photo-current, XRD, and SEM spectra are shown below:

3.2.1 Electronic absorption spectra

3.2.1.1 Effect of deposition time on CBD-CdS thin Film Electrodes

For ECD-CdS film, the resulted films weren't observable, which means that the ECD may give a very thin layer only. Therefore, its characteristics couldn't be investigated.

The effect of deposition time on the fresh prepared CBD- CdS thin films electronic absorption spectra was studied. Electronic absorption spectra were calculated for the new CBD- CdS thin films, which preparing at different times (30, 60, 90, 120, 150 and 180 min), Figure (3.1).

To determine the energy band gap, Figure (3.2). The Tauc method was used by using optical absorbance data plotted with respect to energy. This is explained in the relation $(\alpha h\nu) = A (h\nu - E_{bg})^n$, where $h\nu$ is an energy of the incident radiation, α is the absorption coefficient, E_{bg} is the energy band-gap energy, A is a constant which is based on effective masses of electrons and holes, and n can take values of 0.5 and 2, for direct or indirect band gap transitions [76]. The results are summarized in Table (3.1).

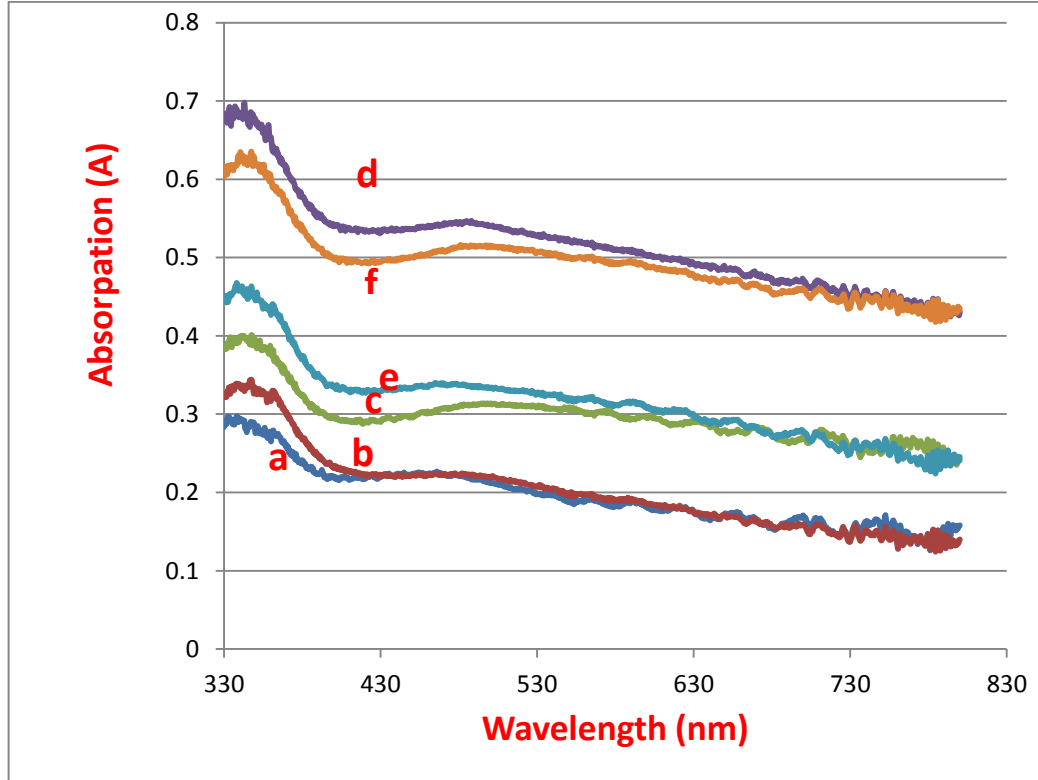


Figure (3.1): Electronic absorption spectra measured for prepared CBD-CdS thin films, deposited at different times a) 30 min, b) 60 min, c) 90 min, d) 120 min e) 150 min and f) 180 min (all one cycle)

The Figure (3.1) shows that the prepared films at 120 min exhibit slightly clearer absorption than the other ones, where this film has a thickness about 0.002 mm.

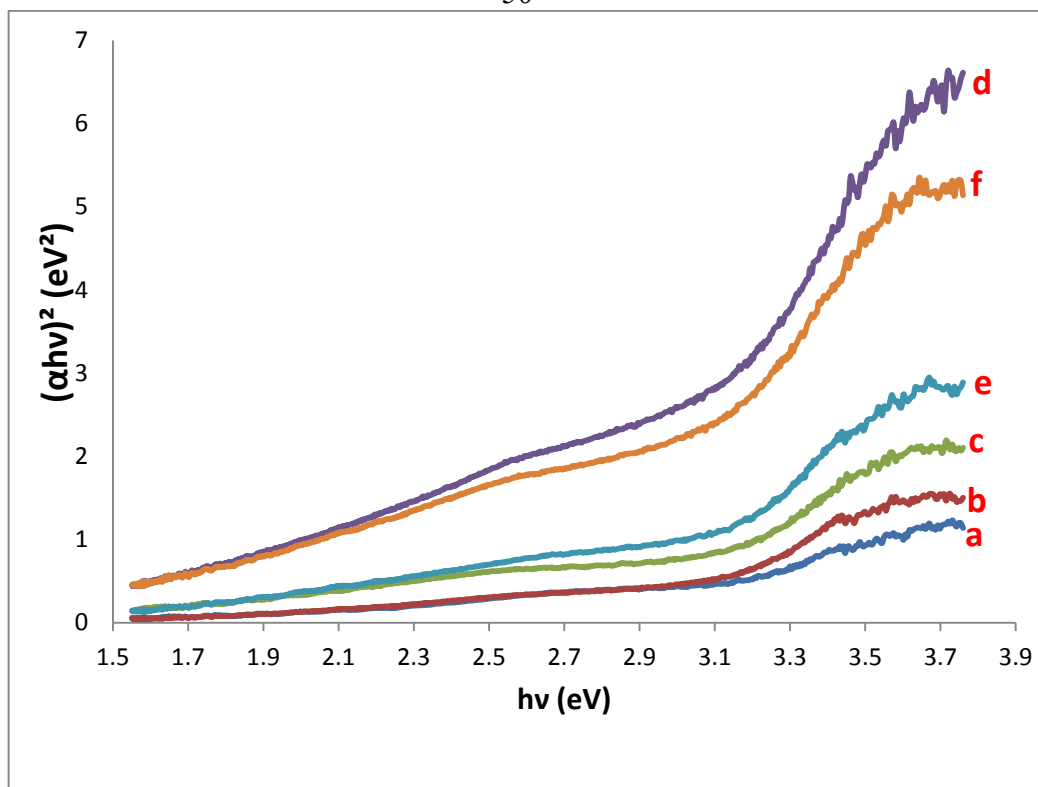


Figure (3.2): Tauc Plot from UV-Vis analysis of fresh prepared CBD-CdS thin films, deposited at different times a) 30 min, b) 60 min, c) 90 min, d) 120 min e) 150 min and f) 180 min

The Tauc method was used to determine the energy band gaps for the films, as described above, in Figure (3.2). Table (3.1) shows that prepared films at different times gave very close values of the energy band gap. The best deposition time is 120 min, which gives a value similar to literature [17]. It can be said from the results, that when the particle size increases, its energy band gap value decreases. This is consistent with literature [77].

Table (3.1): Effect of deposition time on energy band gap value for CBD-CdS thin film electrodes

Sample number	Deposition time	Energy band gap(eV)
1	30 min	~2.90
2	60 min	~2.90
3	90 min	~2.89
4	120 min	~2.91
5	150 min	~2.89
6	180 min	~2.88

3.2.1.2 Effect of deposition cycle on CBD-CdS thin film spectra.

The effects of the cycle of deposition (at 30 min) on the prepared CdS thin film electronic absorption spectra were studied. In this part, the time was fixed and we changed the cycle number of deposition of CdS on the ITO/Plastic films were studied. Primary deposition at (30 min) was started until sixth deposition (single deposition, double, triple, fourth, fifth, sixth deposition). For these CdS thin films, the electronic absorption spectra, Figure (3.3), were measured.

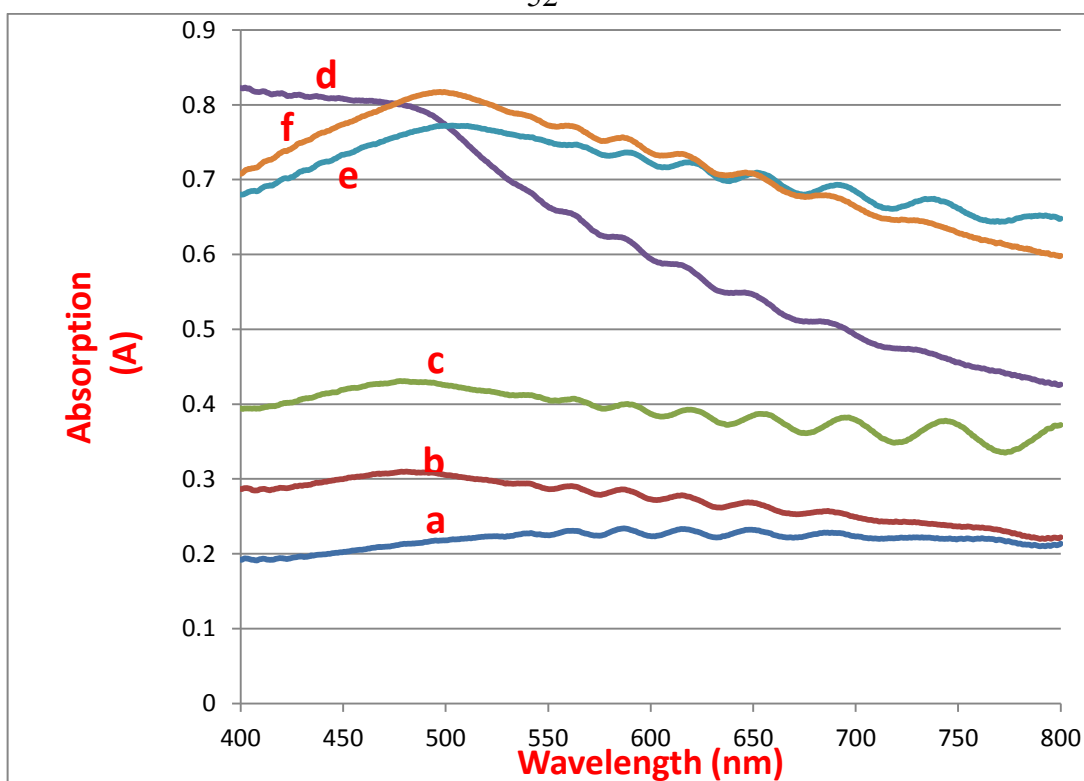


Figure (3.3): Electronic absorption spectra measured for prepared CBD-CdS thin films, deposited in different cycles a) single b) double c) triple d) fourth e) fifth and f) sixth cycle.

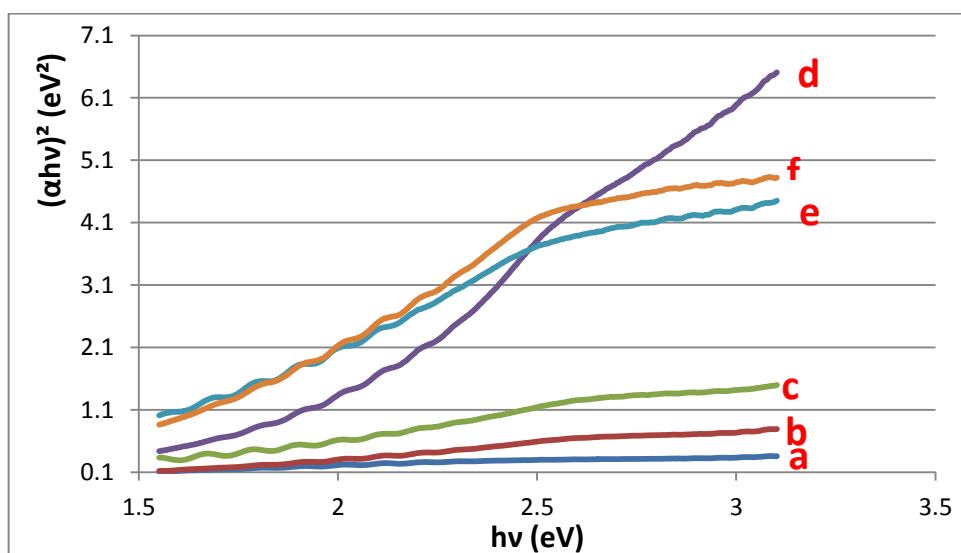


Figure (3.4): Tauc Plot of fresh prepared CBD-CdS thin films, deposited in different cycles a) first b) second c) third d) fourth e) fifth and f) sixth cycle.

Figure (3.3) shows that the prepared films at 30 min for fourth deposition (120 min) exhibit clearer absorption than the other ones, and its thickness nearly 0.003 ml.

The Tauc method was used to determine the energy band gap for thin films, as described above in Figure (3.4). Table (3.2) showed that the prepared films for fourth deposition gave energy band gap close to literature [50]. The results of the Figure are summarized in Table (3.2).

Table (3.2): Effect of the cycle of deposition on energy band gap value for CBD-CdS thin film electrodes

Sample number	Cycle of Deposition	Energy band gap(eV)
1	First	~1.9
2	Second	~1.8
3	Third	~1.7
4	Fourth	~2.0
5	Fifth	~1.5
6	Sixth	~1.6

3.2.1.3 Effect of deposition time on ECD/CBD -CdS thin film spectra

The electronic absorption spectra for the CdS thin films prepared by combined ECD/CBD at different times (30, 60, 90, 120, 15 and 180 min) were investigated, Figure (3.5).

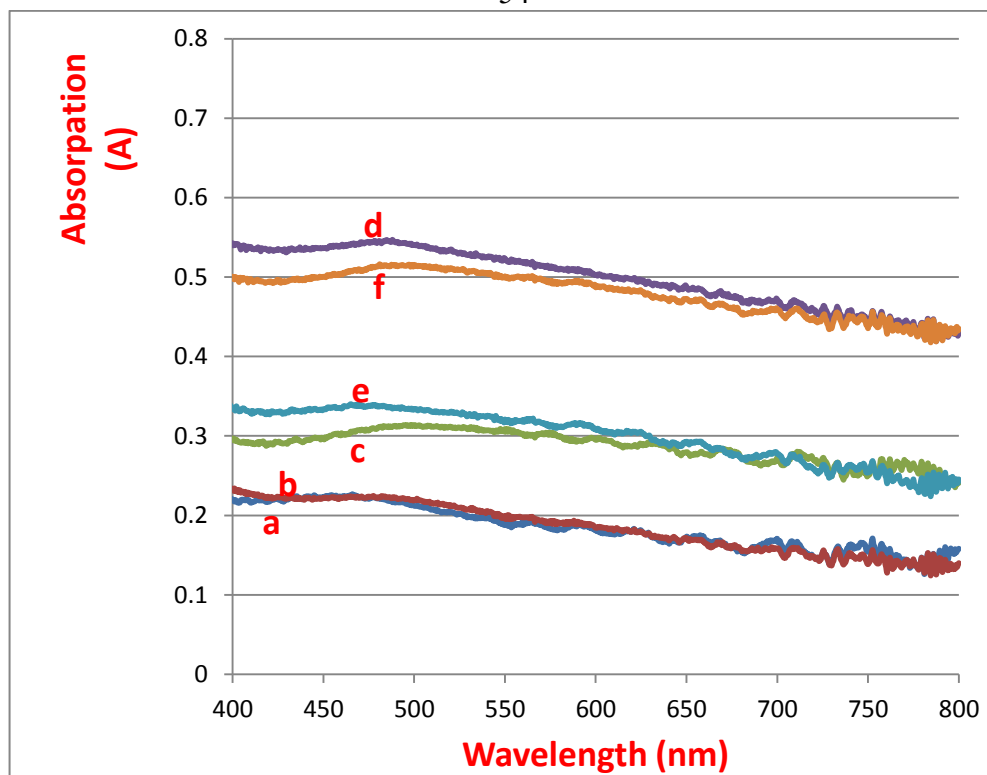


Figure (3.5): Electronic absorption spectra for the ECD/CBD of CdS thin films, deposited in different times a) 30 min, b) 60 min, c) 90 min, d) 120 min, e) 150 min and f) 180 min.

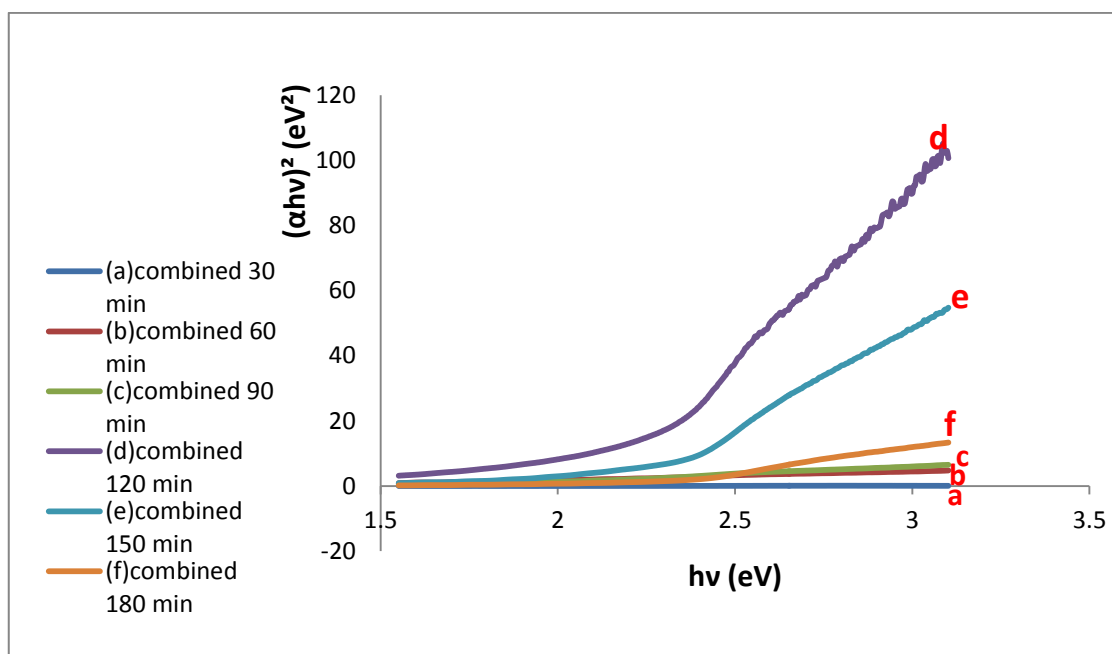


Figure (3.6): Tauc Plot of ECD/CBD-CdS thin films, deposited in different times a) 30 min, b) 60 min, c) 90 min, d) 120 min, e) 150 min and f) 180 min (all one cycle deposition)

The Figure shows that different absorption edge values were present in the prepared films, with band gap values in the range of (2.29-2.6 eV). The energy of the band gap influences the semiconductors' light absorption characteristics.

The Tauc method was used to determine the energy band gap for thin films, Figure (3.6). Table (3.3) shows that the prepared films at different time gave energy band gap that resembles literature [50]. It can be said from the results, that when the particle size becomes increase, its energy band gap value will decrease.

Table (3.3): Effect of deposition time on energy band gap value for ECD/CBD-CdS thin film electrodes

Sample number	Deposition time	Energy band gap(eV)
1	30 min	~2.60
2	60 min	~2.53
3	90 min	~2.50
4	120 min	~2.35
5	150 min	~2.40
6	180 min	~2.45

3.2.1.4 Effect of CdS film preparation method on spectra

Electronic absorption spectra have been investigated for CdS thin films prepared by different techniques (CBD and ECD / CBD), Figure (3.7). The prepared films show different absorption edges, with band gap

values in the range of 2.00-3.2 eV. The best time for the prepared film by the two different techniques was 2 hr. Table (3.4) shows that the combined ECD/CBD films had better spectra than the CBD films.

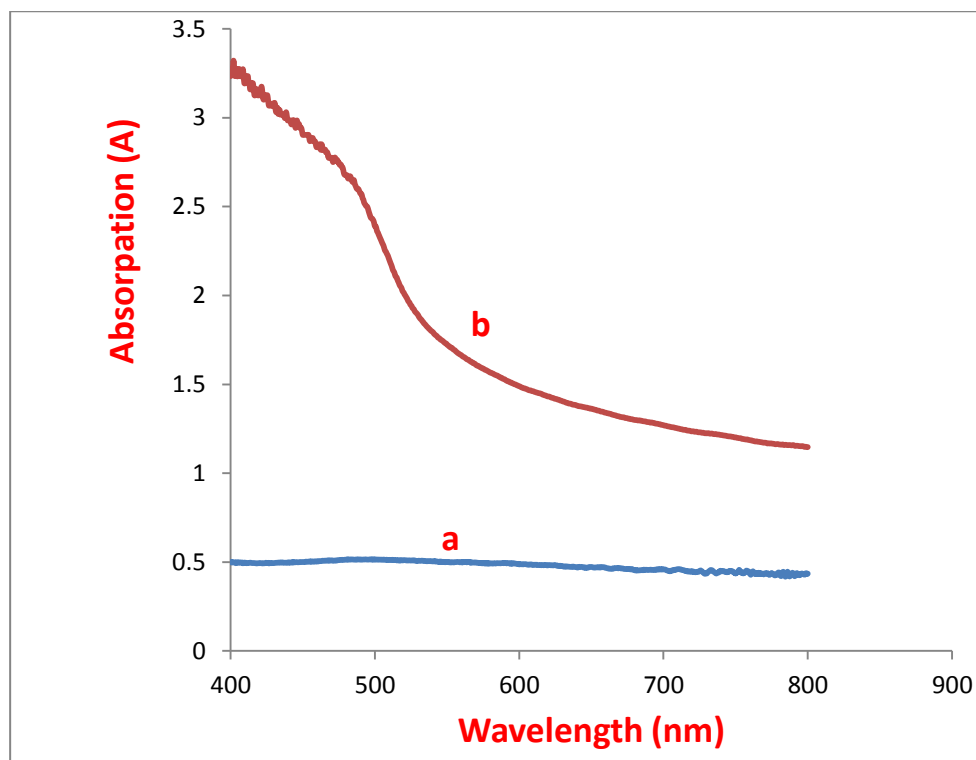


Figure (3.7): Electronic absorption spectra for the CBD & EC/CBD of CdS thin films, deposited at 120 min a) 120 min for CBD and b) 120 min for ECD/CBD (one cycle)

Table (3.4): Effect of the time of deposition on energy band gap value for CBD & combined CdS thin film electrodes

Type	Deposition time	Energy band gap(eV)
CBD	120min	~2.30
Combined	120min	~2.35

3.2.1.5 Effect of annealing and cooling rate on CdS thin film electrodes prepared by fourth cycle of deposition by CBD (fresh electrodes)

Electronic absorption spectra were measured for annealed fresh CdS thin films, which was prepared through fourth cycle deposition at different temperatures (100, 125 and 150 °C), as shown in Figure (3.8). Then, the best-annealed one at 125 °C under N₂ for 15 min, which showed a higher absorptivity was compared with a non-annealed fresh CdS thin film. Moreover, the effects of cooling rate (fast and slow cooling) on the electronic absorption spectra were investigated for the pre-annealed CBD-CdS thin film electrodes at 125 °C under nitrogen for 15 min, Figure (3.9).

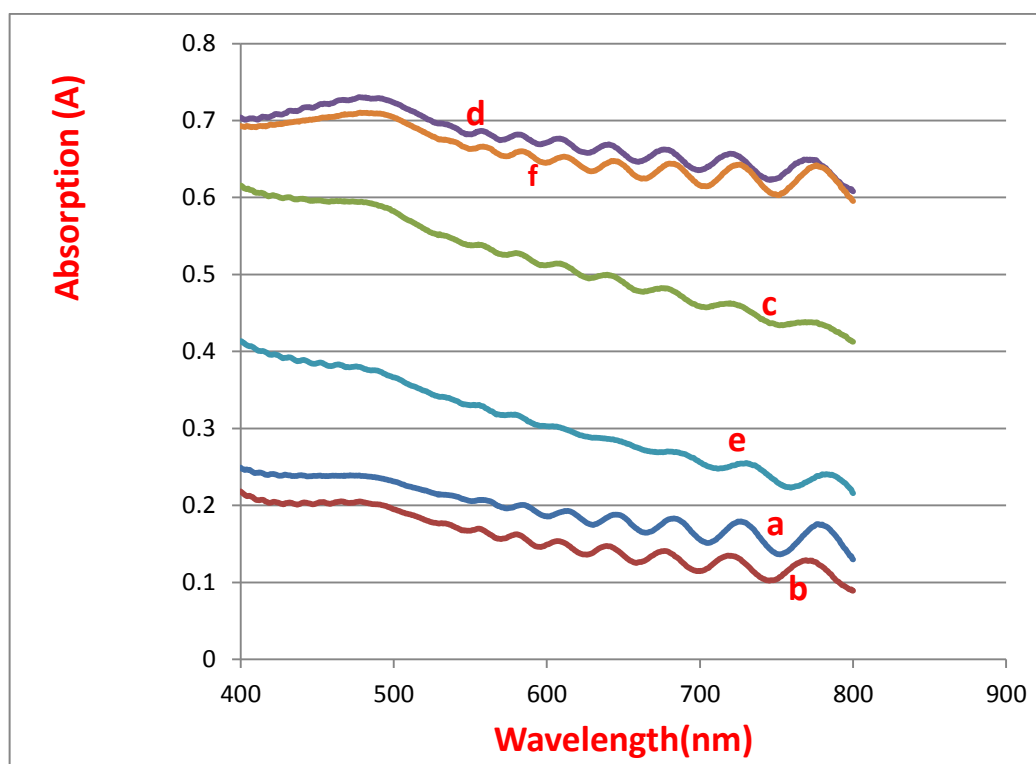


Figure (3.8): Electronic absorption spectra for annealed CBD-CdS thin films, at different temperature a) after annealing at 100 °C and slowly cooled b) after annealing at 100 °C and quickly cooled c) after annealing at 125 °C and slowly cooled d) after annealing at 125 °C and quickly cooled e) after annealing at 150 °C and slowly cooled f) after annealing at 150 °C and quickly cooled

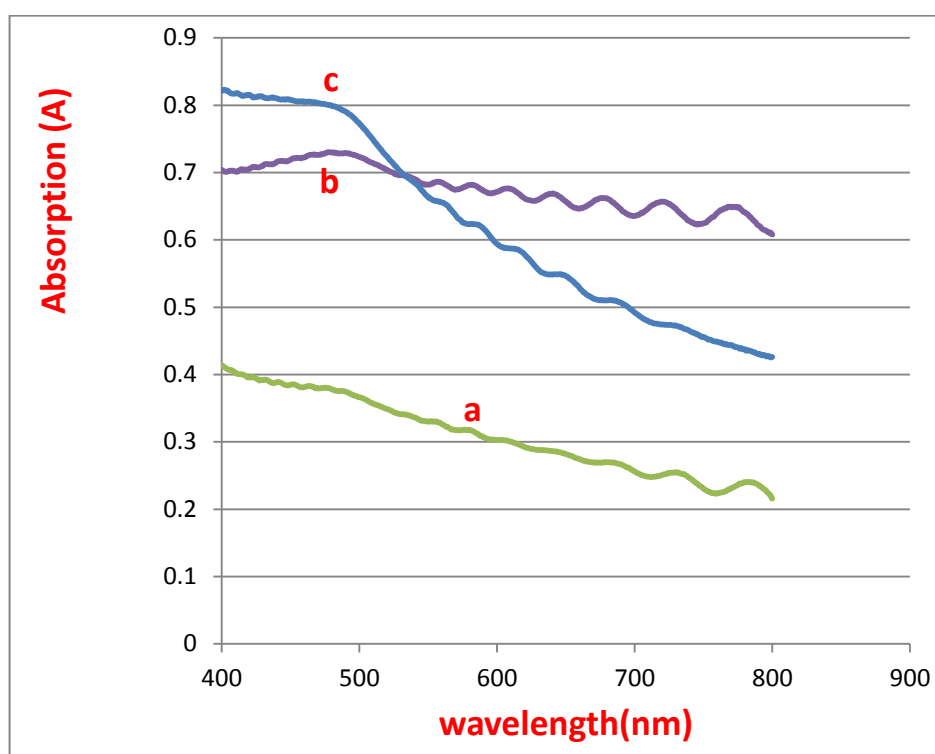


Figure (3.9): Electronic absorption spectra for a) annealed CBD- CdS thin film after annealing at 125 °C and slowly cooled, b) after annealing at 125 °C and quickly cooled and c) non-annealed CBD- CdS thin film

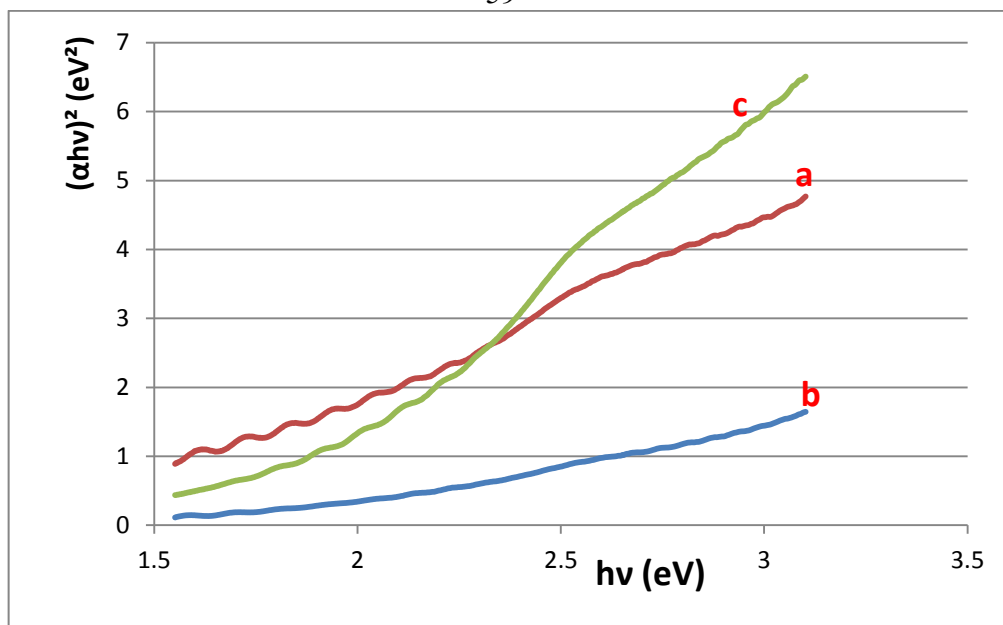


Figure (3.10): Tauc Plots from UV-Vis analysis for a) annealed CBD- CdS thin film after annealing at 125 °C and slowly cooled, b) after annealing at 125 °C and quickly cooled and c) non-annealed CBD- CdS thin film

Figure (3.10), the Tauc method was used to assess the energy band gap for these thin films. The results of the Figure are summarized in the Table (3.5), which shows that the annealed film at 125 °C with fast cooling gave better energy band gap than the non-annealed one, as compared with literature [10].

Table (3.5): Effect of annealing and cooling rate on energy band gap value for CBD-CdS thin film electrodes

	Description	Energy band gap (eV)
Fresh CBD-CdS electrode	Non-annealed	~2.00
	Slowly cooled	~1.90
	Fast cooled	~2.20

3.2.2 XRD patterns

CBD-CdS thin film electrodes at the fourth cycle of deposition

XRD measurements were used to determine the crystallite size and structural phase of the CBD-CdS/ITO/Plastic thin films. CdS may exist in two crystalline structures: cubic structure (zinc blende) and hexagonal (wurtzite type). Depending on the deposition conditions and techniques, CdS films may be grown in either phase [52, 53].

XRD patterns were obtained for CBD-CdS thin films deposited at fourth cycle of deposition. Different parameters (including annealing effect, cooling rate, and coating process) were studied, Figure (3.11).

The particle sizes of CdS were calculated by using Debye-Scherrers' formula, $D = 0.9\lambda/\beta\cos\theta$, in which D is the average grain size (\AA), λ is the X-ray wavelength of Cu $K\alpha$ radiation ($\lambda = 1.5406 \text{ \AA}$), β is the full-width at half-maxima (FWHM) in radians, and θ is the diffraction angle [78-80]. Table (3.6) summarizes the results.

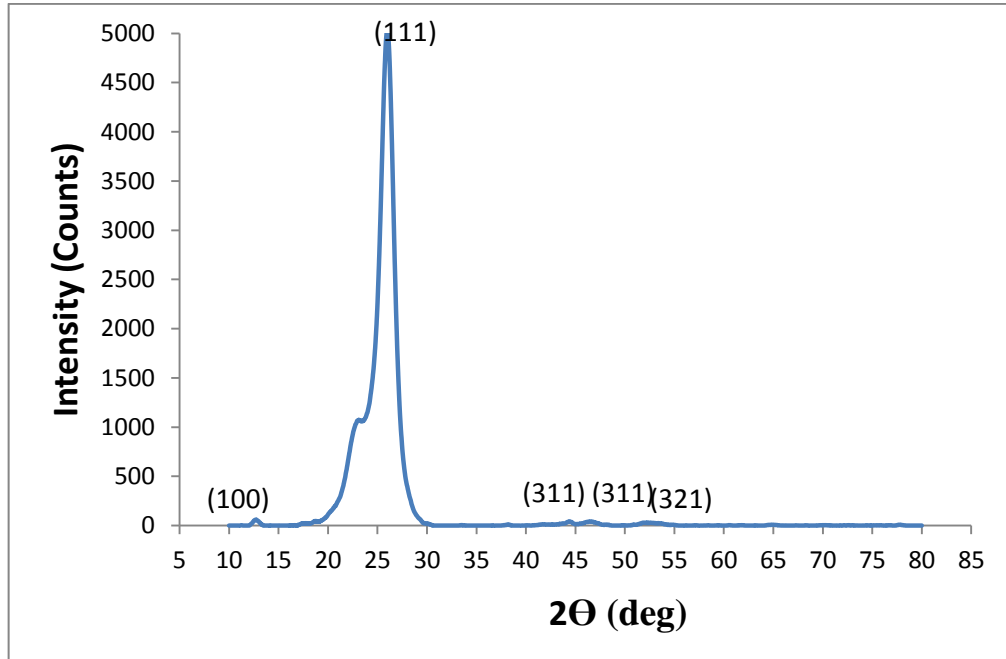


Figure (3.11): XRD patterns for CBD-CdS at fourth cycle of deposition

Table (3.6): Crystallite size values from XRD results for CBD-CdS film

2θ	θ	β (FWHM)	$(\sin\theta)^2$	$N=(h^2+k^2+l^2)$	hkl	D (nm)
13	6.5	2	0.013	1	100	4.18
25	12.5	2	0.04	3	111	4.25
44	22	2	0.14	11	311	4.48
46	23	2	0.15	11	311	4.51
52	26	2	0.19	14	321	4.62

The structure and the orientations were measured of crystal by using Bragg's law, $2d\sin\theta = n\lambda$, in which d is the spacing of the crystal layers, n is an integer, θ is the incident angle, and by using a miller indices equation $d_{hkl} = a/(h^2+k^2+l^2)^{1/2}$ to specify directions and planes of crystal.

XRD data showed that the CBD-CdS film involved crystallites, with average grain size~ 4.408 nm. It had intensity with preferential orientation, Table (3.6). It involved both cubic and hexagonal phases [62, 81].

3.2.2.2 Effect of annealing and cooling rate on CdS thin film electrodes

For annealed CdS thin film at 125 °C with slow and fast cooling rates, XRD measurements were obtained. The annealing temperature of 125 °C provided the best characteristics. This temperature has, therefore, been studied here.

XRD data showed that both fresh and annealed films exhibited crystallites.

Average particle sizes of slowly and fast cooled films~ 4.51 and 4.525 nm respectively. The XRD patterns indicate that annealing at 125 °C and fast cooling, Figure (3.12 b) give higher crystallites than annealing with slow cooling, Figure (3.12 a) and Figure (3.13). Table (3.7) summarized the results.

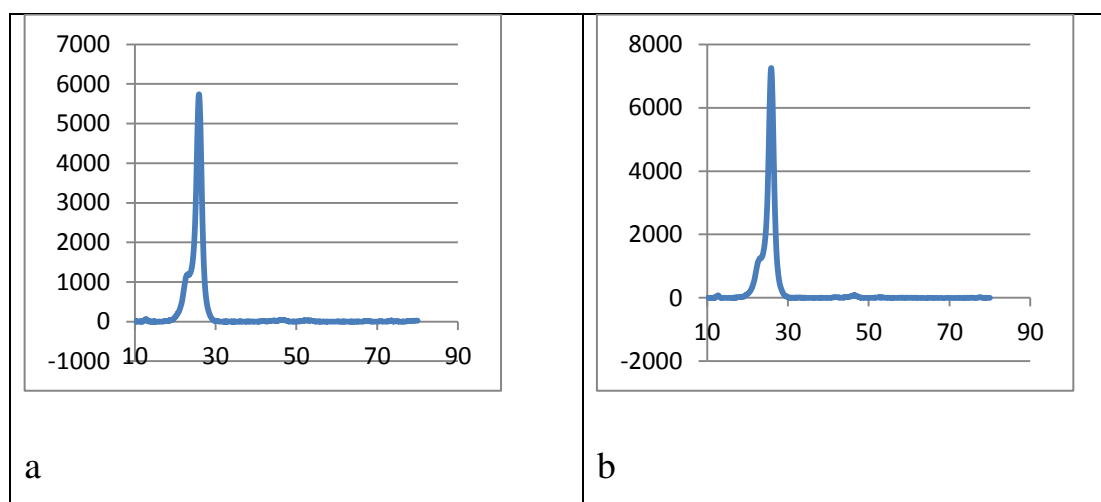


Figure (3.12): XRD patterns for annealing film at 125 °C a) after cooling slowly, b) after cooling quickly

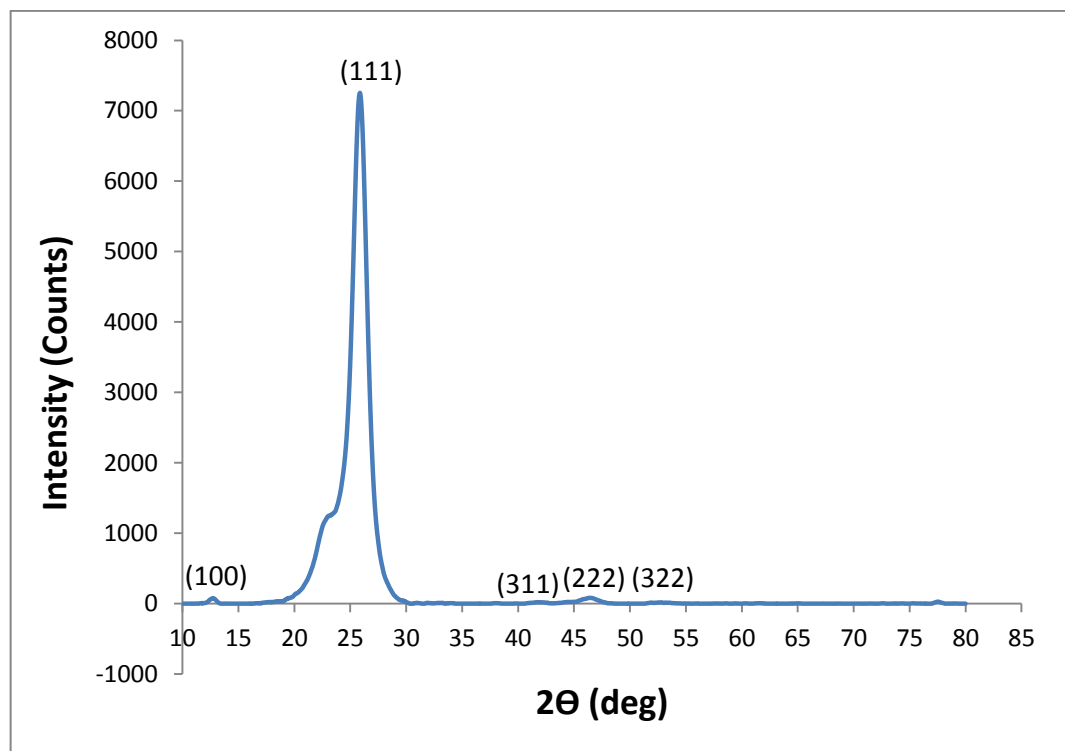


Figure (3.13): XRD patterns for fast cooling film at 125 °C

Table (3.7): Crystallite size values from XRD results for annealed and fast cooled the CBD-CdS film

2 θ	θ	β (FWHM)	$(\sin\theta)^2$	$N=(h^2+k^2+l^2)$	hkl	D (nm)
13	6.5	3	0.012	1	100	4.18
25	12.5	2	0.04	3	111	4.26
44	22	2	0.14	11	311	4.48
46	23	2	0.15	12	222	4.51
52	26	2	0.2	17	322	4.62

XRD data showed that both annealed and non-annealed CBD-CdS films exhibited crystallites, both films involved both cubic and hexagonal phases. Thus, no measurable phase change in the crystal structure of CBD-CdS films occurred by annealing at 125 °C under nitrogen.

3.2.3 SEM micrographs

In order to study the surface quality and morphology of SCs, SEM surface imaging is an important process. In PEC processes, surface quality affects SC performance. SEM surface images were obtained for different parameters including annealing effect, cooling rate, and coating process.

3.2.3.1 SEM Images for CBD-CdS thin film electrodes at the fourth cycle of deposition

SEM surface images have been obtained for CBD-CdS at fourth cycle of deposition (120 min) to see the uniformity and quality of the surface, Figure (3.14). The SEM image for the CBD-CdS at fourth cycle of deposition film showed a surface with coagulates of nano-sized particles. There were various sizes of coagulate (0.87- 1.55 μm). The surface topography showed ups and downs, showing relatively low uniformity.

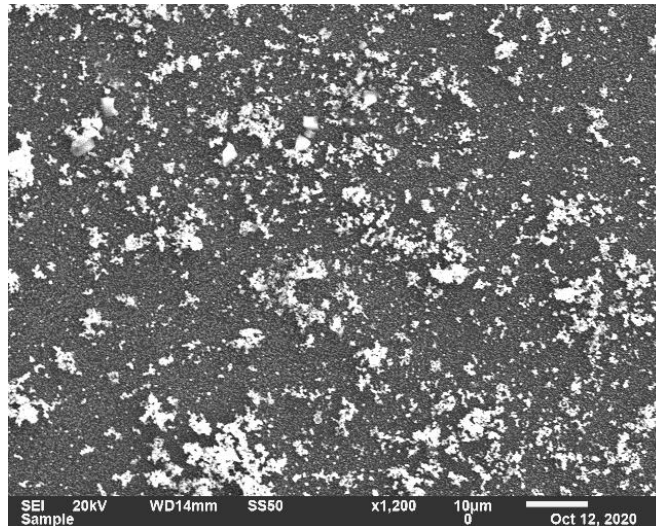


Figure (3.14): SEM surface for CBD-CdS thin film at fourth cycle of deposition

- EDX Spectra for CBD-CdS film at fourth cycle of deposition

The EDX pattern has been obtained for CBD-CdS film at fourth cycle of deposition, Figure (3.15). The EDX results showed different atomic ratios for Cd and S, (Cd:S 0.71: 0.88, respectively), Table (3.8). This means that Sulfur was more than Cadmium. However, in PEC study the film shows n-type behavior, in accordance with earlier literature [82]. This indicates that the excess S, in the film, is not an elemental S⁰ form. It can be due to other sulfur impurities but not elemental.

Table (3.8): EDX atomic analysis for fourth deposition cycle of CBD-CdS

Formula	Mass%	Atom%	Sigma
C	50.86	67.92	0.09
O	28.48	28.56	0.31
S	1.76	0.88	0.05
Cd	4.97	0.71	0.20
In	12.15	1.70	0.23
Sn	1.78	0.24	0.21
Total	100	100	

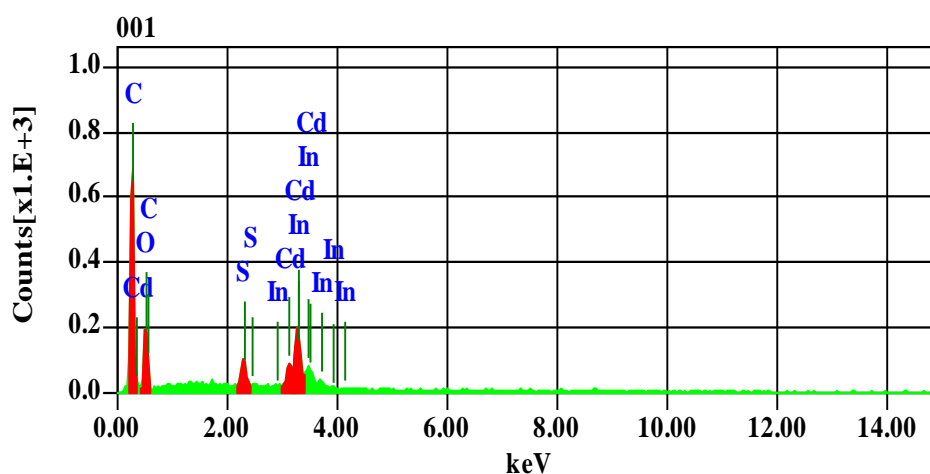


Figure (3.15): EDX patterns for CBD-CdS thin film at fourth cycle of deposition

3.2.3.2 Effect of annealing and cooling rate on CdS thin film electrodes

SEM surface images were obtained for CdS thin films after annealing at 125 °C with fast cooling, because this annealing temperature gave best characteristics in this study. To see the uniformity and quality of the surfaces, SEM was studied. A surface with coagulates of nano-sized particles was shown in the SEM image for the annealed film, Figure (3.16). The coagulate size about (3.15 μm). The surface topography showed ups and downs, indicating relatively low uniformity.

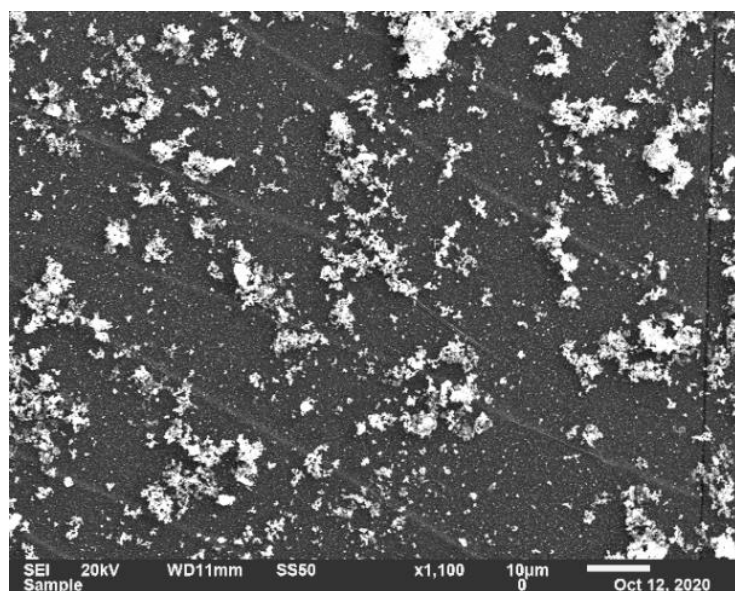


Figure (3.16): SEM surface for CBD-CdS thin film after annealing at 125 °C with fast cooling

- EDX Spectra for annealing CBD-CdS at 125 °C with fast cooling

The EDX pattern has been obtained for CBD-CdS film at fourth cycle of deposition, Figure (3.17). The EDX results showed different atomic ratios for Cd and S, (Cd:S 0.51: 0.60, respectively), Table (3.9). Sulfur was more than Cadmium; this indicates that the excess S, in the film,

is not an elemental S° form. It can be due to other sulfur impurities but not elemental.

Table (3.9): EDX atomic analysis for annealed CBD-CdS at 125 °C with fast cooling rate

Formula	Mass%	Atom%	Sigma
C	49.52	67.02	0.09
O	29.03	29.49	0.30
S	1.18	0.60	0.04
Ca*	0.06	0.02	0.07
Cd	3.51	0.51	0.18
In	14.62	2.07	0.24
Sn*	2.08	0.29	0.24
Total	100	100	

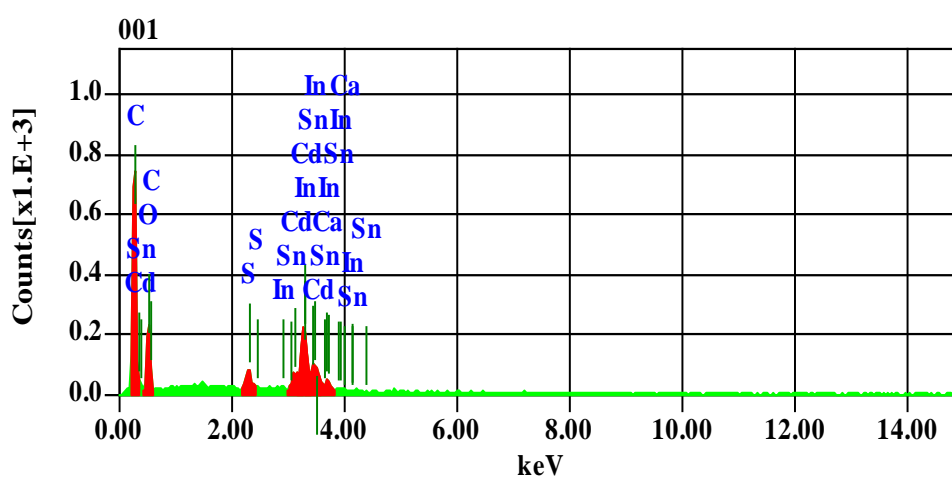


Figure (3.17): EDX patterns for CBD-CdS thin film after annealing at 125 °C with fast cooling

3.2.4 PEC studies on fresh CdS thin film electrodes

ECD-CdS film was too thin to observe. Therefore, the PEC study was not made on it. PEC studies on CBD-CdS thin films were made. The study included photo *J-V* plots, short-circuit current and efficiency. Aqueous poly sulfide redox was studied at room temperature. Effects of annealing (100,125 and 150 °C) and cooling rates were studied.

3.2.4.1 Effect of deposition time

Photo *J-V* plots were measured for fresh CBD-CdS/ITO/Plastic thin film electrodes, with different deposition times.

Photo *J-V* plots were measured for new prepared films deposited in different times (30, 60, 90, 120, 150 and 180 min), Figure (3.18). The Figure results are shown in Table (3.10).

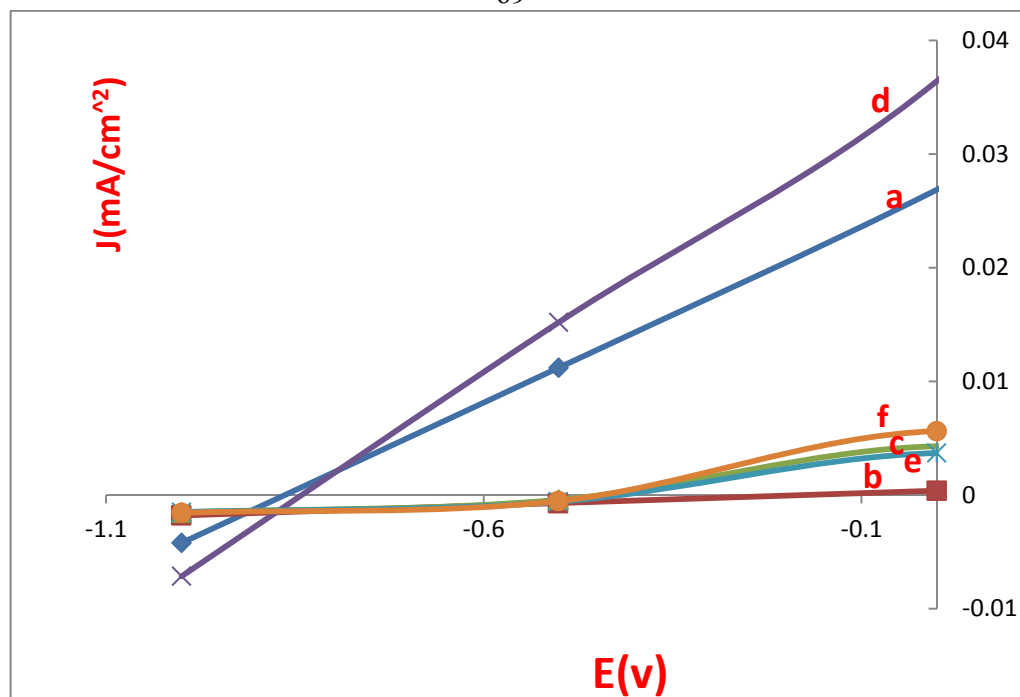


Figure (3.18): Photo J-V plots for CBD- CdS/ITO/Plastic thin film fresh electrodes, deposited in different times a)30 min, b) 60 min, c) 90 min, d) 120 min, e) 150 min and f) 180 min (all one cycle)

Table (3.10): Effect of deposition time on PEC characteristics of fresh CBD- CdS thin film electrodes

	Sample	V_{oc} (V)	J_{sc} (mA/cm ²)
Fresh CdS electrode	30 min	-0.8	0.025
	60 min	-0.2	0.0
	90 min	-0.41	0.005
	120 min	-0.71	0.035
	150 min	-0.45	0.005
	180 min	-0.5	0.01

The V_{oc} and J_{sc} for the 30 min and 120 min deposition times were very close to each other, and they are higher than other values. Values of efficiency (η %) are higher for films deposited in 30 min and 120 min.

Similarly, Fill Factor (***FF***) values are higher for films deposited in 30 min and 120 min.

Based on Figure (3.18), the values of ***η %*** for deposition time 30 and 120 min are **(0.135)**, **(0.1802)** respectively, and the ***FF*** values for deposition time 30 and 120 min are **(0.58)**, **(0.645)** respectively. Thus the most efficient generation of electric current is by films deposited in 120 min

Equations (1) and (2) explain ***η %*** and ***FF***.

$$\eta\% = [(\text{maximum observed power density})/(\text{reach-in power density})] \times 100\% \quad (1)$$

$$FF = [(\text{maximum observed power density})/J_{sc} \times V_{oc}] \times 100\% \quad (2)$$

3.2.4.2 Effect of cycles of deposition

The effect of deposition cycle on the photo *J-V* plots, was studied for fresh CBD- CdS thin film electrodes, Figure (3.19), The results of the Figure are shown in Table (3.11)

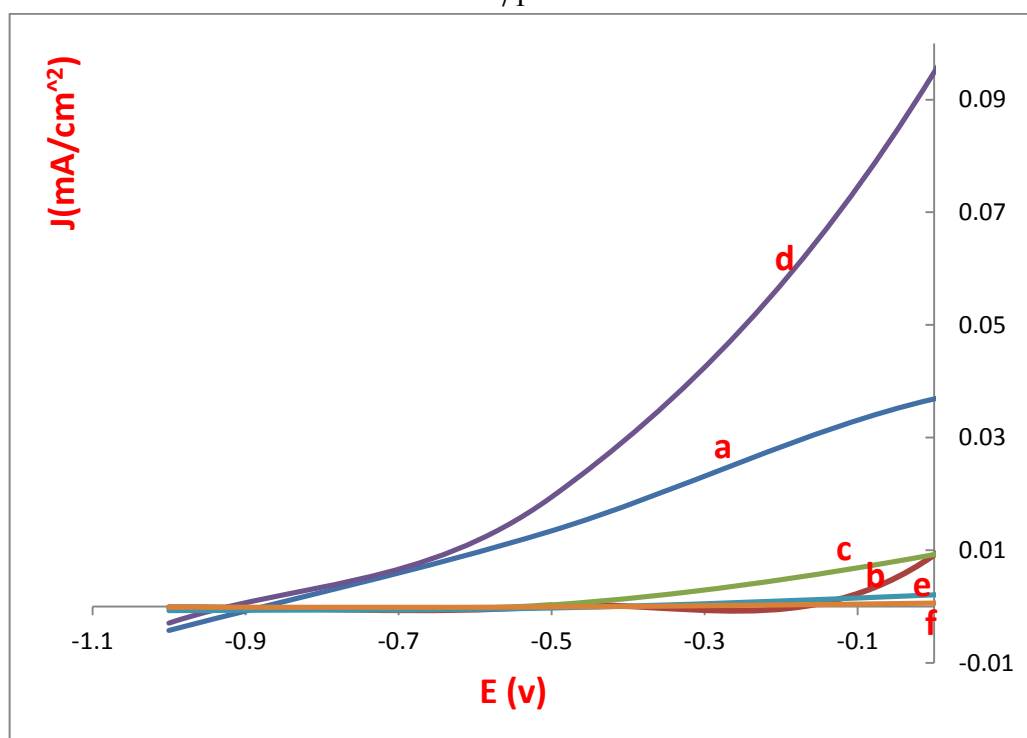


Figure (3.19): Photo J-V plots for CBD-CdS thin film non-annealed fresh electrodes, effect of deposition cycles a) first, b) second, c) third, d) fourth, e) fifth and f) sixth cycle

Table (3.11): Effect of deposition cycle on PEC characteristics of fresh CBD- CdS thin film electrodes

	Sample	V_{oc} (V)	J_{sc} (mA/cm ²)
Fresh CdS electrode	First	-0.88	0.036
	Second	-0.1	0.01
	Third	-0.42	0.01
	Fourth	-0.9	0.095
	Fifth	-0.1	0.003
	Sixth	0.001	0.0012

The V_{oc} and J_{sc} for the fourth and first cycle of deposition were the best, and they are higher than other values. Higher efficiency (η %) values are taken from deposition cycles first and fourth. Values of η % for first and fourth are (0.162) and (3.25) respectively. FF values for first and fourth are (0.44), (0.327) respectively. Thus the most efficient generation of electric current is obtained by the fourth cycle.

3.2.4.3 Effect of different annealing temperature and cooling rate

Effect of annealing (100, 125 and 150 °C) of CBD-CdS/ITO/Plastic on Photo J - V characteristics were studied. Effect of cooling rate was also studied, as shown in Figure (3.20). Table (3.12) summarizes the results.

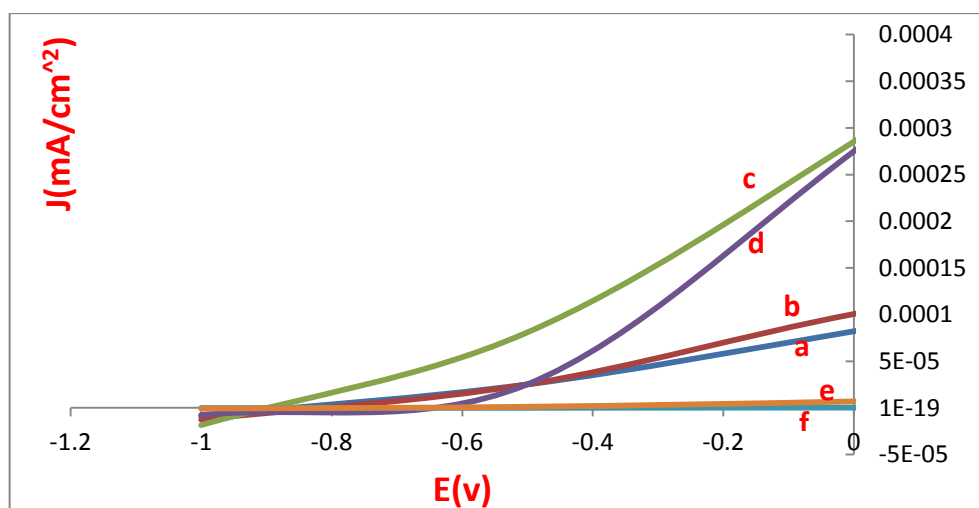


Figure (3.20): Photo J - V plots for CBD-CdS annealed thin film at different temperature
a) after annealing at 100 °C and slowly cooled b) after annealing at 100 °C and quickly cooled c) after annealing at 125 °C and slowly cooled d) after annealing at 125 °C and quickly cooled e) after annealing at 150 °C and slowly cooled f) after annealing at 150 °C and quickly cooled

Table (3.12): Effect of different annealing temperature and cooling rate on PEC characteristics of fresh CBD-CdS thin film electrodes

	Sample	V_{oc}	J_{sc} (mA/cm ²)
Annealed CBD-CdS electrode	Fast (100)	-0.8	0.000056
	Slow (100)	-0.78	0.0001
	Fast (125)	-0.9	0.00026
	Slow (125)	-0.6	0.00023
	Fast (150)	-0.2	0.000001
	Slow (150)	-0.7	0.00002

The values of efficiency are higher for annealed films at 125 °C under nitrogen for 15min with cooling rate (fast and slow). Values of η % for fast cooling and slow cooling are **(0.017)** and **(0.0053)** respectively. Similarly, ***FF*** values are higher for annealed films at 125 °C, where the values of ***FF*** for fast cooling and slow cooling are **(0.641)**, **(0.333)** respectively. Thus the most efficient generation of electric current is obtained by annealing at 125 °C with rapid cooling rate.

3.2.4.4 Effect of annealing (at 125 °C)

Photo J-V plots were measured for non-annealed CBD-CdS/ITO/Plastic thin films, which prepared through fourth cycle deposition, and it compared with the best-annealed ones at 125 °C under nitrogen for 15min. Moreover, the effects of cooling rate (fast and slow) was also studied, Figure (3.21). The results of the Figure are shown in Table (3.13)

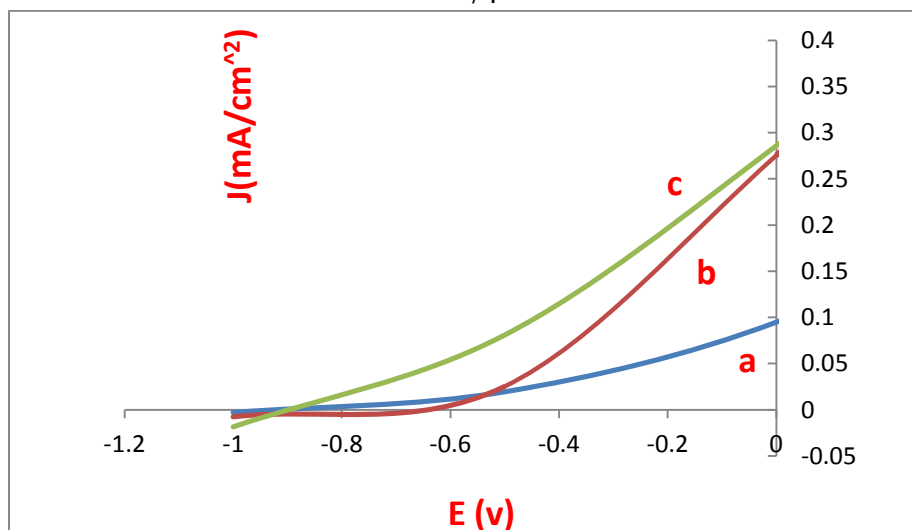


Figure (3.21): Photo J-V plots for a) non-annealed CBD-CdS thin film b) annealed CBD- CdS thin film after annealing at 125 °C and slowly cooled and c) after annealing at 125 °C and quickly cooled

Table (3.13): Effect of annealing and non-annealing on PEC characteristics of fresh CBD- CdS thin film electrodes

	Description	V_{oc} (V)	J_{sc} (mA\cm ²)	η %	FF
Fresh CBD-CdS	Non-annealed	-0.9	0.095	3.25	0.327
	Slowly cooled	-0.7	0.270	8.13	0.370
	Fast cooled	-0.9	0.290	10.46	0.340

From Table (3.13), the non-annealed film deposited in the fourth cycle showed lower V_{oc} and J_{sc} values than the annealed films. Consequently it gave percentage conversion efficiency (η % ~**3.25**) lower than annealed films (η % ~**8.13 and 10.46**). On the other hand, the fast cooled electrode gave a higher efficiency than the slowly cooled electrode.

The films annealed at 125 °C gave higher electronic absorption and better PEC characteristics than the non- annealed film. In order to enhance the particle properties, the annealing process was reported, giving a more organized, compact surface, more homogeneous, and higher crystallites. Annealing reduces crystal defects, enhances particle interaction, decreases harshness of surface, and removes surface states [71].

3.2.4.5 Effect of deposition method

Photo *J-V* plots were measured for CdS thin films prepared by different techniques (CBD and EC/CBD) were investigated, Figure (3.22). Table (3.14) summarizes the results.

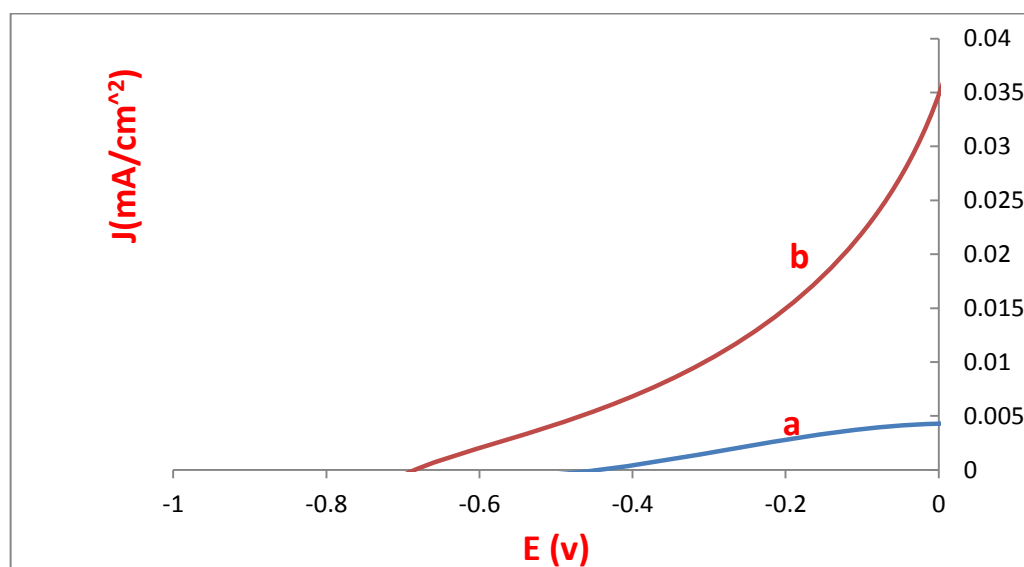


Figure (3.22): Photo *J-V* plots for a) ECD/CBD and b) CBD- CdS thin films which deposited for 120 min at first cycle of deposition

Table (3.14): Comparison the PEC characteristics of CdS thin film electrodes prepared by different techniques

Type of deposition	V_{oc} (V)	J_{sc} (mA/cm ²)	η %	FF
Combined	-0.45	0.0048	0.139	0.55
CBD	-0.71	0.035	0.180	0.64

From Table (3.14), the V_{oc} and J_{sc} for the CBD technique were higher than ECD/CBD (combined) technique. For calculated the efficiency η %, the larger areas was for CBD deposition.

The values η % for CBD and ECD/CBD are **(0.180)** and **(0.139)** respectively. The FF values for CBD and ECD/CBD are **(0.64)** and **(0.55)** respectively. Thus the CBD deposition technique is better than ECD/CBD technique.

3.3 Effect of redox couple on PEC

The effect of redox pairs was measured for fresh CBD-CdS thin film electrodes on the photo J-V plots, Figure (3.23).The results of the Figure are shown in Table (3.15).

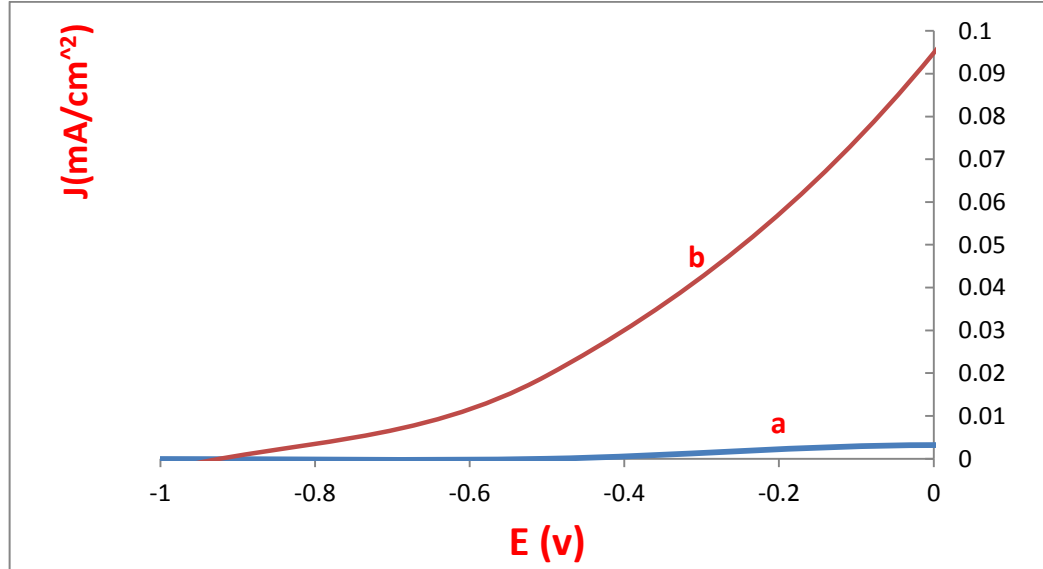


Figure (3.23): Photo J-V plots for fresh CdS thin film, with effect of redox couple a) Iron and b) poly sulfide redox couples

Table (3.15): Effect of redox couple on PEC characteristics of fresh CBD-CdS thin film electrode

Type of redox couple	V_{oc} (V)	J_{sc} (mA/cm ²)	η %	FF
Iron redox couple	-1.00	0.0031	0.05	0.138
Sulfide redox couple	-0.9	0.095	3.25	0.327

Table (3.15) shows that, the J_{sc} value of film in Poly-Sulfide redox couple is higher than in Iron redox couple. But V_{oc} value for the film in Iron redox couple is higher. For calculated the efficiency η %, from a Figure (3.23). Largest efficiency value was for film in Poly-Sulfide redox couple. The value η % for Poly-Sulfide and Iron redox couples are **(3.25)**, **(0.05)** respectively. The FF values for Poly-Sulfide and Iron redox couples

are (0.327), (0.138) respectively. Thus the most efficient generation of electric current is when using the Poly-Sulfide redox couple, which is more efficient than other counterpart. Therefore, the Poly-Sulfide redox couple was used throughout this work.

3.4 Part 2:

Coated CdS thin film electrodes by multi-wall carbon nano tube (MWCNT)

Different characteristics for coated CdS thin-film electrodes, such as electronic absorption, photo-current, XRD, and SEM spectra are shown below:

3.4.1 Electronic absorption spectra

Electronic Absorption Spectra were studied for CdS films coated with MWCNT. After preparing the new thin films by CBD through fourth deposition (120 min), it was coated with MWCNT. The electronic absorption spectra were measured for the CBD- CdS /ITO/Plastic thin films after coating, Figure (3.24).

The Tauc method was used to determine the energy band gap by using optical absorbance data plotted with respect to energy, Figure (3.25).

The results of the Figure are summarized in Table (3.16), which shows that the non-coated CdS electrode for fourth deposition gave lower

energy band gap than the coated ones. However, the E_{bg} value cannot be accurately measured for the coated CdS films.

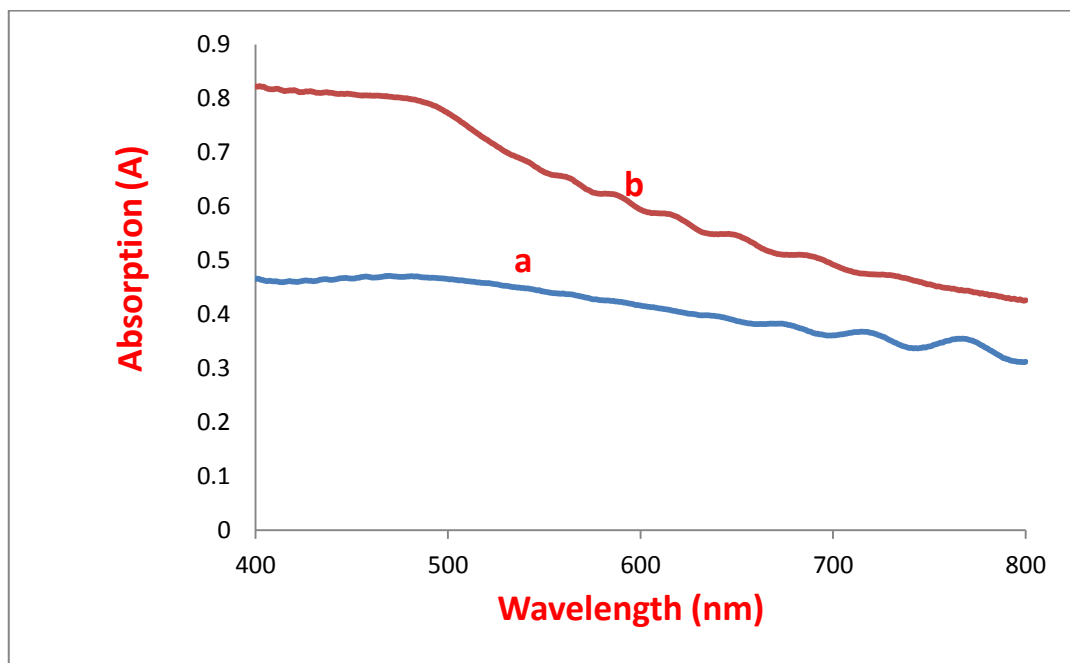


Figure (3.24): Electronic absorption spectra for a) coated and b) fresh CBD-CdS thin films, deposited in the fourth cycle (120 min)

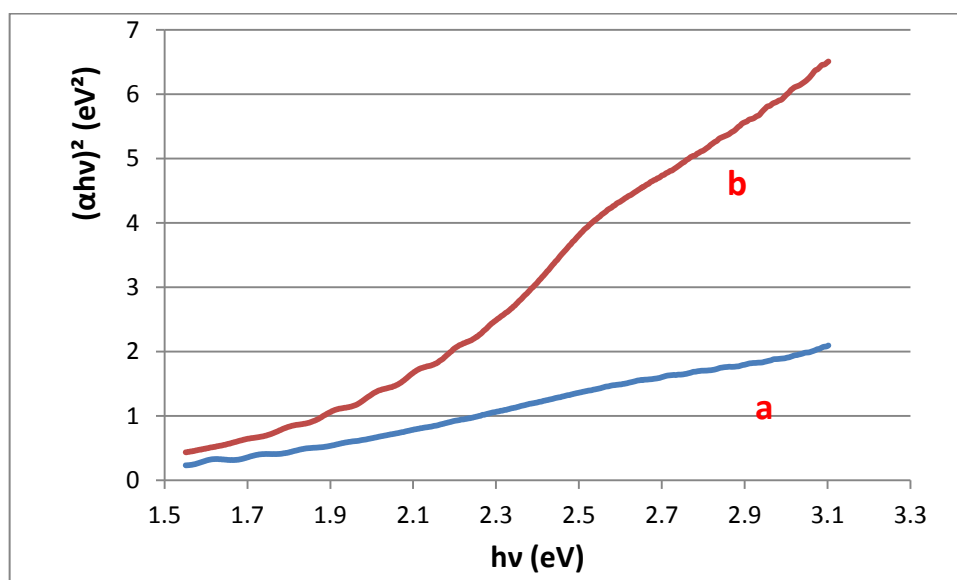


Figure (3.25): Tauc Plot from UV-Vis analysis for a) coated and b) fresh CBD-CdS thin films, deposited in the fourth cycle (120 min)

Table (3.16): Effect of coated with (MWCNT) on energy band gap value of CBD thin film electrodes, by electronic absorption spectra.

Type	Cycle of Deposition	Energy band gap(eV)
Non-coated	Fourth (120 min)	~2.0
Coated electrode	Fourth (120 min)	~2.1

3.4.2 XRD patterns for coated CdS thin films electrodes

XRD patterns were used to determine the crystalline size and structural phase of the coated CBD-CdS Nano crystalline thin films. XRD measurements were obtained for coated CBD-CdS at fourth cycle of deposition (120 min), Figure (3.26). The particle sizes of CdS were calculated. Table (3.17) summarized the results.

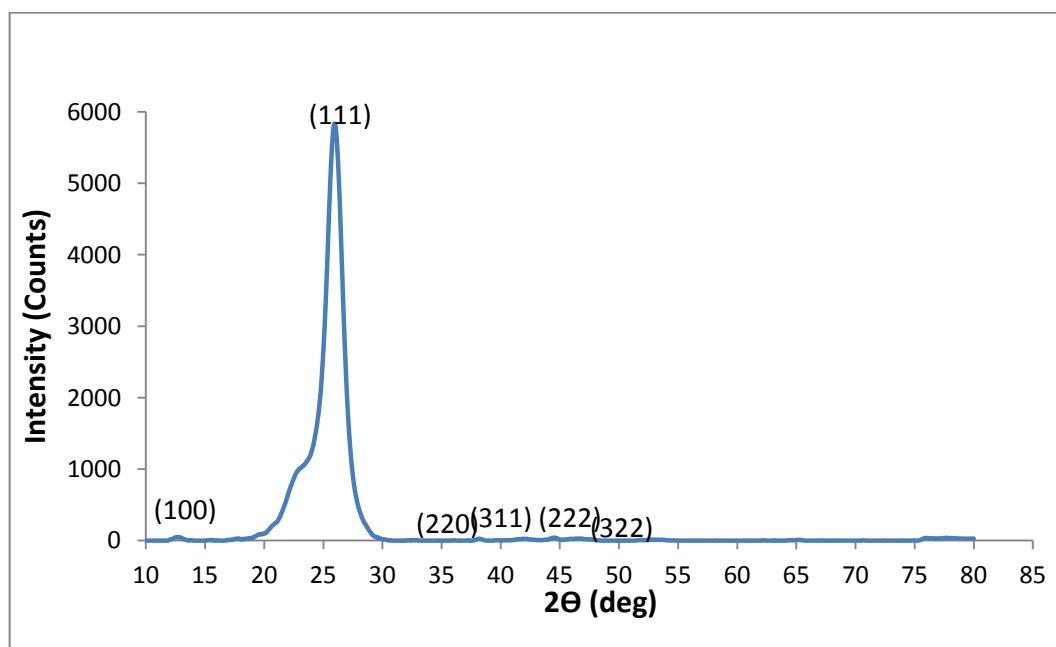


Figure (3.26): XRD patterns measured for coated CdS thin film

Table (3.17): XRD results for coated CBD-CdS thin film

2θ	θ	β (FWHM)	$(\sin\theta)^2$	$N=(h^2+k^2+l^2)$	hkl	D
13	6.5	3	0.012	1	100	4.18
25	12.5	2	0.04	3	111	4.26
38	19	2	0.10	8	220	4.39
44	22	2	0.14	11	311	4.48
46	23	2	0.15	12	222	4.51
52	26	2	0.2	17	322	4.62

The XRD data showed that the coated film exhibited crystallites. The average grain size was ~ 4.406 nm, and it had intensities with preferential orientation; This means that particle size and preferential orientations are identical in both coated and fresh films, Table (3.17). It involved both cubic and hexagonal phases [62]. This means that the coating process by MWCNT didn't affect the original grain size of CdS as it appeared in Figure (3.11), and the particle sizes are approximately the same.

3.4.3 SEM micrographs

SEM surface images have been obtained for coated CBD-CdS Nano crystalline thin films, to see the uniformity and quality of the surface, as in Figure (3.27). The SEM image showed a surface with nano-sized particles coagulating. There have various sizes of coagulates (4.06- 5.13 μm). The surface topography showed low uniformity.

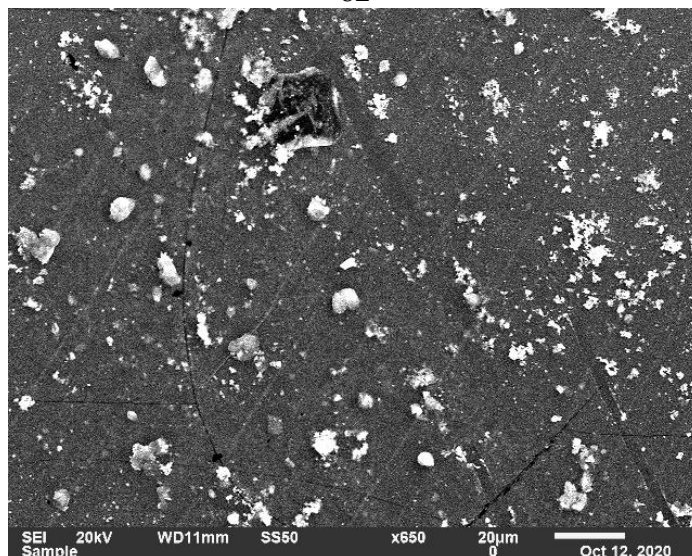


Figure (3.27): SEM surface for coated CdS thin film

- EDX Spectra for coated CBD-CdS thin film Electrodes

EDX patterns have been obtained for coated CBD-CdS, Figure (3.28). The EDX analysis showed the disappearance of the sulfur atoms, and showed only small amount Cadmium atoms. This may be due to the fact that the carbon atoms covered the sulfur atoms. Thus, the atomic quantity of Cd is 0.20 and 67.69 for Carbon atom, as shown in Table (3.18).

Table (3.18): EDX atomic analysis for coated CBD-CdS

Formula	Mass%	Atom%	Sigma
C	52.38	67.92	0.08
O	29.78	28.89	0.27
Na	0.78	0.53	0.06
Si	1.40	0.78	0.06
Cd	1.42	0.20	0.13
In	11.93	1.61	0.19
Sn	2.30	0.30	0.18
Total	100	100	

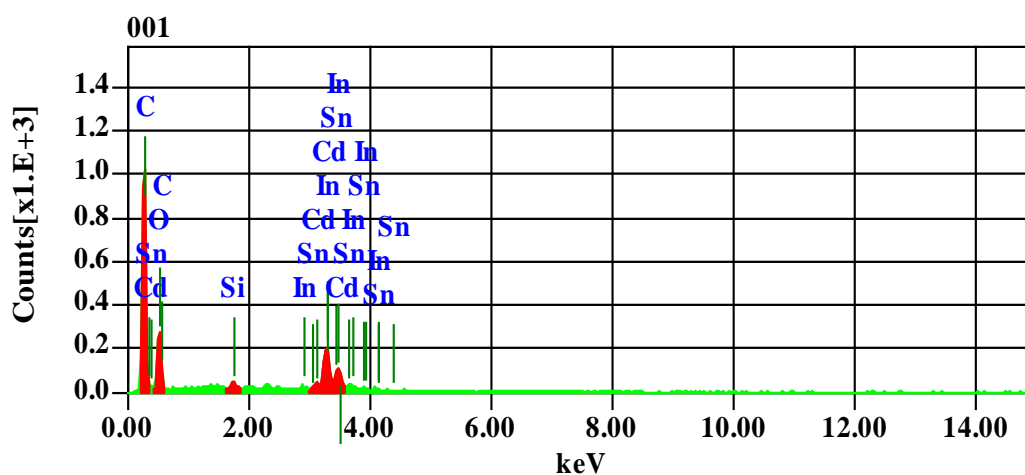


Figure (3.28): EDX patterns for coated CBD-CdS thin film

3.4.4 PEC studies for coated and fresh CdS thin film electrodes

PEC values including photo J-V plots, short-circuit current and efficiency, were studied in aqueous S^{2-}/S_x^{2-} redox couple at room temperature.

Photo J-V plots were measured for coated and fresh CBD-CdS films, Figure (3.29). Table (3.19) summarized the results.

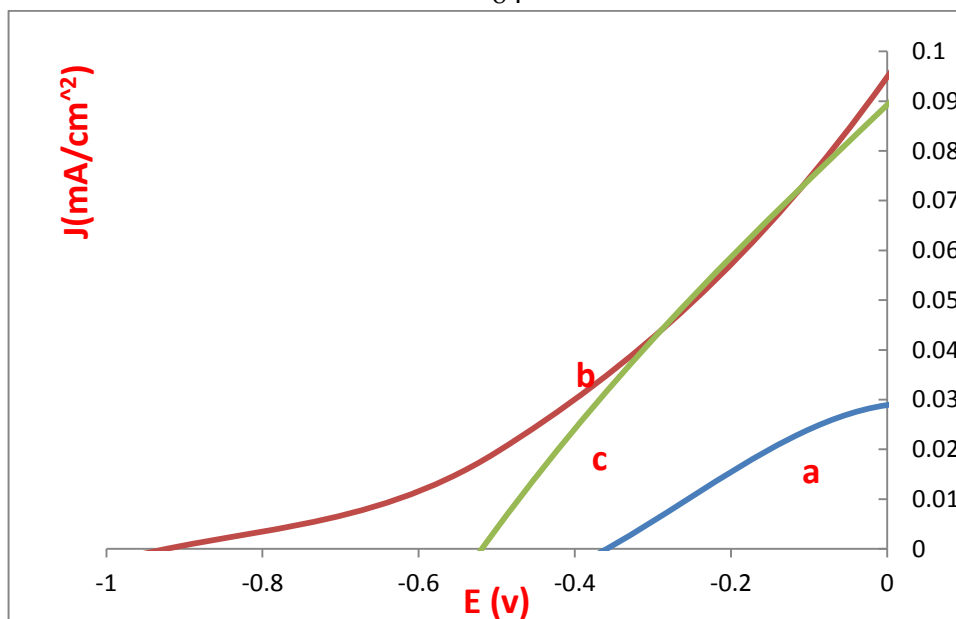


Figure (3.29): Photo J-V plots for a) coated CBD-CdS b) fresh CBD-CdS thin films and c) back side of coating electron, which deposited in fourth cycle

Table (3.19): Comparison the PEC characteristics of coated and fresh CdS thin films electrodes prepared by fourth deposition

Description of electrode	V_{oc} (V)	J_{sc} (mA/cm ²)	η %	FF
Fresh electrode	-0.9	0.095	3.25	0.327
From Side of coated electrode	-0.35	0.028	0.77	0.670
Back side of coating	-0.50	0.089	2.79	0.540

From the Table (3.19), the V_{oc} and J_{sc} for the non-coated (fresh) film was the highest than the coated one. For calculated the efficiency η %, the largest and best value was for fresh film.

The FF values for fresh and coated films are **(0.327)**, **(0.67)** respectively. Thus the most efficient generation of electric current is from the fresh film, which is higher than other counterparts.

3.5 Part 3:

Recycled CdS thin film electrodes

For recycled CdS thin-film electrodes, different characteristics, such as photo-current and electronic absorption are shown below:

3.5.1 Electronic absorption spectra

After prepared the new CBD-CdS/ITO/Plastic electrode, and recycled other thin films through CBD technique for fourth deposition (about 120min), electronic absorption spectra was measured for these fresh and recycled thin films.

- Effect of annealing and cooling rate

Electronic absorption spectra were measured for non-annealed fresh and recycled CBD- CdS/ITO/Plastic thin films, and for annealed ones at 125 °C under nitrogen for 15 min. Moreover, the effects of cooling rate (fast and slow) for both electrodes were studied, Figure (3.30).

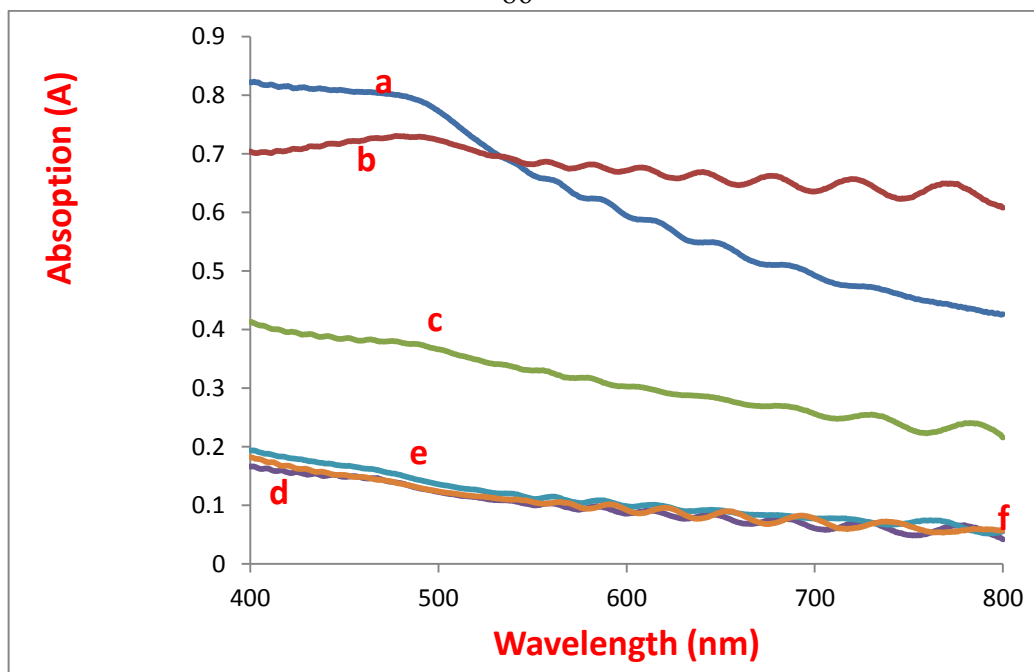


Figure (3.30): Electronic absorption spectra for a) non- annealed fresh electrodes, b) after annealing at 125 °C and quickly cooled fresh, c) after annealing at 125 °C and slowly cooled fresh, d) non-annealed recycled, e) after annealing at 125 °C and slowly cooled recycled, f) after annealing at 125 °C and quickly cooled recycled

To determine the energy band gap, the Tauc plots were made, Figure (3.31). The results of the Figure are summarized in Table (3.20). The Table shows that recycled and fresh films gave comparable gaps in the energy band, and the energy band gaps are marginally influenced by annealing. In contrast with annealed films, the recycled and fresh non-annealed films showed higher energy band gaps. The lowest energy band gap values were provided by quickly cooled films.

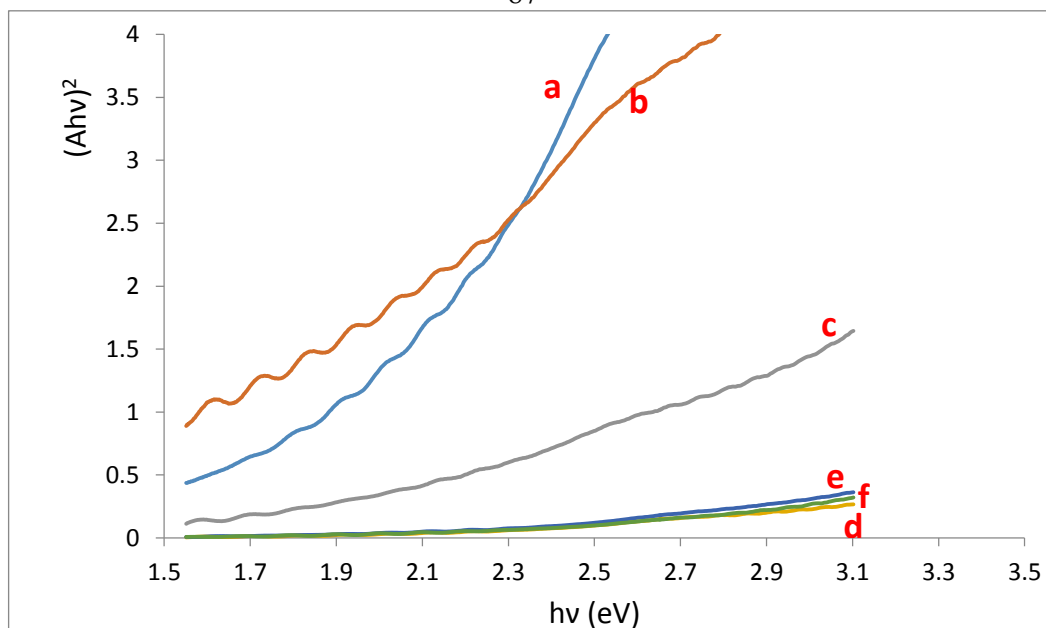


Figure (3.31): Tauc Plot from UV-Vis analysis for a) non- annealed fresh electrodes, b) after annealing at 125 °C and quickly cooled fresh, c) after annealing at 125 °C and slowly cooled fresh, d) non-annealed recycled, e) after annealing at 125 °C and slowly cooled recycled, f) after annealing at 125 °C and quickly cooled recycled.

Table (3.20): Effect of annealing and cooling rate on energy band gap values of CBD-CdS thin film electrodes (fresh and recycled)

CdS type	Description	energy band gap (eV)
Fresh	Non-annealed	~1.70
	Slowly cooled	~1.72
	Fast cooled	~1.71
Recycled	Non-annealed	~2.10
	Slowly cooled	~2.20
	Fast cooled	~2.25

3.5.2 PEC studies for recycled and fresh CdS thin film electrodes

PEC results for recycled and fresh electrodes, prepared by CBD technique, including photo J-V plots, the value of short-circuit current and efficiency was studied in aqueous S^{2-}/S_x^{2-} redox couple at room temperature, Figure (3.32). Table (3.21) summarized the results.

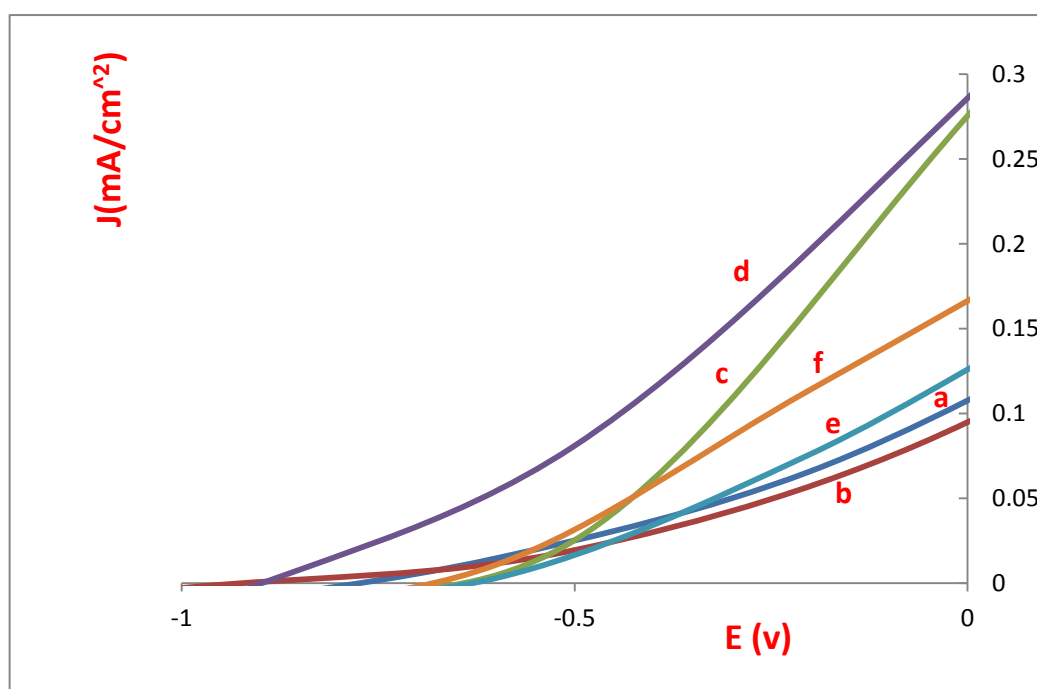


Figure (3.32): Photo J-V plots for a) non- annealed recycled, b) non-annealed fresh c) after annealing at 125 °C and slowly cooled fresh, d) after annealing at 125 °C and quickly cooled fresh, e) after annealing at 125 °C and slowly cooled recycled, f) after annealing at 125 °C and quickly cooled recycled

Table (3.21): Effect of annealing and cooling rate on PEC characteristics of fresh and recycled CBD-CdS thin film electrodes

CdS type	Description	V_{oc} (V)	J_{sc} (mA/cm ²)	η %	FF
fresh	Non-annealed	-0.9	0.095	3.25	0.327
	Slow cooling	-0.7	0.27	8.13	0.37
	Fast cooling	-0.9	0.29	10.46	0.34
recycled	Non-annealed	-0.72	0.11	3.83	0.420
	Slow cooling	-0.6	0.125	4.06	0.46
	Fast cooling	-0.67	0.152	5.93	0.504

From the Table (3.21), the fresh films showed higher V_{oc} and J_{sc} values than recycled ones. For percent conversion efficiencies, the fresh and recycled annealed films showed the higher conversion efficiency than the other films.

The quenched film, gave higher percent conversion efficiency than the slowly cooled ones. From a Figure (3.32), the largest and best η % value was for quenched fresh film (**10.46**). The $FF\%$ values for recycled films are higher than fresh film; especially the quenched films (**0.504**).

As mentioned earlier, the annealed films in both types (fresh and recycled) at 125 °C gave better PEC characteristics than the non- annealed films. The annealing process was reported to enhance contact the particle and its properties, giving a more orderly and compact surface. In addition, it provides more homogenous and higher crystallites and eliminates the crystal defects [71].

Here, quenched films showed better PEC characteristics than the slowly cooled ones. The fast cooling protects crystallites from extra exposure to heat, and possibly eliminates film distortion. Annealed films with slow cooling have more imperfection, because the heated crystal is exposed to more heat [83, 84].

3.6 Stability of the CdS thin film electrodes

The stability under PEC conditions was investigated for various CBD-CdS/ITO/Plastic thin film electrodes, Figure (3.33). The value of J_{sc} vs. **time** was measured at (0.0 V) applied potential with respect to Calomel electrode. The illumination intensity on the electrode was measured, and it was $\sim 0.0086 \text{ W.cm}^{-2}$.

The effect of annealing and fast cooling rate on J_{sc} vs. **time** plots on fresh and recycled films has been studied. The films that were recycled showed higher J_{sc} vs. **time** than fresh films. The annealed CdS films showed higher J_{sc} vs. **time** than the non-annealed CdS films, while quenched films showed J_{sc} vs. **time** higher than slowly cooled films.

Compared to annealed CdS with slowly cooled and non-annealed thin films under PEC conditions, this suggests relative stability of the quenched annealed films.

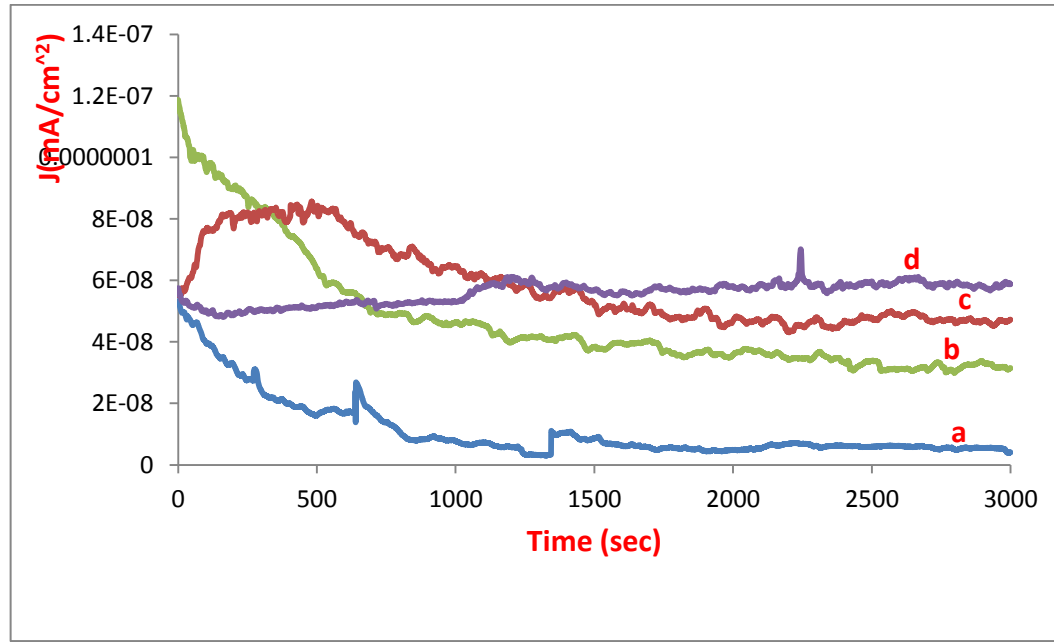


Figure (3.33): Short circuit current density vs. time measured for a) non-annealed fresh, b) non- annealed recycled c) after annealing at 125 °C and quickly cooled recycled, d) after annealing at 125 °C and quickly cooled fresh

Chapter Four

Conclusions

Chapter Four

Conclusions

1. CdS thin films electrode-based solar cells, were prepared by different techniques onto ITO/Plastic substrate, including ECD, CBD and ECD/CBD techniques. All films showed PEC behaviors, except ECD film.
2. CBD-CdS thin films showed higher efficiency in PEC systems than its EC/CBD-CdS counterparts.
3. ECD technique gives a very thin layer of CdS, because the resulting film wasn't observable. Thus, the characteristics for this technique can't be obtained.
4. Poly-Sulfide redox couple showed higher efficiency in PEC systems than Iron redox couple.
5. CBD-CdS thin films, prepared through fourth cycle of deposition (120 min) showed higher efficiency in PEC systems than other counterparts.
6. Annealing and fast cooling process showed enhancement in PEC cell efficiency for CBD-CdS thin film electrodes.
7. Covering CBD-CdS films with carbon couldn't enhance the PEC characteristics.
8. CdS thin films electrode-based solar cells can be recycled as confirmed in this work.

9. Annealing process and fast cooling enhance PEC cell efficiency and stability for fresh and recycled CBD-CdS films.

Suggestions for Future Work:

It is recommended to investigate the following:

1. Use the ITO/Plastic substrates for other types of semiconductors (CdTe, CuSe, CuO, and others).
2. Doping the CdS film with different types of dopants.
3. Coating the film electrode with electro active materials to improve charge transfer between the electrode and the Redox couple.
4. Recycling of other types of semiconductor film electrodes.
5. Studying different experimental conditions and different redox couples to enhance electrode efficiency and stability is recommended.

References

1. Tromly, K., *Renewable energy: An overview*. 2001, National Renewable Energy Lab., Golden, CO (US).
2. Gunerhan, H., A. Hepbasli, and U. Giresunlu, *Environmental impacts from the solar energy systems*. Energy Sources, Part A: Recovery, Utilization, and Environmental Effects, 2008. **31**(2): p. 131-138.
3. Laposata, M. and J. Pratte, *The ESA21 Project: Environmental Science Activities for the 21st Century*. 2005: DigitalCommons@ Kennesaw State University.
4. Knödel, K., G. Lange, and H.-J. Voigt, *Environmental geology: handbook of field methods and case studies*. 2007: Springer Science & Business Media.
5. Lopes, R.M. and T.K. Gregg, *Volcanic worlds: exploring the solar system's volcanoes*. 2004: Springer Science & Business Media.
6. Stephens, G.L., et al., *An update on Earth's energy balance in light of the latest global observations*. Nature Geoscience, 2012. **5**(10): p. 691-696.
7. Wallace, J.M. and P.V. Hobbs, *Atmospheric science: an introductory survey*. Vol. 92. 2006: Elsevier.
8. Prasad, A.R., S. Singh, and H. Nagar, *Importance of Solar Energy Technologies for Development of Rural Area in India*. 2017.

9. Ghiani, E. and G. Pisano, *Impact of renewable energy sources and energy storage technologies on the operation and planning of smart distribution networks*, in *Operation of Distributed Energy Resources in Smart Distribution Networks*. 2018, Elsevier. p. 25-48.
10. Khudruj, S.M.A., *CdS thin film photo-Electrochemical electrodes: Combined Electrochemical and chemical bath depositions*. 2011.
11. Stephens, G.L. and T. L'Ecuyer, *The Earth's energy balance*. Atmospheric Research, 2015. **166**: p. 195-203.
12. Potočník, J. and A. Pielbalgs, *Photovoltaic Solar Energy Development and current research*. Luxembourg: Office for Official Publications of the European Union, 2009: p. 5.
13. Murtada, K.A.Q., *Combined Electrochemical and Chemical Bath Deposition Techniques to Prepare CuSe Thin Film Electrodes for Solar Energy Purposes*. 2014.
14. Kaldis, E., *Current Topics in Materials Science*. Vol. 9. 1982: North-Holland.
15. Yoder, M.N., *Wide bandgap semiconductor materials and devices*. IEEE Transactions on Electron Devices, 1996. **43**(10): p. 1633-1636.
16. Kissell, T.E., *Introduction to solar principles*. 2011: Pearson Higher Ed.

17. Isa, T., M. Morisue, and I. Kawamata, *Semiconductor device, electronic device, and method of manufacturing semiconductor device*. 2009, Google Patents.
18. Zahedi, A., *The engineering and economics of solar photovoltaic energy systems*. 2004: New World Publishing.
19. Takimiya, K., et al., *Organic semiconductors based on [1] benzothieno [3, 2-b][1] benzothiophene substructure*. Accounts of chemical research, 2014. **47**(5): p. 1493-1502.
20. Brabec, C., U. Scherf, and V. Dyakonov, *Organic photovoltaics: materials, device physics, and manufacturing technologies*. 2011: John Wiley & Sons.
21. Landsberg, P.T., *Basic properties of semiconductors*. 2016: Elsevier.
22. Swaminathan, P., *ELECTRONIC MATERIALS, DEVICES, AND FABRICATION*. 2015, A JOHN WILEY & SONS, INC.,.
23. Neamen, D.A., *Semiconductor physics and devices: basic principles*. 2012: New York, NY: McGraw-Hill.
24. Meyers, H. and H. Myers, *Introductory solid state physics*. 1997: CRC press.
25. Klein, C., *Simple explanation of the electron-hole pair creation energy puzzle in germanium*. Physics Letters A, 1967. **24**(10): p. 513-514.

26. Chao, T., *Introduction to semiconductor manufacturing technology*. 2001: SPIE PRESS.
27. Enderlein, R. and N.J. Horing, *Fundamentals of semiconductor physics and devices*. 1997: World Scientific.
28. Basak, M.K. and M. Joarder, Sourov Mazum “*Simulation of A 2d PN Junction in Silicon Thin Film Incorporating Quantum Transport For Carriers*” *Der*. 2017, Daffodil International University.
29. Tyona, M., *Doped zinc oxide nanostructures for photovoltaic solar cells application*, in *Zinc Oxide Based Nano Materials and Devices*. 2019, IntechOpen.
30. Mead, C. and W. Spitzer, *Fermi level position at metal-semiconductor interfaces*. *Physical Review*, 1964. **134**(3A): p. A713.
31. Goldsmid, H.J., *Generator materials*. The Physics of Thermoelectric Energy Conversion, 2017.
32. Walukiewicz, W., *Mechanism of Fermi-level stabilization in semiconductors*. *Physical Review B*, 1988. **37**(9): p. 4760.
33. Chandra, S., *Recent trends in high efficiency photo-electrochemical solar cell using dye-sensitised photo-electrodes and ionic liquid based redox electrolytes*. *Proceedings of the National Academy of Sciences, India Section A: Physical Sciences*, 2012. **82**(1): p. 5-19.
34. Matsuoka, L. *Economic Evaluation of Space Solar Power System*. in *Solar Power from Space-SPS'04*. 2004.

35. Kalogirou, S.A., *Solar energy engineering: processes and systems*. 2013: Academic Press.
36. Barbarino, G., et al., *Silicon photo multipliers detectors operating in geiger regime: an unlimited device for future applications*, in *Photodiodes-World Activities in 2011*. 2011, InTechOpen.
37. Rajeshwar, K., P. Singh, and J. DuBow, *Energy conversion in photoelectrochemical systems—a review*. *Electrochimica Acta*, 1978. **23**(11): p. 1117-1144.
38. Muhibbullah, M. and A.M.A. Haleem, *Estimation of the Open Circuit Voltage of a pn Junction Based on Photoelectrochemical Measurements*. *Transactions of the Materials Research Society of Japan*, 2015. **40**(3): p. 247-252.
39. Sahu, S. and S. Chandra, *Chemical-bath-deposited CdS and CdS: Li films and their use in photoelectrochemical solar cells*. *Solar Cells*, 1987. **22**(3): p. 163-173.
40. d Boer, R., *Technologies and prospects for photochemical conversion and storage of solar energy: a survey of the state-of-the-art*. 2001: Petten: ECN.
41. Nozik, A.J., *Photoelectrochemistry: applications to solar energy conversion*. *Annual review of physical chemistry*, 1978. **29**(1): p. 189-222.

42. Claesson, S., B. Holmström, and P. Carlsson, *Solar energy: photochemical processes available for energy conversion*. 1982: National Swedish board for energy source development [Nämnden för
43. Brett, C. and A.M. Oliveira Brett, *Electrochemistry: principles, methods, and applications*. 1993.
44. Ismail, R.M.A.-A., *Enhancement of Photoelectrochemical Characteristics of CdS Thin Film Electrodes Prepared by Chemical Bath Deposition: Effect of Annealing and Rate of Cooling*. 2008, An-Najah National University.
45. Finklea, H.O., *Semiconductor electrodes*. 1988.
46. Toivola, M. and T. Pilvi, *ALD for a Sustainable Future-Paving the Way to a Cleaner World from Sub-Nanometer Level*. ECS Transactions, 2011. **41**(2): p. 203.
47. Islam, A., *Characterization of copper selenide thin films deposited by chemical bath deposition technique*. Applied surface science, 2004. **238**(1-4): p. 184-188.
48. Lindfors, S., *Coating a substrate web by atomic layer deposition*. 2015, Google Patents.
49. Xu, D., et al., *Preparation of CdS single-crystal nanowires by electrochemically induced deposition*. Advanced Materials, 2000. **12**(7): p. 520-522.

50. Jia, H., et al., *Synthesis and photoelectrochemical behavior of nanocrystalline CdS film electrodes*. Electrochemistry communications, 2006. **8**(8): p. 1381-1385.
51. Patidar, D., et al. *Energy band gap studies of CdS nanomaterials*. in *Journal of Nano Research*. 2008. Trans Tech Publ.
52. Enríquez, J.P. and X. Mathew, *Influence of the thickness on structural, optical and electrical properties of chemical bath deposited CdS thin films*. Solar Energy Materials and Solar Cells, 2003. **76**(3): p. 313-322.
53. Antony, A., *Preparation and characterisation of certain II-VI, I-III-VI₂ semiconductor thin films and transparent conducting oxides*. Department of Physics Cochin University of Science and Technology Cochin-682022, Kerala, India, 2004.
54. Oliva, A., et al., *Comparison of properties of CdS thin films grown by two techniques*. Applied surface science, 2003. **205**(1-4): p. 56-64.
55. Patil, B.N., D. Naik, and V. Shrivastava, *Synthesis and characterization of Al doped CdS thin films grown by chemical bath deposition method and its application to remove dye by photocatalytic treatment*. Chalcogenide lett, 2011. **8**(2): p. 117-121.
56. Islam, M. and M.S. Islam, *Electro-deposition method for platinum nano-particles synthesis*. Saidul, Electro-Deposition Method for Platinum Nano-Particles Synthesis, 2013.

57. Mirmohseni, A., D. Farshbaf, and M. Zarrabi, *Electrodeposition Coating of Epoxy Resin on Phosphated Steel: Optimization of Key Factors*. International Journal of Polymeric Materials, 2004. **53**(8): p. 621-632.
58. Sasikala, G., R. Dhanasekaran, and C. Subramanian, *Electrodeposition and optical characterisation of CdS thin films on ITO-coated glass*. Thin Solid Films, 1997. **302**(1-2): p. 71-76.
59. Kadirgan, F., et al., *Properties of electrodeposited cadmium sulfide films for photovoltaic devices with comparison to CdS films prepared by other methods*. Turkish Journal of Chemistry, 2000. **24**(1): p. 21-34.
60. Lincot, D. and R.O. Borges, *Chemical bath deposition of cadmium sulfide thin films. In situ growth and structural studies by combined quartz crystal microbalance and electrochemical impedance techniques*. Journal of the Electrochemical Society, 1992. **139**(7): p. 1880.
61. Soundeswaran, S., O.S. Kumar, and R. Dhanasekaran, *Effect of ammonium sulphate on chemical bath deposition of CdS thin films*. Materials letters, 2004. **58**(19): p. 2381-2385.
62. Ramaiah, K.S., et al., *Structural and optical investigations on CdS thin films grown by chemical bath technique*. Materials chemistry and physics, 2001. **68**(1-3): p. 22-30.

63. Martinez, M., C. Guillen, and J. Herrero, *Morphological and structural studies of CBD-CdS thin films by microscopy and diffraction techniques*. Applied Surface Science, 1998. **136**(1-2): p. 8-16.
64. Rami, M., et al., *Effect of the cadmium ion source on the structural and optical properties of chemical bath deposited CdS thin films*. Solid state sciences, 1999. **1**(4): p. 179-188.
65. Hilal, H.S., et al., *Effect of annealing and of effect of annealing and of cooling rates on n-GaAs electrode photoelectrochemical characteristics*. Active and passive electronic components, 2004. **27**.
66. El Maliki, H., et al., *Study of the influence of annealing on the properties of CBD-CdS thin films*. Applied Surface Science, 2003. **205**(1-4): p. 65-79.
67. Zinoviev, K. and O. Zelaya-Angel, *Influence of low temperature thermal annealing on the dark resistivity of chemical bath deposited CdS films*. Materials Chemistry and Physics, 2001. **70**(1): p. 100-102.
68. Metin, H. and R. Esen, *Annealing studies on CBD grown CdS thin films*. Journal of Crystal Growth, 2003. **258**(1-2): p. 141-148.
69. Goto, F., K. Shirai, and M. Ichimura, *Defect reduction in electrochemically deposited CdS thin films by annealing in O₂*. Solar Energy Materials and Solar Cells, 1998. **50**(1-4): p. 147-153.

70. Olmedo, P., et al., *Determination of toxic elements (mercury, cadmium, lead, tin and arsenic) in fish and shellfish samples. Risk assessment for the consumers*. Environment international, 2013. **59**: p. 63-72.
71. Zyoud, A., et al., *Recycled polycrystalline CdS film electrodes with enhanced photo-electrochemical characteristics*. Materials Science in Semiconductor Processing, 2018. **74**: p. 277-283.
72. Purkayastha, D., U. Mishra, and S. Biswas, *A comprehensive review on Cd (II) removal from aqueous solution*. Journal of water process engineering, 2014. **2**: p. 105-128.
73. Hilal, H.S., et al., *Effect of cooling rate of pre-annealed CdS thin film electrodes prepared by chemical bath deposition: Enhancement of photoelectrochemical characteristics*. Electrochimica acta, 2009. **54**(12): p. 3433-3440.
74. Dona, J. and J. Herrero, *Chemical bath deposition of CdS thin films: an approach to the chemical mechanism through study of the film microstructure*. Journal of the Electrochemical Society, 1997. **144**(11): p. 4081.
75. Al Yamani, S.M.M., *Recycling CdS Thin Film Solar Cells Prepared by Chemical Bath Deposition*. 2014.
76. Martin, D.J., *Investigation into high efficiency visible light photocatalysts for water reduction and oxidation*. 2015: Springer.

77. Singh, M., M. Goyal, and K. Devlal, *Size and shape effects on the band gap of semiconductor compound nanomaterials*. Journal of Taibah University for Science, 2018. **12**(4): p. 470-475.
78. Pawar, M. and S. Chaure, *Synthesis of CdS nanoparticles using glucose as a capping agent*. Chalcogenide Lett, 2009. **6**(12): p. 689-693.
79. Manickathai, K., S.K. Viswanathan, and M. Alagar, *Synthesis and characterization of CdO and CdS nanoparticles*. 2008.
80. Warren, B.E., *X-ray Diffraction*. 1990: Courier Corporation.
81. Andrade, E.N.D.C. and K.Y. Lonsdale, *William Henry Bragg, 1862-1942*. 1943, The Royal Society London.
82. Rajpal, S. and V. Bandyopadhyay, *Structural and optical properties of CdS thin film grown by chemical bath deposition*. Журнал нано-та електронної фізики, 2013(5, № 3 (1)): p. 03021-1-03021-3.
83. Zyoud, A., et al., *Enhanced PEC characteristics of pre-annealed CuS film electrodes by metalloporphyrin/polymer matrices*. Solar Energy Materials and Solar Cells, 2016. **144**: p. 429-437.
84. Hilal, H.S., et al., *Effects of annealing temperature and cooling rate on photo-electrochemical performance of pristine polycrystalline metal-chalcogenide film electrodes*. Solar Energy, 2019. **183**: p. 704-715.

جامعة النجاح الوطنية

كلية الدراسات العليا

إعادة تدوير الخلايا الشمسية من أفلام CdS العادمة بواسطة
طرق الترسيب المختلفة

إعداد

مجد إبراهيم راشد صبيح

إشراف

أ.د حكمت هلال

د. عاهد زيود

قدمت هذه الأطروحة استكمالاً لمتطلبات الحصول على درجة الماجستير في الكيمياء بكلية الدراسات العليا في جامعة النجاح الوطنية في نابلس، فلسطين.

2020

ب

إعادة تدوير الخلايا الشمسية من أفلام CdS العادمة بواسطة طرق الترسيب المختلفة

إعداد

مجد إبراهيم راشد صبيح

إشراف

أ.د. حكمت هلال

د. عاهد زيود

الملخص

في هذا البحث تم ترسيب أفلام CdS الرقيقة نانوية الحبيبات لأول مرة على شرائح بلاستيكية مغطاة بطبقة رقيقة موصلة شفافة من أكسيد القصدير الالمطعم بالإنديوم (ITO/Plastic) ، وذلك باستخدام تقنيات مختلفة، وهي:

الترسيب الكهروكيميائي (ECD)، والترسيب الكيميائي (CBD) وطريقة مشتركة تعتمد على الترسيب الكهروكيميائي تليها تقنية الترسيب الكيميائي (ECD / CBD). تم التأكد من وجود طبقة CdS على سطح البلاستيك عن طريق المسح المجهر الإلكتروني (SEM)، حيود الأشعة السينية (XRD)، وطيف الامتصاص الإلكتروني.

درست كفاءة الأفلام المحضرة في تحويل الضوء إلى كهرباء بالطريقة الفوتو كهروكيميائية (PEC) لأقطاب الأفلام المختلفة من حيث عوامل مختلفة مثل منحنيات كثافة تيار الاضاءة (photo J-V) مقابل الجهد، كثافة تيار الدارة القصيرة (J_{sc})، جهد الدارة المفتوحة (V_{oc})، وكفاءة التحويل، ومعامل الملء (FF)، وثبات الأفلام بعد تحضيرها، حيث كان لطريقة الترسيب الكيميائي والمعالجة أثر كبير على خصائص فيلم CdS.

أظهرت الخصائص الفوتو كهروكيميائية PEC للأفلام المختلفة سلوكيات مختلفة. أعطت أفلام ECD فيلم CdS رقيقاً جداً بحيث لا يمكن تمييزه، وأظهرت أفلام ECD / CBD كفاءة أقل في تحويل الضوء إلى الكهرباء من أفلام CBD. علاوة على ذلك ، أظهرت أغشية CBD ، التي

تم تحضيرها خلال الدورة الرابعة للترسيب ، قيمًا أعلى لكفاءة التحويل والاستقرار من نظيراتها الأخرى. يعطي هذا فكرة عن أهمية الأفلام الموصوفة الجديدة.

وتم محاولة طلاء فيلم CBD-CdS بأنابيب نانوية كربونية متعددة الجدران (MWCNT)، لكن ذلك لم يؤد إلى تحسين خصائص PEC.

كان لتأثير زوج التأكسد والاختزال دور في جودة منحنيات كثافة تيار الاضاءة (photo J-V) مقابل الجهد لأفلام CBD-CdS الرقيقة، أعطى نظام بولي كبريتيد / S^{-2} / NaOH كفاءة أعلى في تحويل الضوء إلى الكهرباء. S_x^{-2}

نظرًا للطبيعة الخطرة لأيونات الكاديوم وتأثيرها السلبي على البيئة ، وصف هذا العمل آلية إعادة تدوير أفلام الكاديوم التالفة إلى أفلام جديدة وفعالة. وذلك بإعادة ترسيبها مرة أخرى على شرائح بلاستيكية (ITO/Plastic) باستخدام الترسيب الكيميائي (CBD).

تمت دراسة تأثير عملية الشئ عند 125 درجة مئوية والتبريد لدرجة حرارة الغرفة بوجود غاز النيتروجين، باستخدام طريقتين مختلفتين: التبريد السريع والبطيء على خصائص أفلام CBD-CdS المحضرة لأول مرة والمعاد تدويرها، بما في ذلك: أطياف الامتصاص الالكتروني، منحنيات كثافة تيار الاضاءة (photo J-V) مقابل الجهد، كثافة تيار الدارة القصيرة (J_{sc})، جهد الدارة المفتوحة (V_{oc})، وكفاءة التحويل، وعامل الملء (FF)، وثبات الأفلام. وقد أظهرت الأفلام المعالجة بالشئ (التلدين) والتبريد السريع كفاءة تحويل واستقرار أعلى من تلك غير الملدنة في كلا النوعين من الأفلام (الجديدة والمعاد تدويرها، ولكن أظهر فيلم CdS المعاد تدويره كفاءة PEC أقل عند الشئ 125 درجة مئوية بوجود غاز النيتروجين، مقارنة بنظيره من الأفلام الجديدة.